Preparation and Characterization of Polymer TiO_2 Nanocomposites via *In-situ* Polymerization

by

Feng Lin

A thesis
presented to the University of Waterloo
in fulfillment of the
thesis requirement of the degree of
Master of Applied Science
in Chemical Engineering

Waterloo, Ontario, Canada, 2006

AUTHOR'S DECLARATION FOR ELECTRONIC SUBMISSION OF A THESIS

I hereby declare that I am the sole author of this thesis. This is a true copy of the thesis, including any required final revisions, as accepted by my examiners.

I understand that my thesis may be made electronically available to the public.

Abstract

Polymer nanocomposites are already a part of many important of worldwide businesses: automotive (molded part in cars), electronics and electrical engineering, household products, packaging industry, aircraft interiors, appliance components, security equipments. Among many nanocomposite precursors, TiO_2 nanopowder is increasingly being investigated due to its special properties.

The objective of this work is to synthesize and characterize polymer-TiO_2 hybrid nanocomposites. When dispersed at the nanoscale level TiO_2 could act as visually transparent UV filters and high-thermomechanical-performance materials. The synthesis strategy involved two steps. Firstly, aggregated TiO_2, as received, was modified by 3-trimethoxysilyl propylmethacrylate aimed at altering its surface characteristics. The effect of modifier concentration on changing the physicochemical properties of TiO_2 surface was evaluated. Size distribution of unmodified and modified TiO_2 nanopowders was measured using a particle size analyzer. The qualitative and quantitative grafting of vinyl groups on TiO_2 surface was investigated with Fourier transform-infrared (FTIR) and proton nuclear magnetic resonance (^{1}H-NMR) spectroscopy. Secondly, styrene monomer was then added to carry out copolymerization with vinyl groups on the modified TiO_2 by free radical initiator 2,2-azobis isobutyronitrile (AIBN) in bulk medium. FTIR spectra confirmed the formation of nanocomposites with polystyrene chains chemically linked to the surface of TiO_2 nanopowders. Thermogravimetric analysis (TGA) and differential scanning calorimetry (DSC) indicated that the resulting nanocomposites displayed higher thermal stability and maintained similar glass transition temperatures (T_g) compared with pure PS. Ultraviolet –visible spectroscopy (UV-Vis) investigated that these nanocomposites have improved optical properties potentially acting as visually transparent UV filters. Such incremented properties were attributed to the nancoscale dispersion (20-50nm size) of TiO_2 into polystyrene matrix, which morphology was observed by scanning electron microscopy (SEM).

Acknowledgements

First of all, I am greatly grateful to my supervisor, Dr. Leonardo C. Simon, not only for his giving me a once in my lifetime opportunity to go further distance, but for his invaluable guidance, encouragement and inspiration in both my academic work and daily life. His thoughtfulness deeply motivated me throughout this research process.

I would like to acknowledge Dr. Elkamel and Dr. Henneke for their reviewing my thesis; Dr. Soares, Dr. Penlidis and Dr. Legge for their allowing the use of several instruments in their labs. Many thanks are extended to Mamdouh, Sang-Young (Anthony) and other members of our research group, for their selfless helps and enjoyable discussions during my research work. I am also indebted to Qingxin, Matthew and Dominik for their willingness to provide me technical trainings of some instruments and to answer many of my "dumb questions".

Special appreciation is given to Mohammad Al-Saleh for his friendship, for his encouragement in exploring my potential and sharing my happiness and sadness as well as making me close to home. His support was fundamental and helped me to better survive every single challenge in these last two years.

And, I could not complete this thesis without plentiful supports from my family, namely, my brother and sister for taking care of the whole family business and errands; my parents for giving me example of being positive, unbeatable and honest and keeping promise; my beautiful wife for her endless love without asking any rewards, I still have no idea of how bravely she has stood side by side with me to get through all the difficulties as immigrant.

Financial supports from Emerging Materials Knowledge-Materials and Manufacturing Ontario (EMK-MMO) and Ontario Graduate Scholarship at Science and Technology (OGSST) are also deeply thankful.

Contents

List of Figures

List of Tables

Nomenclature

1D: one dimensional

2D: two dimensional

3D: Three dimensional

ABS: absorbance

AEAPS: N-(2-aminoethyl) 3-aminopropyl-trimethoxysilane

AFM: atom force microscopy

AIBN: 2,2'-azobis(isobutyronitrile)

AOT: sodium bis(2-ethyl hexyl) sulphosuccinate

ATRP: atom transfer radical polymerization

ATRSIP: atom transfer radical surface-initiated polymerization

BI: Brookhaven Instruments

BPDA: 3,3′,4,4′-biphenyl tetracarboxylic dianhydride

BTDA: 3′,4,4′-benzophenonetetracarboxylic acid dianhydride

BPO: benzoyl peroxide

CDES: (2-(4-chloromethylphenyl)ethyl) dimethylethoxysilane

CRT: cathode ray tubes

CNTs: carbon nanotubes

CTE: coefficient of thermal expansion

CV: cyclic voltammetric

DBSA: dodecylbenzenesulfonic acid

DCP: Disc Centrifuge Photosedimentometer Size Analyser

DMAC: dimethylacetamide

DMF: dimethylformamide

DPE: 1,1-diphenylethylene

DSC: differential scanning calorimetry

DTG: derivative thermogravimetric

$E_{0:}$ cumulative failure probability

FT-IR: Fourier transform-infrared

GTP: group transfer polymerization

h: hours

^{1}H-NMR: proton nuclear magnetic resonance

HREELS: high resolution electron energy loss spectroscopy

HVOF: high velocity oxy-fuel

IPNs: interpenetrating networks

LASIP: living anionic surface-initiated polymerization

LCSIP: living cationic surface-initiated polymerization

LDPE: low-density polyethylene

LFRSIP: living free radical surface-initiated polymerization

$LiBF_4$: lithium tetrafluoroborate

LROP: living ring opening polymerization

LS: layered silicate

IR: infrared

M: mol/l

MAO: methylaluminoxane

min: minutes

MMA: methyl methacrylate

MMT: montmorillonite

MPS: 3-trimethoxysilyl propylmethacrylate

MT: modified TiO_2

MWNT: multi-walled nanotube

NMR: nuclear magnetic resonance

PA: polyamide

PAAM: polyacrylamide

PBa: polybenzoxazine

PDAA: poly-3-hydroxy-2,3-dimethylacrylic acid

PDLLA: poly-D,L lactid acid

PDMS: polydimethylsiloxane

PE: polyethylene

PEG: polyethylene glycol

PEK: polyarylene ether ketone

PEO: polyethylene oxide

PET: polyethylene terephthalate

PGMA: propylene glycol methyl ether acetate

PI: polyimide

PLS: polymer/layered silicate

PMDA-ODA: pyromellitic dianhydride-4,4'-oxydianiline

PMDA: pyromellitic dianhydride

PMMA: polymethyl methacrylate

POSS: polyhedral oligomeric silsesquioxanes

PP: polypropylene

PPO: polypropylene oxide

PPV: poly-*p*-phenylenevinylene

PS: polystyrene

PSF: polyacrylene sulfone

PSMA: polystyrene maleic anhydride

PSTN: polystyrene TiO_2 Nanocomposites

PU: polyurethane

PVAL: polyvinyl alcohol

PVAC: polyvinyl acetate

PVC: polyvinyl chloride

PVPO: polyvinylpyrrolidone

PVPY: polyvinyl pyridine

R: radius

RF: radio frequency

ROMP: ring-opening metathesis polymerization

SCA: silane coupling agent

SGC: surface grafting conversion

SGD: surface grafting density

S/V: surface-to-volume

SEM: scanning electron microscopy

STM: scanning tuning microscopy

SWNT: single-walled nanotube

TEOS: tetraethyloxysilane

T_g: glass transition temperature

TGA: thermogravimetric analysis

THF: tetrahydrofuran

T_m: melting temperature

TMS: tetramethylsilane

TIP: titanium iso-propoxide

TPD: temperature programmed desorption

UHV: ultra high vacuum

UV: ultraviolet

UV-Vis: ultraviolet –visible spectroscopy

VDA: vinyl dianhydride

XPS: X-ray photoelectron spectroscopy

XRD: X-ray diffraction

Chapter 1 Introduction

1.1 Motivation and Objective

Manufacturers traditionally reinforce polymers with micrometer fillers to gain higher strength and stiffness, to improve solvent or fire resistance, or simply to reduce cost. However, these microfillers also impart several drawbacks such as brittleness and opacity. Nanocomposites, for which at least one dimension of the filler is less than 100 nm [Rosoff, 2002], give a new way to overcome the limitations of traditional counterparts. One can distinguish three categories of nanocomposites, depending on geometry of the nanofillers including one dimensional (1D) nanotube fillers such as carbon nanotubes, two dimensional (2D) plate-like nanofillers such as clay, and nanopowders such as nanoalumina or nanosilica.

Because of significantly increased interfacial interaction between inorganic and organic phases and size-dependent phenomena of nanoscale particles, polymer nanocomposites are capable of dramatically improving the mechanical and thermal properties including stiffness and heat resistance, gas and solvent barrier property, flame retardance without losing good ductility of polymer (i.e. toughness), affecting optical transparency and increasing density or difficulty of processing as compared with homopolymer or traditional microcomposites. In addition, these properties improvements in nanocomposites are achieved at very low loadings of the nanoscale inorganic component (<5wt%) while traditional microcomposites usually require a much high loading of the order of 25-40 wt% [Saujanya, 2001].

Therefore, polymer nanocomposites are already a part of important of worldwide business sections: automotive (molded parts in cars), electronics and electrical engineering, household products, packaging industry, aircraft interiors, appliance components. A number of polymer nanocomposites based on layered silicates have been recently commercialized, such as the polyamide-clay nanocomposites pioneered by

Toyota in 1993 [Usuki, 1992] and polypropylene-clay nanocomposites by General Motors in 2002 [Stewart, 2004].

To achieve the desired properties for an application, a method of producing polymer nanocomposites capable of controlling the interface is quite important. Several methods have recently been employed ranging from simply mixing polymer with fillers to more elaborated approaches. A key challenge in the preparation of nanocomposite materials is the establishment of good dispersion of nanosize inorganic phase into the polymer matrix and the efficiency to prevent re-aggregation of nanoparticles

Our research group in the Department of Chemical Engineering, at the University of Waterloo, has investigated new methods to produce a nano-filler well dispersed into the polyolefin matrix and the effect on the physicochemical properties. We have focused on the study of the chemical modification of nano fillers (clay and Al_2O_3) and their interaction with the polymerization mechanism to create hybrid materials. This new class of materials has polyolefin chains covalently bonded to the surface of nano-fillers during the polymerization reaction [Shin, 2003; Zhang, 2005].

Among many nanocomposite precursors, TiO_2 nanopowder is increasingly being investigated because it is non-toxic, chemically inert, low cost, has a high refractive index, is a broadband UV filter, kills bacteria by photo irradiation, is corrosion resistant and has a high hardness [Solomon, 1983]. Literature has also shown that nanoscale TiO_2 reinforcement brings new optical, electrical, physiochemical properties attained at very low TiO_2 content, which make polymer TiO_2 nanocomposites a promising new class of materials. One can foresee that they will be commercially beneficial for widespread fields. Nevertheless, the study of TiO_2-based nanocomposites is still in its infancy and much research remains to be carried out to explore improved synthesis techniques yielding the different nanocomposite structures and to fully understand the actual structure/properties relationships.

The objective of my work is to investigate the feasibility of preparing hybrid polymer TiO_2 nanocomposites acting as visually transparent UV filters without losing thermomechanical performance materials by using two-step strategy, one of which is the preparation and characterization of modified TiO_2 and the other the preparation and characterization of polymer TiO_2 nanocomposites via *in-situ* polymerization. Styrene was employed as one model of vinyl monomers with low cost and widespread use. TiO_2 as received was modified by 3-trimethoxysilyl propylmethacrylate aimed at altering its surface characteristics. After modification, styrene monomer was then added to carry out copolymerization with vinyl groups on the modified TiO_2 resulting in the formation of nanocomposites with polymer chains chemically linked to the surface of titania nanopowders.

1.2 Thesis Scope

This thesis is organized in such that each chapter has its own introduction, list of references, and appendix if applicable. The comprehensive review in Chapter 2 discusses overall background information about the development of various categories of nanofillers dispersed polymer nanocomposites, about size-dependent phenomena of nanopowders, about the surface chemistry and modification of TiO_2 as well as its applications, and finally about the preparation methods and properties gains of nanoTiO_2 filled polymers. Several surface characterization methods can be found in the appendix at end of this chapter.

Chapter 3 describes the experimental method used to modify TiO_2 surface and the techniques used to analyze the modified TiO_2. Main results are included and explained in the main body of Chapter 3 to demonstrate the results, while supplementary data are provided in the appendix.

Chapter 4 gives a detailed account of the in-situ polymerization of polymer TiO_2 nanocomposites. Included here are also the characterization methods and results of the

final nanocomposites structure and properties. These results are then compared with experiments where homopolymers are run under identical conditions.

Finally, concluding remarks are summarized in Chapter 5, along with recommendations for further work.

1.3 References

Rosoff, M.; *Nano-surface Chemistry*, Marcel Dekker Inc., New York, 2002

Saujanya, C.; Radhakrishnan, S.; *Polymer*, 2001, 42, 6723

Shin, S-Y; Simon, L. C.; Soares, B. P.; Scholz, G.; *Polymer*, 2003, 44, 5317

Solomon, D. H.; Hawthorne, D. G.; *Chemistry of Pigments and Fillers*, John Wiley & Sons Inc., New York, 1983

Stewart, R.; *Plast. Eng*. 2004, *60*, 23

Usuki, A.; Kojima, Y.; Kamigaito, O.; *J. Mater. Res*., 1992, 8, 1179

Zhang, X.; Simon, L. C.; *Macromol. Mater. Eng.,* 2005, 290, 573

Chapter 2 Literature Review

This review is written with purpose to obtain general understanding of the preparation of such materials for different applications. We start with an overview of recent accomplishments in the field of developing polymer filled nanocomposites, followed by a short glimpse of nanopowders. General comprehension of the surface chemistry, modification of TiO_2 and its applications is to be summarized in the third section. Finally, preparation, properties and applications of TiO_2 polymer nanocomposites are also discussed in details. The principles of operation and capabilities of surface characterization can be found in an appendix at end of this chapter.

2.1 Polymer Filled Nanocomposites: Synthesis

2.1.1 Introduction

Conventional polymer composites, usually reinforced by micrometer-scale fillers into polymer matrices, have found large-scale applications for decades in automobile, construction, electronics, and consumer products. Composites gain enhanced properties such as higher strength and stiffness compared with neat polymer [Akita, 1999; Mark, 1996]. However, properties achieved by these traditional composites involve compromises. For example, stiffness is obtained at cost of toughness, which is also traded for optical clarity. Recently, nanoscale filled polymer composites give a new way to overcome the limitations of traditional counterparts.

An idea suggested by current micromechanics theories [Jordan, 2005] is that the effective properties of polymer microscale filled composites rely on constituents, volume fraction of components, shape and arrangement of fillers, and polymer/filler interface. Based on this idea, properties of polymer composites are thus independent of the size of fillers. Obviously, this may not be correct for polymer nanocomposites. The most prominent difference of nanocomposites compared with their traditional counterparts is the small

size of the fillers, which could bring added specific phenomena. For example, nanotube fillers possess strength as high as 500 GPa and modulus as high as 1 TPa. Nanoparticles are optically active and do not scatter light significantly, which can be combined into a polymer to obtain the optical gain of the material. Very small fillers do not build large stress concentrations and therefore do not compromise the ductility of the polymer. In addition, the small decrease in size of the fillers less than 100 nm leads to dramatically augmented interfacial area per unit volume or weight of the dispersed phase, which control the degree of interaction between the polymer and filler phase and thus controls the properties. Hence, the greatest challenge in making polymer nanocomposites is to learn how to control the interface.

To realize the novel properties of polymer nanocomposites, synthetic methods which have effect on controlling particle size distribution, dispersion, and interfacial interactions are critical. Synthetic techniques for nanocomposites are quite different from those for conventional microscale-filled composites and creating one universal technique for developing polymer nanocomposites is impossible due to the physiochemical differences between each system. Each polymer system may require a special set of processing conditions to be formed and different synthetic techniques in general could yield nonequivalent results [Park, 2001]. Despite numerous challenges, considerable research has been done to develop appropriate synthetic techniques for making good polymer nanocomposites in the literature.

This section is to review what we feel are important synthetic methods and possible interpretations of those methods for developing polymer nanocomposites.

2.1.2 Synthetic Methods

Among several factors in selecting a synthetic method, the most prominent to be considered is geometry of the nanofillers, which are generally classified into three categories. 1) One dimensional (1D) nanotube fillers, which have one diameter less than 100 nm and an aspect ratio of more than 100, such as carbon nanotubes (CNTs) first

noticed in 1991 by Sumio Injima [Iijima, 1991] ; 2) 2D plate-like nanofillers, typically defined as layered materials with a thickness on the order of 1nm and an aspect ratio in the other two dimensions of at least 25 such as layered silicate; 3) Nanopowders, which are equi-axed particles with less than 100 nm in their largest dimension such as nanosilica. For ease of review, the following subsections are to present a variety of synthesis methods organized by these three categories.

2.1.2.1 Polymer/Nanotube Composites Synthesis

The synthesis of polymer nanotube composites is still in its infancy and the most common nanotubes used are carbon nanotubes which include multi-walled nanotube (MWNT) and single-walled nanotube (SWNT). CNTs are exceptionally stiff and strong materials which are able to be tailored into polymers to make composites with improved mechanical and electrical properties. However, strong van der Waals forces which lead to agglomerate and poor solubility in most solvents hinder their potential applications.

To tackle this obstacle, the physical or/and chemical modification [Velasco-Santos, 2002; Liu, 1998; Wong, 1998; Chen, 1998A-B] of the surface of CNTs with or without the aid of surfactants [Gong, 2000] is one effective approach in achieving good dispersion of CNTs into a polymer. Physical modification has poor miscibility and the resulted dispersions often re-agglomerate in time. Chemical modification becomes an increasing way to functionalize CNTs. A variety of chemical functionalization including chemically etched CNTs [Chen, 1998A; Riggs, 2000], covalent [Bahr, 2001A-B; Boul, 1999;] and non-covalent [O'Connell, 2001; Star, 2001; Chen, 2001; Dalton, 2000] sidewall functionalization as well as sidewall functionalization of CNTs via nucleophilic reaction, cycloaddition reaction [Sun, 2001; Bahr, 2001A-B; Holzinger, 2001], and radical addition have been reported in the recent years. The modification surfactants used widely are long aliphatic amines [Chen, 1998A], organosilane [Velasco-Santos, 2002], fluorine [Mickelson, 1999], alkanes [Mcnamara, 1999].

In-situ polymerization [Li, 2002; Park, 2003; Park, 2002; Maser, 2003; Feng, 2003; Jia, 1999; Wagner, 1998] of a monomer in pre-modified CNTs is the most common synthetic strategy studied by many researchers to develop good polymer nanocomposites. For example, S. J. Park et al. reported that nanocomposites with polymethylmethacrylate (PMMA) and MWNT were prepared by first performing treatment of pristine MWNT with 3 M HNO_3 at 60^oC for 12 h and 5 M HCl at 120^oC for 6 h, which make MWNT more dispersible in common organic solvents. Then, the acid-treated MWNT was dispersed in a liquid state of methylmethacrylate (MMA). Ultrasound was applied to the MWNT dispersion for 5 h at 25^oC. Finally polymerization of MMA/MWNT dispersion was conducted at 65^oC by using 2, 2-azoisobutyronitrile (AIBN) as an initiator. This method produced more uniformly dispersed PMMA composites with MWNT about 38nm in size [Park, 2003]. Polyaniline/CNTs [Park, 2003; Park, 2002 Maser, 2003; Feng, 2003; Jia, 1999], polyurethane/MWNT [Wagner, 1998] nanocomposites were fabricated by this processing method. In C. Park, an *in-situ* process of effectively disperse SWNT in an aromatic polymer was demonstrated. The pre-dispersed SWNT in dimethylformamide (DMF) solvent remained stable throughout the polymerization of diamine and dianhydride solution. This was explained by 1) SWNT surface was repulsed by implosion of the cavitation bubbles [Park, 2002]. 2) High-viscosity solution at the completion of polymerization restricted Brownian motion and sedimentation [Mark, 1984], thus stabilizing the nanotube dispersion from re-aggregation. 3) Ultrasound might aid in the removal of amorphous carbon, thus making more of the SWNT surface available for interaction with monomers [Mason, 1990]. 4) Diamine and dianhydride were able to interact with the graphene surface of the nanotubes via $\pi-\pi$ overlap interaction [Chen, 2001; Eklund, 2002], further stabilizing of the solution.

Direct mixing [Safadi, 2002; Curran, 1998; Ajayan, 2003] is another technique that has been used to make polymer nanotube composites. CNTs have been successfully incorporated by this process into polyphenylene/polyamide commercially, which lead to conductive thermoplastics for electrostatic painting with maintaining mechanical properties [Ajayan, 2003].

2.1.2.2 Polymer/Layered Nanofiller Composites Synthesis

The most common 2D fillers are layered silicates (LS), well known as clay including mica and talc. Since 1993 when Toyota Motor commercially introduced an automobile timing-belt cover from a Nylon 6-LS nanocomposite [Usuki, 1992A-B; Kojima, 1992], polymer/layered silicate (PLS) nanocomposites have extensively been investigated and prepared. Two challenges are being faced in developing this type of nanocomposites. i). Dispersion of the LS in polymers is hindered by the inherent tendency to form face-to-face agglomerates due to high interlayer energy. ii). Hydrophilic LS are incompatible with hydrophobic polymers. To solve these problems, treatment or functionalization of LS is usual routine to weaken interlayer cohesive energy, thus expanding the LS galleries, and to match the polarity of the LS surface to the polymer, thus improving compatibility between them. This can be done either by ion exchanging an organic cation for and inorganic cation via surfactants such as ammonium salts, onium ions and organometallic compounds or by directly using synthetic LS or a sintered clay-like fluoromica.

Depending on different extents of dispersion of the LS in a monomer or polymer, three types of composites can be formed as illustrated in **Error! Reference source not found.** [Alexandre, 2000]. The first type is an immiscible conventional composite in which the LS tactoids are poorly dispersed forming a segregated phase. The second type is intercalated PLS nanocomposite in which a single, extended polymer chain is intercalated between the silicate layers resulting in a well ordered multilayer with a distance of a few nanometers. The third type is exfoliated PLS nanocomposites in which the silicate layers are ultrafinely dispersed in a continuous polymer matrix. Exfoliated is the most desirable system which shows unlimited solvability.

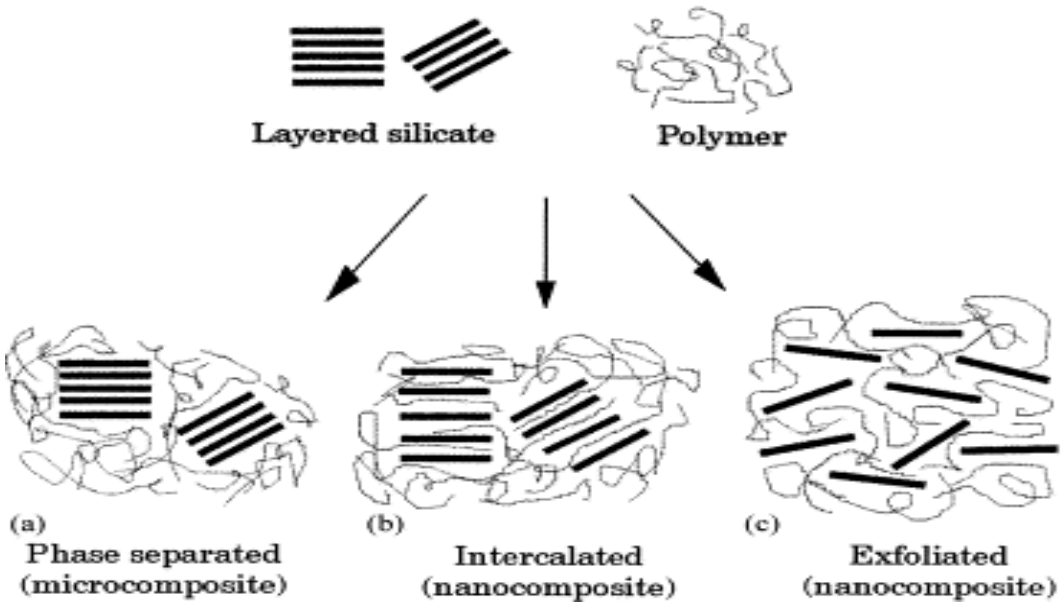

Figure 1: Illustration of three type o f PLS composites [Alexandre, 2000]

Typically, synthesis of PLS nanocomposites has involved the following three approaches. The first approach is to intercalate the pre-treated LS with a suitable monomer or precursor followed by *in situ* polymerization, which is called *in situ* polymerization route. Ion-exchanged treatments give the swelling of the LS and polymerization of monomers occurs in its galleries. In addition, the LS nanolayers are further forced apart upon polymerization and thus highly exfoliated nanocomposites are formed. However, in situ polymerization only works with suitable monomers. To date, this route has been applied to several systems including those with such polymers as amides [Usuki, 1992A-B; Kojima, 1992], olefins [Ma, 2001; Shin, 2003; Ray, 2005; Kuo, 2003], styrene [Fu, 2000], methylmethacrylate [Okamoto, 2000; Chen, 1999; Dietsche, 2000], epoxies [Wang, 1994; Wang, 1998A], urethane [Wang, 1998B], rubber [Laus, 1997], dimethylsiloxane [Burnside, 1995]. The second approach is called as solution intercalation route and involves dissolving a polymer and the LS in a compatible polymer-silicate solvent. It is well known that water-soluble polymers easily intercalate into the LS layers in aqueous solutions. A comprehensive review was done by Theng [Theng, 1986]. Recent interests have concentrated on the mixing of the modified LS with polymers dissolved with organic solvents [Ogata, 1997; Yano, 1997; Tyan, 1999A-B;

Yang, 1999; Zhu, 1999; Lan, 1994; Chen, 2000]. This approach was used to prepare polyethylene oxide (PEO)/LS [Ogata, 1997], polyimide (PI)/LS [Yano, 1997; Tyan, 1999A-B; Yang, 1999; Zhu, 1999; Lan, 1994], polyurethane (PU)/LS [Chen, 2000] nanocomposites. The third method is melt intercalation route, which involves mixing the LS with the polymer and heating the mixture above the T_g or T_m of the polymer and the LS [Vaia, 1999; Liu, 2002; Kurokawa, 1997; Usuki, 1997; Hasegawa, 1998; Kato, 1997; Phang, 2005; Liu, 2003A; Zhang, 2005; Gopakumar, 2002]. This route is the preferred process with respect to environmental and economical issues. But direct intercalation has quite slow kinetics due to diffusion phenomena and thus relatively low exfoliated composites are formed. This process is again enhanced by alkyl ammonium ions.

2.1.2.3 Polymer/Nanopowder Composites Synthesis

Nanopowders primarily involve metals, semiconductors, metal oxides. This subsection primarily reviews how to form nanocomposites with metal oxides and polymers. Generally, three ways have been applied to disperse nanopowders in polymers. The first is direct mixing or blending of the polymer and the nanopowder either as discrete phases (known as melt mixing) or in solution (solution mixing). The second is sol-gel process which starts with molecular precursor at ambient temperature and then forms metal or metal oxide framework by hydrolysis and condensation. The third is in situ grafting polymerization of macromolecular chains on the surface of nanopowder.

2.1.2.3.1 Direct Mixing

Melt mixing is the fastest method for introducing new nanocomposites to market since it can take full advantage of well-built polymer processing equipments including extruders or injectors. For example, nanoscale silica or $CaCO_3$ filled Nylon composites have successfully been produced by using high velocity oxy-fuel (HVOF) combustion spray process as shown in Figure 2 [Petrovicova, 2000].

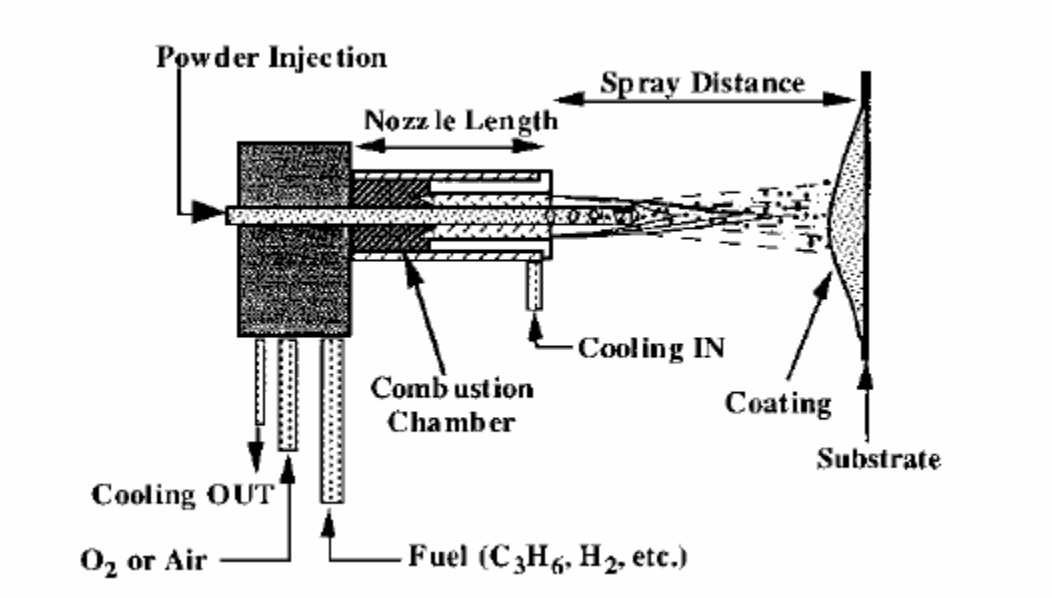

Figure 2: Schematic of the HVOF Process [Petrovicova, 2000]

Hong and coworkers also reported that nano-ZnO and low-density PE were melt-compound in a high-shear mixer to prepare nanocomposites with an increase in the resistance to thermal degradation [Hong, 2002]. In Bhimaraj, a nanocomposite was synthesized by melt mixing polyethylene terephthalate (PET) with nanoalumina under an inert atmosphere in a batch melt mixer and wear resistance of PET increases nearly twice with the addition of 2 wt% 38 nm alumina particles [Bhimaraj, 2005]. In addition, PP/nanosilica [Rong, 2001B], Nylon 6/nanosilica [Garcia, 2004] composites were reported to be processed in a twin-screw extruder.

Although being successful in many cases, melt mixing method has several drawbacks. First, this process only builds up relatively weak interaction force between the polymer and the nanopowder. Nanopowders have a very strong tendency to aggregate and the dispersion was successfully achieved only after modification of the surface of inorganic nanopowders [Petrovicova, 2000; Hong, 2002; Bhimaraj, 2005; Rong, 2001B; Garcia, 2004]. Second, for some polymers, this processing method may be limited due to rapid increase of the viscosity with the addition of a few volume fractions of nanopowders.

Some of the limitations of melt mixing can be overcome if both the polymer and the nanoparticles are dissolved or dispersed in solution. This allows modification of the particle surface without drying, which reduces particle agglomeration [Carotenuto, 1996]. After dispersion, the polymer nanoparticle solution can then be casted into a solid, or be isolated from solution by solvent evaporation or precipitation. Further processing can be done by conventional techniques.

2.1.2.3.2 Sol-Gel Processing

The sol-gel processing of the nanopowders inside the polymer dissolved in non-aqueous or aqueous solution as generally described in Figure 3 [Brinker, 1990] is the ideal procedure for the formation of interpenetrating networks between inorganic and organic moieties at the milder temperature in improving good compatibility and building strong interfacial interaction between two phases. This process has been used successfully to prepare nanocomposites with silica, alumina, calcium oxide, titania in a range of polymer matrices.

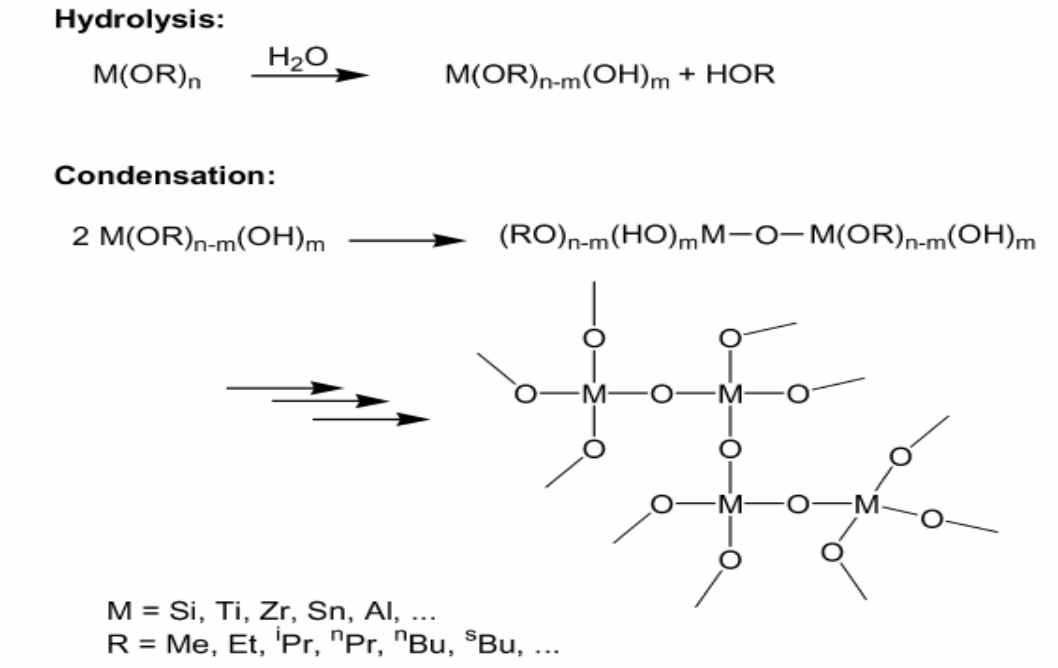

Figure 3: Sol-gel Process [Brinker, 1990]

Several strategies for the sol-gel process are applied for formation of the hybrid materials. One method involves the polymerization of organic functional groups from a preformed sol–gel network; vinyl [Hsiue, 2000A] or epoxy groups [Crivello, 2001] and free-radical or cationic polymerization processes are common. Hsiue showed an example of the process for PS/silica nanocomposites. Miscibility of the PS-silica copolymers was enhanced via incorporating PS matrix with silica covalently. During drying, the polymer blocked phase-separate and the silica region coalesce [Hsiue, 2000A].

Alternatively, the sol–gel hydrolysis and condensation of a precursor such as tetraethyloxysilane (TEOS), tetrabutyl titanate, aluminum iso-propoxide are carried out starting from a preformed functional organic polymer such as polyvinyl acetate [Fitzgerald, 1992], polymethylmethacrylate [Silveira, 1995], polyetherimide [Nunes, 1999], polyvinyl alcohol [Suzuki, 1990;], polyamides [Sengupta, 2005], polyimide [Hsiue, 2000B] and several other polymers [Mauritz, 1989; Stefanithis, 1990]. For example, a recent report on the nonaqueous sol-gel process by polycondensation of phenyltriethoxysilane mixing with PI in a polyamic acid solution resulted in excellent dispersion of nanoscale silica in PI. Comparatively, mechanical mixing of SiO_2 to the PI melt led to serious aggregation.

A combination of the above two methods has been used to synthesize polydimethylsiloxane (PDMS)/silica nanocomposites. The unfilled PDMS network was first formed with the stoichiometric amount of TEOS as an end-linking agent. Next the network was swollen with additional TEOS which was suspended in excess water containing the catalyst such as an acid or base and the sol-gel reaction was catalyzed [McCarthy, 1998]. Significant study on determining the parameters to affect particle size has been accomplished with this method [Breiner, 1999].

Finally, the two distinct polymerization processes can be carried out simultaneously, although in this case coupling or compatibilization of the two main components, and thus formation of a true hybrid, can be an elusive task. For example, PS/silica nanocomposites were found with the simultaneous polymerization of styrene and tetraethyl orthosilicate,

which resulted in a continuous interpenetrating network of silica and PS [Wei, 1992]. So, the sol- gel process is a rich chemistry which has been reviewed elsewhere on the processing of materials from glass to polymers [Garcia, 2004; Gomez-Romero, 2001].

2.1.2.3.3 Graft Polymerization

Another method for avoiding phase-separate is graft polymerization, where nanopowders are dispersed in the monomer or monomer solution, and the resulting mixture is polymerized by standard polymerization methods. This process provides flexibility in our ability to engineer the powder surface being placed in composites. Besides tailoring specific properties in composites via relatively strong interaction, the layer of polymer bonded to the nanopowders can control aggregation of the nanopowders.

Generally speaking, there are two approaches (Figure 4) for graft polymerization in the literature [Kickelbick, 2003]. One approach is “grafting to”, also termed "tethering", which consists of immobilization of polymerizable groups on the nanopowder surface for copolymerization. The other is “grafting from” approach, also known as surface-initiated polymerization, which involves grafting an initiator onto the nanopowder surface to form polymer chains from the surface.

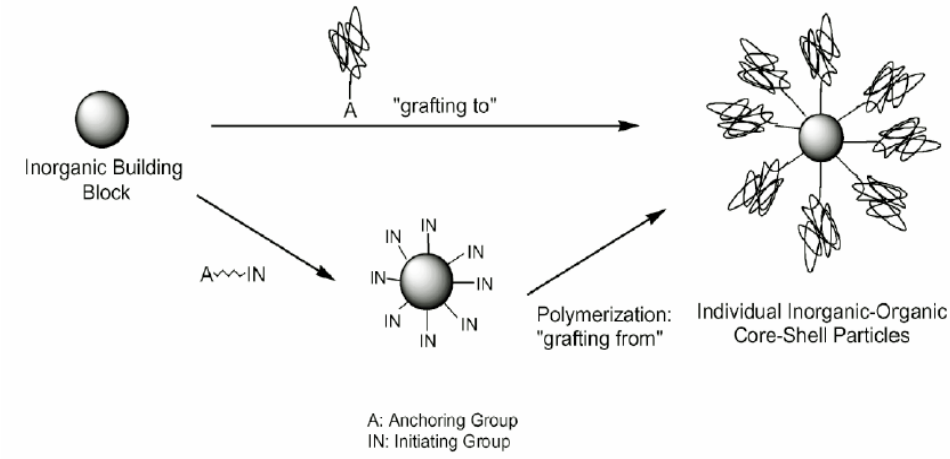

Figure 4: Two approaches of graft polymerization [Kickelbick, 2003]

2.1.2.3.3.1 Grafting to Approach

Mostly, grafting to approach (Figure 5) has been conducted via two routes: i) monomers are copolymerized from the active compounds covalently attached to the inorganic particle surface. Surfactants such as silane coupling agents, polyhedral oligomeric silsesquioxanes (POSS) and $R_8Si_8O_{12}$ nanoclusters are used for modification of the particle surface to introduce polymerizable groups. ii) ready made polymers with reactive ends react with the functional groups of different monomers pre-grafting into the nanopowder surface through physical treatment such as irradiation [Kickelbick, 2003].

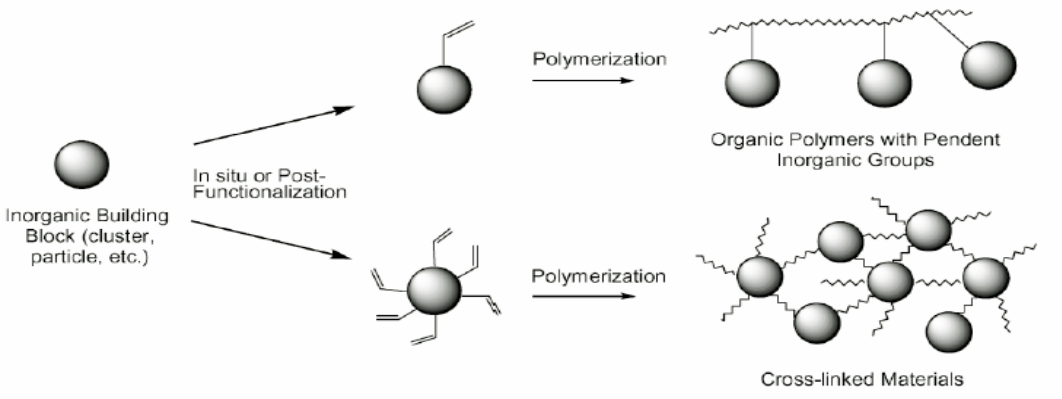

Figure 5: Graft to approach [Kickelbick, 2003]

Rong et al. reported a new polymer nanocomposite with excellent tribological properties by the process (Figure 6) that graft polymerization of PS and PAAM onto nanosized alumina particles was accomplished through free-radical polymerization at the double bonds of the particle surfaces. The double bonds were pre-introduced by a silane coupling agent modification of the alumina. At the initial reaction, grafting of PAAM and growth of the grafted PAAM was predominant. Prolonged reaction time helped to promote the grafting reaction of PS, but reduced the percentage of grafting and the grafting efficiency of PAAM. In addition, homopolymerization of PAAM became significant with a lapse of time. High concentration of monomers was favorable to grafting polymerization due to diffusion blocking and molecular weight and the density of the grafted macromolecules

could be controlled by the way of monomer feeding. Strong interaction between the grafted polymers and alumina was observed [Rong, 2002].

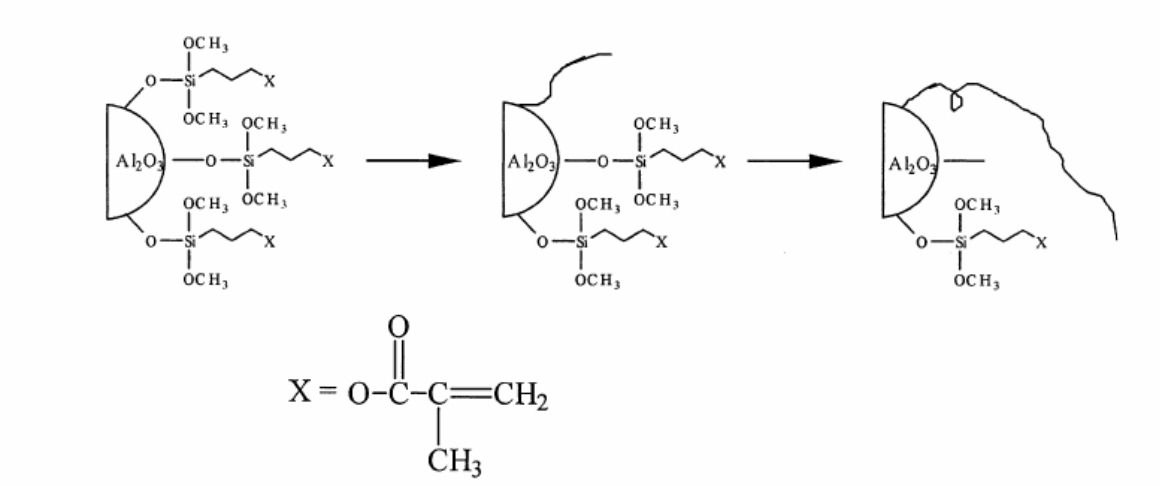

Figure 6: Graft polymerization of PS and PAAM onto nanoalumina [Rong, 2002]

In some case, the polymer is not directly grafted onto but interacts strongly with the surface via hydrogen bonding. For example, carboxylic acids are intensively adsorbed to alumina. If the acid contains a polymerizable group such as maleic acid, the polymer can be grown the molecule attached to the surface after adsorption. Mao et al. showed that maleic acid adsorbed on alumina and was used to copolymerize with 1-alkenes to form monolayers of polymer that were tightly anchored on the alumina surface [Mao, 1998].

One previous work done by Rong represented another route of grafting to approach which was used to place nanopowders (in this case fumed silica) into a monomer such as styrene or MMA. The mixture was then irradiated by ^{60}Co γ-ray under atomsphere. The monomer penetrated into the silica aggregates, and after grafting, the surfaces became hydrophobic and blended easily with polymers such as polypropylene. This treatment result in more uniform distribution of the powder and greatly enhanced interfacial interaction [Rong, 2001A].

Although being less complex than the grafting from approach, the grafting to approach has not widely been used in the literature. This can be explained by that the grafting to

approach is hampered by steric constraints and kinetic factors. Slowing diffusion of additional long chains through the existing polymer film prevents reaching the high grafting density. Moreover, space constraints around these potential reactive sites further limit the grafting density. This barrier becomes even greater as the layer thickness increases, and the process becomes self-limiting [Edmondson, 2004].

2.1.2.3.3.2 Grafting from Approach

The grafting from approach has attracted considerable attention in the preparation of grafting polymers on a nanopowder surface. In the first step, the particle is modified with initiator-bearing self-assembled monolayers. These monolayers can be formed on almost any surface, as long as the anchor functionality is chosen right. Next, the nanopowder surfaces with grafted initiator are exposed to solutions containing catalyst and monomer (plus solvent if necessary). This polymerization is surface-initiated and surface-confined.

To achieve most appropriate polymer grafting density, polydispersity, composition and microstructure, the polymerization has to be precisely controlled [Edmondson, 2004]. In the last decades, this field has rapidly developed and many controlled polymerization strategies have been used. This subsection overview some examples of controlled surface initiated polymerizations commonly used.

Living anionic surface-initiated polymerization (LASIP)

Anionic polymerization is an attractive choice for making well-defined architectures of polymers. It has also been employed to graft polymers from various small particles such as silica [Zhou, 2002], graphite and carbon black [Tsubokawa, 1991] and also flat surface [Zhou, 2001]. Zhou and coworkers used anionic polymerization to form polystyrene grafted from silica nanoparticle surfaces. They utilized 1,1-diphenylethylene (DPE) with a chlorosilane end group as an initiator precursor attached to silica nanoparticles. After being activated with excess *n*-BuLi, each DPE group initiated growth of one polystyrene chain. A small amount of tetrahydrofuran (THF) was used to reduce the aggregates of *n*-BuLi to speed up the reaction of *n*-BuLi with DPE. High polymer density with a low

polydispersity and covalent bonding between interfacial phases were observed on nanosilica surfaces [Zhou, 2002].

Living cationic surface-initiated polymerization (LCSIP)

Cationic polymerization has little been applied to the grafting of polymer on nanoparticles. Brittain and Zhao investigated the synthesis of grafting polystyrene (PS) from silicate substrates via *LCSIP* [Zhao, 2000]. The cumyl methyl ether moieties were immobilized on particle surfaces. Activation with $TiCl_4$ in the presence of styrene and a proton scavenger (di-*tert*-butylpyridine) leads to the growth of brushes up to 30 nm thick in under an hour. Even with the addition of proton scavenger, initiation by protons leads to the formation of polystyrene in solution. The polymerization was shown to be living by re-initiation of the polymer chains to grow further polystyrene. Recently, tethered poly(*N*-propionylethylenimine) on gold surfaces was synthesized [Jordan, 2001].

Living free radical surface-initiated polymerization (LFRSIP)

Controlled radical polymerizations including atom transfer radical polymerization (ATRP), reverse ATRP, nitroxide -mediated and iniferter radical polymerizations have been extensively used to synthesize tethered polymer on particle surfaces in achieving a better control of molecular weight and weight distribution. The kinetics and mechanism of LFRSIP were investigated by Prucker and Ruhe [Prucher, 1998]. They found that polymerization mechanism on surface was much different from that of in solution, especially the termination step. In solution, the rate of termination decreased with increasing graft density of the attached chains due to diffusion and the molecular weight of the newly growing chains became a function of the number of already attached chains. However, on the surface, transfer reactions to solvent, monomer or transfer agent could lead to termination of the growth of the surface-attached chains and the film growth was completely stopped.

Atom transfer radical surface-initiated polymerization (ATRSIP)

Of these *LFRSIP methods*, ATRSIP has become the most popular route, mostly due to its tolerance to a wide range of functional monomers and less stringent experimental

conditions. Wene et al. yielded a nanocomposite with a nanosilica core and an outer layer of covalently attached, well-defined PS chains via this technique [Weme, 1999]. The surface ATRSIP initiator, (2-(4-chloromethylphenyl)ethyl) dimethylethoxysilane (CDES), was deposited on the surface of the nanoparticles using a neat siloxane mixture in order to minimize the solvolysis of CDES by ethanol. This group also found that polymerization of various hydrophilic methacrylates at the surface of nanosilica preceded efficiently via aqueous ATRSIP even at room temperature [Perruchot, 2001]. Sedjo and coworkers developed this idea to prepare PS-block-PMMA diblock copolymers on nanosilica [Sedjo, 2000].

Other surface-initiated polymerization methods

Living ring opening polymerization (LROP), ring-opening metathesis polymerization (ROMP), group transfer polymerization (GTP), hyper-branched polymerization and other polymerization methods have also been employed in the synthesis of tethered polymer on the nanoparticle surfaces. Chang and Frank [Chang, 1998] reported a novel dry process for surface deposition-polymerization of vapor phase α-amino acid *N*-carboxy anhydride from a surface immobilized initiator layer. The silicon surface was modified with the coupling agent, (3-aminopropyl) triethoxysilane, in which the primary amine was a good initiator for LROP of γ-benzyl-L-glutamate *N*-carboxy anhydride. A film with thickness of 40 nm was obtained by this method. Herrman and coworkers [Herrmann, 1996] immobilized a tris(neopentyl)nitridomolybdenum metathesis catalyst onto silica and performed ROMP of norbornene.

2.2 Nanopowders: Properties

As mentioned earlier, nanopowders are the three dimensional relatively uni-axial nanosized objects at a level intermediate between atom/molecule and bulk. Although nanopowders involving metals (Au, Pt, Pd, Cu, etc.), semiconductors (ZnS, CdS, CdSe, etc.), metal oxides (SiO_2, Al_2O_3, TiO_2, ZrO_2, Fe_2O_3, etc.) are everywhere in nature, they grow into micro-powders or macroscopic materials instantaneously and then lose their specific features. Therefore, how to produce a nanopowder with controlled size and

degree of aggregation is a key issue which attracts many efforts. Recently, significant progress in the diversity of preparative methods has been made. Good reviews in this area have been presented elsewhere in the literature, which involve gas-phase synthesis of nanopowders (flame hydrolysis, gas condensation, chemical vapor condensation, pyrolysis, laser ablation, etc.) given by Kammler et al [Kammler, 2001], Kruis et al. [Kruis,1998], Hahn [Hahn, 1997], and Swihart [Swihart, 2003]; liquid-phase synthesis (co-precipitation, sol-gel processing, micro-emulsion, hydrothermal and solvothermal processing, templated synthesis, etc.) by Grieve et al. [Grieve, 2000], Trindade et al. [Trindade, 2001], Murray et al. [Murray, 2000], and Cushing et al. [Cushing,2004].

The primary driver for this growing synthetic interest is the effect of powder size on properties. For example, the optical absorption spectrum of gold (Au) changes with the size of the Au nanoparticles. The electroluminescene of semiconductors is also size-dependent. Generally, nanopowders do not exhibit classical bulk properties, while on the other hand they also differ from the molecules or atoms that in some way represent pieces of matter related to the bulk material they originate from. In this section we discuss some typical physicochemical characteristics of nanopowders, with emphasis on size-dependent phenomena.

2.2.1 High Surface-to-Volume (S/V) Ratio

The size and surface characteristics of nanopowders are interrelated. Suppose a spherical particle, it is obvious that the surface-to-volume ratio is inversely proportional to its radius, R, S/V =3/R. Likewise, for another 3D particle, the *S*/*V* ratio also increases as the size decreases. Assuming that the thickness per shell is 6 Å, Burda et al. calculated the S/V ratio as shown in Figure 7: S/V ratio as a function of the particle size [Burda, 2005] [Burda, 2005]. As a powder size shrinks to between tens of nanometers and about a nanometer, it will possess increasing and significantly high surface areas and a large fraction of these atoms will be exposed on the surface. In addition, the surface atoms are chemically more active compared to the bulk atoms because they usually have fewer adjacent coordinate atoms and unsaturated sites or more dangling bonds. Consequently,

the surface characteristics of nanopowders play a key role in their fundamental properties, from phase transformation via light emission to reactivity.

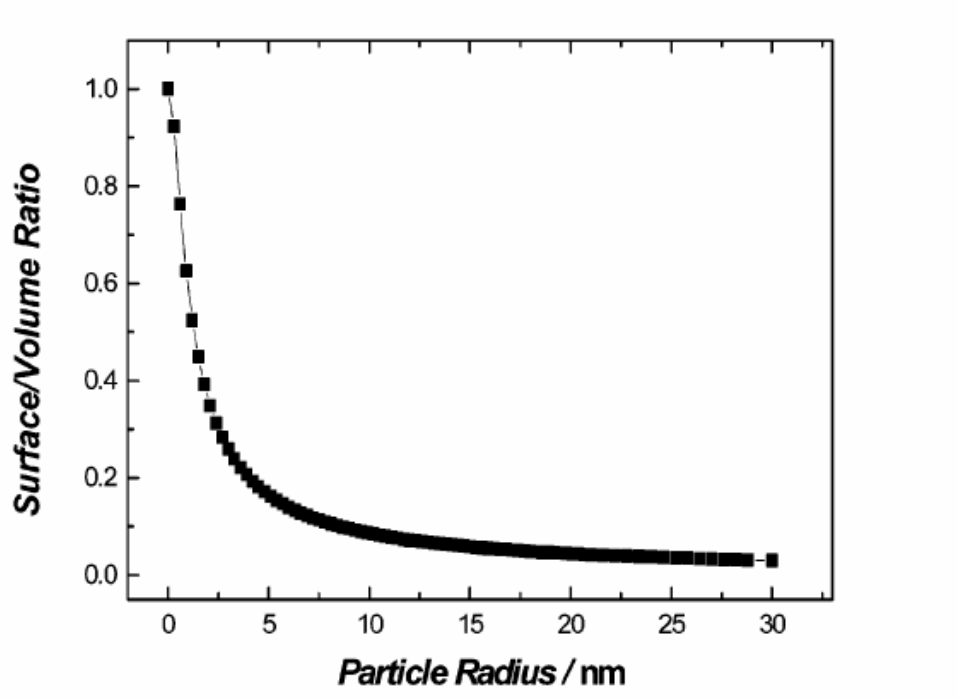

Figure 7: S/V ratio as a function of the particle size [Burda, 2005]

2.2.2 Depressed Melting Temperature (T_m)

Melting is one important type of phase transformations widely studied in thermodynamics. In quite a large quantity of materials ranging from metals to semiconductors to insulators, a decrease in T_m has been observed with decreasing nanopowder size [Coombes, 1972; Buffat, 1976; Beck, 1991; Martin, 1994; Goldstein, 1992]. A sample of the magnitude of the effect was presented in Figure 8 for experiments performed on CdS nanopowders. Melting point depressions of over 50% were observed for sufficiently small sized nanopowders [Goldstein, 1992]. This depression can be explained by considering the fact that a large energy is associated with the surface due to coordinatively unsaturated surface atoms and the surface energy is always lower in the liquid phase compared to the solid phase. By melting, the total surface energy is reduced, thus stabilizing the liquid phase over the solid. The smaller the

nanopowder, the larger the contribution made by the surface energy to the overall energy of the system and thus the more dramatic the T_m depression [Ercolessi, 1991].

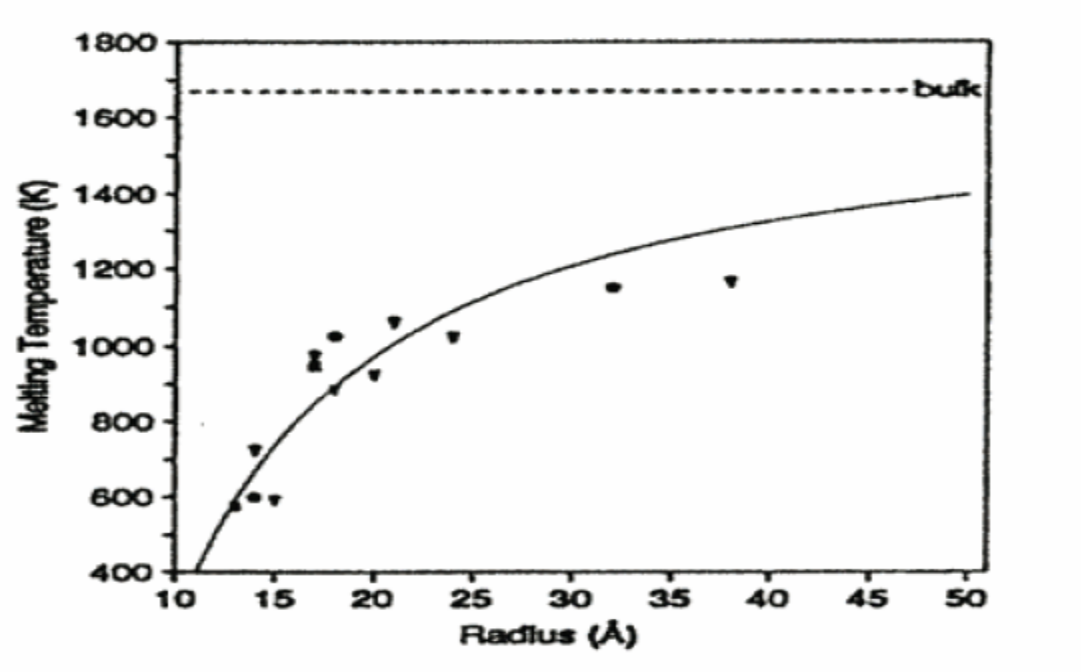

Figure 8: Melting temperature vs size for CdS nanopowder [Goldstein, 1992]

2.2.3 Discrete Electronic Structure

For small powders, the electronic energy levels are not continuous as in bulk materials but are discrete, due to the confinement of the electron wavefunction because of the physical dimensions of the powders. As a result, electronic, magnetic, optical properties of a nanopowder become size dependent. In electric conductivity, an important gain result from wide investigations of metallic nanopowders of various sizes by photoelectron spectroscopic measurement is that as the metal particle size decreases, the core-level bonding energy of metals such as Ag, Hg, Au, Ni, Cu increases dramatically [Johnson, 1985; Volokitin, 1996; Vijayakrishnan, 1992]. This increase is a manifestation of the size induced conductive-nonconductive transition phenomena in nano-metals.

Rademann et al. showed that Hg, the same element, behaves as either a metal or a non-metal, depending on its particle size [Rademann, 1992].

Among several techniques of investigating size-dependent optical properties, optical absorption spectra generally exhibit peak at the threshold which is assigned to the creation of the excitons. The position and shape strongly dependent on the particle size have been observed in many nanopowder systems. Figure 9 shows the absorption spectra for a series of CdSe nanoparticles of different sizes. In addition, it shows how the first absorption peak changes as the nanoparticle size changes for CdSe, CdS, CdTe [Qu, 2001; Yu, 2003].

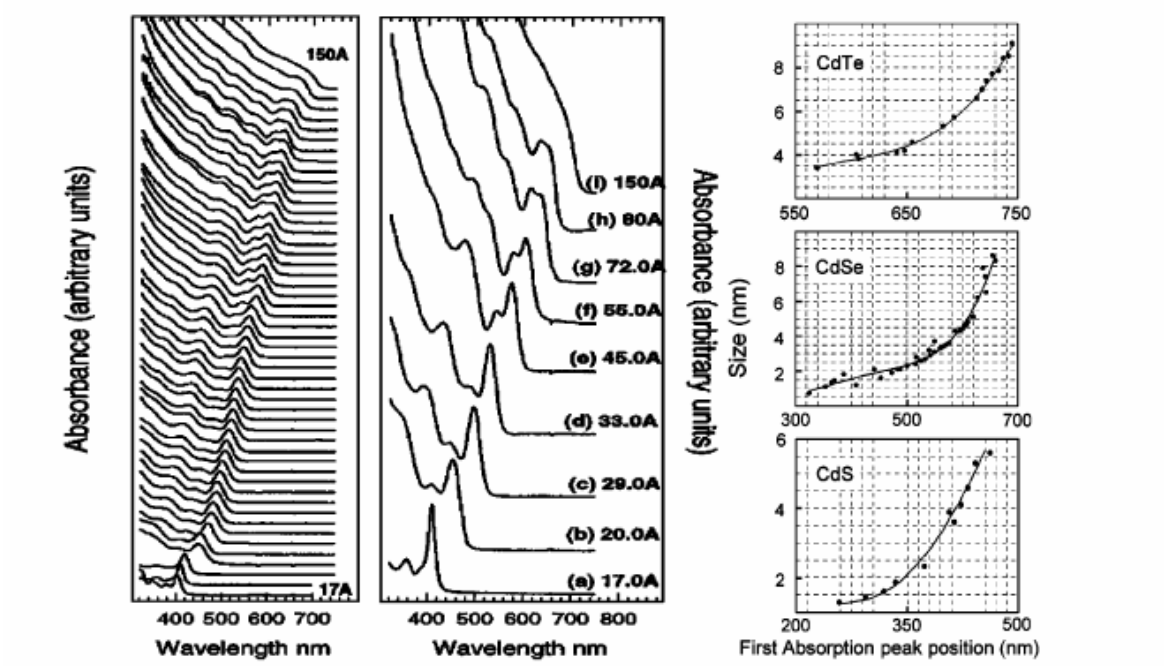

Figure 9 (Left, middle) Observation of discrete electronic transitions in optical absorption for a series of sizes of nano-CdSe (Right) First absorption peak change versus the size of the nanopowders [Yu, 2003].

Magnetic properties of nanopowders of transition metals such as Ni, Co and metal oxides such as Fe_2O_3 also show remarkable changes with size. We know that in the nanometric domain, the coercivity (H_c) of the particles tends to zero. Hence, the nanopowder behaves as superparamagnets with no associated H_c. The blocking temperature that marks the

onset of this superparamagnetism also rises with the nanopowder size. Moreover, the magnetic moment per atom is seen to increase with the decreasing size of a powder [Schmid, 2004]

2.2.4 High Reactivity

Due to a large fraction of surface atoms and a higher surface area, a nanopowder would be expected to be more active. Furthermore, the qualitative change in the electronic structure arising due to quantum confinement in tiny nanopowders also bestow unusual catalytic properties on these powders, totally different from those of the bulk. The ability of supported or non-supported metal nanopowders such as Ni, Cu, Pt, Au, Pd as catalysts and metal oxides such as SiO_2, TiO_2 and Al_2O_3 as catalyst supports has been investigated. We will give a few examples to show these important aspects. Rao et al revealed that the significant dependence of the reaction of elemental O_2 with Ag was on the particle size of Ag. The smaller Ag powders were more capable to dissociate O_2 molecules to atomic oxygen O, unlike oxygen ion predominantly adsorbed on the bulk Ag. They also reported that unlike bulk Ni, small nanopowders exhibit less dependence in their catalytic activity on ambient temperature as they interacted with H_2S and different sizes of nanopowders show different temperature profiles [Rao, 1992]. This conclusion was similar to that found supports from an earlier study on chemisorption of Cl_2 on Ag, Cu [Baetzold, 1981], on Pt [Baetzold, 1982] and of CO on Pd [Grunze, 1978], on Pt [Heiz, 1999].

One study of Valden et al. showed another significant example that Au nanopowders supported on a TiO_2 surface have a marked size effect on their catalytic ability for CO oxidation reaction, with Au nanopowders in the range of 3.5nm exhibiting the maximum chemical reactivity. Although bulk Au is well-known noble metal, a metal-to-nanometal transition was observed in the I-V spectra as the Au size is decreased to below 3.5 nm [Valden, 1998]. Similar results were obtained with Au particles on a ZnO_2 surface and Pd nanopowders supported on oxide substrate [Xu, 1997].

2.3 Titanium-dioxide

2.3.1 General Remarks

Titanium dioxide adopts at least 8 structures. Besides its four polymorphs found in nature (i.e. rutile, anatase, brookite, TiO_2 (B)), additional high-pressure forms have been synthesized: TiO_2 (II) with the α-PbO_2 structure, TiO_2 (H) with hollandite, baddelleyite with ZrO_2, Cotunnite with $PdCl_2$ [Banfield, 2001]. Among them, rutile, anatase are mostly manufactured in chemical industry as microcrystalline materials. The two polymorphs are based on interconnected TiO_6 octahedra, but their linkages and degree of edge and face sharing differ. Anatase can be regarded to be built-up from octahedrals that are connected by their vertices; in rutile, the edges are connected.

Thermodynamic calculations show that rutile is the most stable phase at all temperatures and pressures below 60 kbar, when TiO_2 (II) becomes the favorable phase [Banfield, 2001]. Reverse phase stability is described by particle size experiments due to size effect on surface energy. Anatase is most stable at sizes less than 11 nm, brookite at sizes between 11-35 nm, rutile at sizes greater than 35 nm [Zhang, 2000].

Basically, the enthalpy of phase transformation between anatase and rutile is low. The synthesis methods of TiO_2 as well as the monotropic anatase $\leftrightarrow$ rutile conversion have been of a wide interest for the application-driven reason, that is, the anatase or rutile phase of TiO_2 is one of the most critical parameters determining its uses. Generally, TiO_2 may be manufactured by either the sulfate or the chlorine process [Solomon, 1983]. The decision of choosing one process instead of the other is based by considering such factors as raw material availability, freight, and waste disposal costs. The sulfate process is relative simpler and TiO_2 modifications and titanium chemicals can be made from one process; on the other hand, the chlorine process is less environmentally invasive and yields higher pure TiO_2.

TiO_2 has received a great amount of applications due to its strong oxidizing power of the photogenerated holes, chemical inertness, non-toxicity, low cost, high refractive index

and other advantageous surface properties. In this section, we begin with a brief discussion of applications of TiO_2 and then dwelt on actual surface science results of TiO_2.

2.3.2 Applications of TiO_2

Titanium dioxide was first industrially introduced to replace toxic lead oxides as a white paint pigment in 1900's. Nowadays, the annual world consumption of TiO_2 exceeds 4.4 million tons [Adams, 2005]. It is used in as a white pigment in paints, plastics, paper and cosmetic products which represent the major end-use sectors of TiO_2. The consumption of TiO_2 increased in the last few years in a number of minor end-use sectors such as a photocatalyst, as a catalyst support or promoter, as gas sensor, as in electric and electrochromic devices, and so on.

2.3.2.1 White Pigment

TiO_2 has recently become a main white pigment source of light scattering as a consequence of its highest refractive index of colorless, stablility and its relatively low and uniform absorption of visible light. Half of all TiO_2 pigment produced is consumed in decorative and architectural paints widely serving to house buildings, wood or furniture, industrial coating, and automobile finishes. TiO_2 is non-toxic, safe, and corrosion-protective and can be dispersed easily as well as absorbs incident UV and protects the paint from direct photochemical degradation of organic binder, making it ideally suited for the paint industry [Preuss, 1974].

Due to its excellent optical transmittance in the visible and near-infrared region, high dielectric constant, TiO_2 pigment is used extensively in thin-film optical devices including antireflective coatings, dielectric mirrors for lasers, metal mirrors with enhanced reflection, and filters. Such coatings are based on the interference effects between light reflected from both the upper and lower interface of a thin film. The relative ratios between transmission and reflection of light are governed by the index of refraction of the thin film and the surrounding media. By depositing a stack of layers with

the appropriate optical index, the refraction/transmission properties of a stack of thin layers on a glass substrate can be designed to meet the aforementioned applications [Selhofer, 1999]

TiO_2 is also added to opacify the plastic materials and improve photodurability. The requirements for TiO_2 are good dispersibility in polymer system, blue undertone, and good heat stability. In the paper industry, TiO_2 is use in conjunction with clay, $CaCO_3$, and other pigments to impart brightness and opacity. Its levels are adjusted, depending on the quality of the paper pulp, to meet the performance and cost goals [Braun, 1992]. For white hiding, TiO_2 is the right pigment of choice for ink production. The type of TiO_2 can affect the ink rheology, abrasiveness, gloss, redispersibility. Additional ink applications with TiO_2 include inks for wood molding, marking pens, decorative sheets. Ink correction fluid for paper depends on TiO_2 to hide errors. Inks for concealed writing such as scratch-off lottery tickets likewise use TiO_2 because of the superior hiding power. Even the marking on gelatine capsule can contain TiO_2 [Bissett, 1979]. In addition, pure TiO_2 is highly effective as a new sun screener, applied to many cosmetic products [Hewitt, 1999]; as an anticorrosive additive, applied to food industry [Phillips, 1997].

2.3.2.2 Photocatalysis

TiO_2 photocatalysis has its origins in early research effort into photoelectrochemical systems for solar to chemical energy conversion. A major landmark in the study of Fujishima and Honda in 1972 found that TiO_2 could be used as catalytic electrode in photoelectrolysis cell to decompose water into H_2 and O_2, without the application of an external voltage [Fujishima, 1972]. After a few years it was realized that this Fujishima-Honda micro-cells, consisting TiO_2 particles with deposit of Pt on them, was also able to work as photocatalysis for splitting H_2O.

Since then, much active attention was given to the use of TiO_2 for photo-assisted degradation of organic compounds and reduction of inorganic compounds. As a semiconductor oxide, a wide-band gap TiO_2 is easy to be irradiated by sunlight (especially UV light) to create the excited electron–hole pairs which could separate and

the resulting charge carriers might migrate to the surface where they react with adsorbed water and oxygen to produce radical species. These radicals attack any adsorbed organic or even micro-organic molecules, resulting in complete or selective decomposition; or transform inorganic molecules into their oxidized and/or reduced states. Such a number of research efforts in photocatalysis have emerged that offer potential for commercial applications. Of particular promises are the following subjects:

i) Selective organic synthesis, for example, the selectivity of the epoxidation of 1-decene is improved by using rutile [Ohno, 2001]; selective oxidation of alcohol catalyzed by light-activated TiO_2 yields very high carbonyl compounds such as ketones ad aldehydes [Pillai, 2002].

ii) Non-selective destruction of organic and inorganic waste materials under normal temperature and pressure, such as wastewater purification [Mills, 1993], pollutant air cleaning [Peral, 1992], indoor or car odor removal [Kim, 2002].

iii) Photokilling of pathogenic organisms (viruses, bacteria, algae, protozoa and cancer cells), for instance, desinfection in operating rooms in hospitals [Maness, 1999] or anti-tumoral activity in the experiment of subcutaneous injection of a TiO_2 in rats under near-UV illumination [Cai, 1991].

iv) Use of self-cleaning or antifogging materials, ranging from self-cleaning facades (e.g. the preservation of ancient marble Greek status against environmental damage [Poulios, 1999]) to antifogging films on car windshields [Paz, 1995].

2.3.2.3 Catalyst Support or Promoter

The importance of TiO_2 in heterogeneous catalysis is also profound and the performances of many metals or metal oxides on high-surface-area TiO_2 support have been studied. These metal oxide/TiO_2 systems often serve as a model for other metal/oxide surfaces. It is well known that the role of TiO_2 on catalytic activity is more complex than simple to increase catalyst surface area and interactions between the catalyst and TiO_2 may occur that lead to changes in reactivity and selectivity [Martin, 1991]. One famous example of these systems is that V_2O_5 supported on TiO_2 is superior catalyst to unsupported V_2O_5

used for partial oxidation reaction of many hydrocarbons or selective catalytic reduction of nitric oxides [Satterfield, 1991]. The mechanism by which TiO_2 modifies the properties of the supported V_2O_5 was the subject of numerous investigations by several research groups [Zhang, 1992; Sambi, 1996; Biener, 1999; Guo, 1999].

Although TiO_2 is not suitable as a structural support material for metals compared with Al_2O_3 and SiO_2, small additions of TiO_2 can modify metal-based catalysts to a significant extent. Encapsulation of the metal particles by a reduced TiO_x overlayer may lead to the so-called strong metal-support interaction. This phenomenon was certified by current surface science techniques [Pan, 1993; Pesty, 1995; Bennett, 1999; Dulub, 2000]. Many metals such as Fe, Ag, Pt, Ru, Rh, Pd and Au loaded TiO_2 catalysts have recently been reported, of which Au/TiO_2 used for CO oxidation at low temperature was the most excited discovery [Boccuzzi, 1996]. Many experiments that may clarify Au/ TiO_2 system are still underway [Valden, 1998; Bondzie, 1999].

2.3.2.4 Gas Sensor

Another successfully existing utilization of TiO_2 is as gas sensor because it may change its electrical conductivity upon gas adsorption like SnO_2 and ZnO semiconductors. So far, TiO_2 is commonly used as an oxygen gas sensor, e.g. to evaluate the combustion process of fuel in car engines for controlling fuel consumption and environmental pollution [Xu, 1993]. Kirner et al. studied that TiO_2-based oxygen sensors had different detection principles when operating in two different temperature regimes. At high temperatures, TiO_2 devices acted as thermodynamically controlled bulk defect sensors, providing oxygen partial pressure measurements over a very large range. The intrinsic behavior of the defects responsible for the sensing mechanism could be controlled by doping with tri- and pentavalent ions. However, at low temperatures, they found that the Pt/TiO_2 Schottky-diodes as oxygen sensors showed reversible current-voltage shift characteristics and changed sensitively upon changes in the oxygen partial pressures [Kirner,1990].

2.3.2.5 Other Applications

TiO_2 is a semiconductor with varistor properties, which presents strong non-linearity between the current density and the electric field, thus being suitable as in electric switching device for transient voltage suppression. Doped TiO_2 ceramics possess non-linearity coefficient (α) values in the range α=3–12, α being defined by the relationship $I=CV^{\alpha,}$ where I is the current, V the voltage, and C the proportionality constant [Pennewiss, 1990].

To overcome the limitation of SiO_2 devices, the TiO_2 potential replacement as well-suited dielectric gate insulator becomes one hot issue currently debated in materials science. This new gate insulator should satisfy very strict demands, e.g. no surface states, virtually pin-hole free, stoichiometric ultrathin films, good interface formation with the Si substrate [Gupta, 2000]. Rutile TiO_2 might be an ideal candidate for this application due to its high dielectric constant and < 2.0 nm thickness. Furthermore, TiO_2 deposited on Si show excellent electric characteristics, but a low resistivity layer, probably SiO_2, forms at the interface [Campbell, 1999].

One interesting finding is that anatase TiO_2 film becomes ferromagnetic at room temperature after doping with a few amount of Co, although TiO_2 itself does not show any magnetic character. In addition to its optical transparency and semi conducting characteristic, such film could be an attractive candidate for spin-based electronic devices [Matsumoto, 2001].

Another novel application of nano-crystalline TiO_2 films is as an electrode in electrochromic devices which control light transmission in windows or light reflection in mirrors and displays. For example, Bonhote et al combined TiO_2 and WO_3 two complementary electrodes based on the color change upon reduction/oxidation cycles induced by an electrical current to elaborate an efficient electrochromic device [Bonhote, 1999].

TiO_2 is an oxide with corrosion resistance and can be applied as an implant biomaterial in human body (e.g., as a bone substitute and reinforcing mechanical support [Sittig, 1999].

2.3.3 Surface of TiO_2

TiO2-x with x=0.0001 to 0.0004 is found in bulk materials. Its surface is a complex and extremely sensitive to thermo chemical history such as temperature, pressure, cooling rate, impurity. Principally the surface contains several atoms, ions and molecules via ionic, covalent or coordinated bonding such as basic terminal and acidic bridged-hydroxyl groups; labile Ti-O-Ti bonds; water molecules adsorbed at Lewis acid sites or bound to surface hydroxyl groups; adsorbed anions such as sulfate or chloride process residues; potential electron donor and acceptor sites; possibly adsorbed oxidants such as hydroxyl or hydroperoxyl radicals; or activated oxygen species generated by photocatalytic processes [Solomon, 1983]. There are also many surface defects on TiO_2 that include step edges, oxygen vacancies, line deficiencies, foreign cations, crystallographic shear planes. In addition, TiO_2 involve several surface planes. The surface of rutile is formed from three crystal planes including the (1 1 0), (0 0 1) and (1 0 0), with (1 1 0) being the most stable one. For anatase, the (1 0 1), (1 0 0) and (0 1 0) surface planes are found in powders, together with some (0 0 1).

Such complex TiO_2 surface plays a vital role in all the aforementioned wide range of applications. Because of this importance, overall insight into its surface characteristics increasingly occupied the center of many research objects and several excellent reviews of different aspects of TiO_2 surfaces were written in the last decade [Henrich, 1994; Diebold, 2003]. Only a selective outline of TiO_2 surface chemistry and modification is given here.

2.3.3.1 Chemistry of TiO_2 Surface

TiO_2 surface is capable of absorbing, dissociating or reacting (oxidizing/reducing) with a wide variety of inorganic and organic molecules and atoms under certain conditions. The most important among them is the H_2O dissociative or nondissociatve adsorption behavior on TiO_2, which determines TiO_2 wetting and dispersing abilities in aqueous or non-aqueous medium and other surface properties.

So far many experimental and theoretical studies on water adsorption on TiO_2 have not yet resulted in unanimous agreements on the details of adsorption. The results drawn from room-temperature adsorption measurements on the "stoichiometric and nearly perfect" TiO_2 surfaces include: i) the surface is completely inert, chemisorbing neither OH ions nor H_2O; ii) H_2O adsorbs only molecularly; iii) H_2O adsorbs only dissociatively, with the saturating monolayer of adsorbed OH ions; iv) H_2O dissociates at low exposure, but for higher exposure molecular H_2O adsorbs in addition to the OH ions.

These scenarios cover two possibilities. One is that different measurements were involved to identify the phenomena and various groups explained different spectra in different ways. Another problem aroused from preparing and selecting the "nearly perfect" investigation surfaces is that TiO_2 has different surface planes in each polymorph and each surface has in reality a different density of step and point defects.

On rutile (1 1 0), most experiments conclude that H_2O does not dissociate on this flat, unperturbed face, but dissociate at defect sites. For example, Brinkley et al. investigated the dynamical adsorption properties of water by a molecular beam scattering. The H_2O molecule was trapped, with enough time to sample the potential energy surface of TiO_2 (1 1 0) before desorption. It was also found that very few of the molecules dissociate, even in the limit of zero coverage [Brinkley, 1998]. This is in agreement with many temperature programmed desorption (TPD) spectroscopy studies. A high-temperature tail in TPD spectra was attributed to recombinative desorption of water that has dissociated at defects, i.e., oxygen vacancies [Henderson, 1996A, B; Hegenschmiolt, 1994]. Most of the photoemission and other spectroscopic experiments are consistent with this idea, although there is some deviation in the details. For example, there is disagreement about the temperature at which water dissociates at point defects [Henderson, 1996B; Kurtz, 1989]. Recent scanning tunneling microscopy (STM) studies also support the earlier experimental results [Brookes, 2001; Schanb, 2001; Suziki, 2001]. In stark contrast to the experimental results on H_2O/rutile (1 1 0), most theoretical calculations predict dissociative adsorption. Intermolecular H bonding was invoked to act as a stabilizing factor for a mixed dissociated/molecular state [Lindan, 1996, 1998]. Other calculations

point out that, while dissociative adsorption on rutile (1 1 0) is thermodynamically favored, it might be hindered by a potential barrier [Ferris, 1998].

For perfect rutile (1 0 0), most experimental and theoretical studies, not all of them [Langel, 2002], indicate that H_2O adsorbs both dissociatively and molecularly, independent of steps, point defects and the Ti^{3+} sites present [Henderson, 1996A; Muryn, 1991; Bourgeois, 1992; Wang,1997B; Fahmi, 1994; Ferris, 1998; Nalewajski,1993]. Adsorption/desorption occurs reversibly, i.e., molecular water is the only desorption product, and the surface generally does not become oxidized. It has been reported that very high doses of water vapor or exposures to liquid water [Wang, 1997B] causes oxidation of defects, but these results have not been reproduced in other studies [Wang, 1997A , 1999].

The adsorption behavior of thicker H_2O layers on rutile surfaces was also widely investigated. On rutile (1 1 0), a distinct second layer peak at 180 K is observed in TPD. This was interpreted as a 'bilayer' structure, where the second water layer lays flat [Hugenschmidt, 1994] and, based on additional high resolution electron energy loss spectroscopy (HREELS) measurements, it was concluded that water in this second layer interacts only with the bridging oxygen atoms [Henderson, 1996B]. Water multilayers on rutile (1 0 0) followed a zeroth-order desorption behavior. This is in contrast to multilayers on TiO_2 (1 1 0), where deviations from this desorption behavior were found [Henderson, 1994; 1996A, B].

The adsorption of water on anatase surfaces has so far been mostly studied theoretically. On the basis of DFT and first-principles molecular dynamics calculations, Selloni et al. [Vittadini, 1998] concluded that water adsorbs molecularly on anatase (1 0 1). A TPD/X-ray photoelectron spectroscopy (XPS) study by Herman et al. confirmed this prediction [Herman, 2003]. Calculations of water adsorption on the anatase (0 0 1) surface [Vittadini, 1998; Fahmi, 1994] predict dissociative adsorption but have not yet to be confirmed by measurements.

Improving the surface wetting ability of TiO_2 is useful in many photochemical applications such as antifogging and self-cleaning coatings. Wang et al reported that water dissociation at surface defects may affect this wetting ability. Dried TiO_2 surfaces are oleophilic and hydrophobic and water droplets do not wet before ultraviolet irradiation (Figure 10-a). After irradiation, TiO_2 surfaces become amphiphilic and water droplet speed out on the film (Figure 10-b). This change in wetting ability was clearer when a TiO_2-coated glass was exposed to water vapor. Without ultraviolet irradiation the glass fogged (Figure 10-c) but on irradiation the glass became transparent (Figure 10-d). The reconversion of hydrophilic to hydrophobic surfaces was also obtained upon storage in the dark due to the replacement of the adsorbed hydroxyl groups by oxygen. The surface stays oleophilic at all times. Based on ultra high vacuum (UHV) studies, this is attributed to the creation of surface vacancies that dissociate water and form microscopic hydrophilic domains [Wang, 1997A, 1999A].

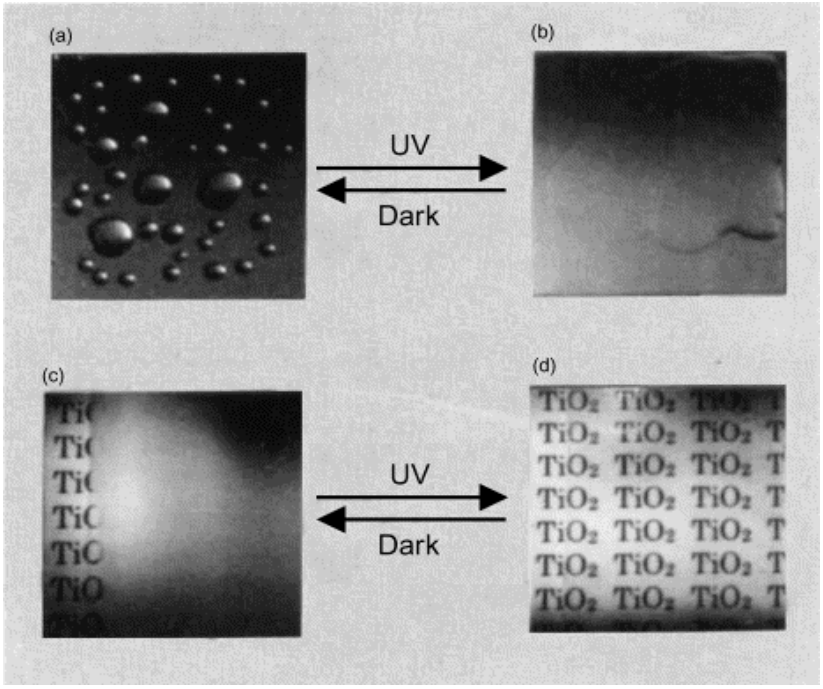

Figure 10: Photographs from a TiO_2 (1 1 0) [Wang, 1997A]

2.3.3.2 Modification of TiO_2 Surface

The photoactivity of titanias is generally detrimental for their application as pigments or fillers into polymers that oxidatively degrade, leading to embrittlement and chalking when exposed to sunlight or UV irradiation, especially in presence of moisture. Hence some form of modification is implemented in order to reduce the surface photoactivity, to alter their hydrophobic/hydrophilic character and improve their dispersibility in various media, to introduce new functional groups which can react with organic molecules and enhance their compatibility with organic polymers.

There have been many patents and papers issued for TiO_2 modifying methods, which can be divided into four groups for the purpose of discussion. i) Modification by chemisorption of small molecules in which coordination, hydrogen bond formation, or proton transfer occurs. ii) Modification by coupling agents involving covalent bond formation between the adsorbed species and hydroxyl reactive groups present on TiO_2 surface. iii) Modification by the adsorption of polymers. iv) Modification by the grafting of polymers or monomers on TiO_2 surface, which is the similar method already discussed in Section 2.1.2.3.3. The scope of this section is limited to a brief summary of the first three modifying methods.

2.3.3.2.1 Modification by Chemisorption of Small Molecules

Although most small molecules can be attracted to TiO_2 surface by van der Waals forces, these forces are so weak that small molecules may not be effectively adsorbed, unless the molecule contain functional groups that can react with TiO_2 surface, resulting in chemisorption. The chemisorption processes discussed in this subsection include hydrogen bond formation, proton transfer, and coordination. The absorbed species are organic acids, bases, salts and neutral compounds.

The most commonly used acids are C_{10} to C_{18} carboxylic acids. The hydrated titania surfaces are amphoteric and are expected to form surface carboxylates. These treatments can be used to impart hydrophobicity and to reduce rheological yield stress of TiO_2 in

paraffin oil, a medium frequently for nonpolar polymers [Plueddemann, 1978]. Treatment with unsaturated acids such as acrylic or linoleic acid can provide a hydrophobic, graft-forming surface which can undergo radical-induced homo-polymerization or copolymerization with other adsorbed monomers. Similarly, dicarboxylic acids can provide a carboxylic acid functional surface, capable of obtaining grafts by condensation with a polymer with reactive centers [Nollen, 1969].

The acidity of the anatase bridged hydroxyls is sufficient for the protonation by trialkylamine, but not by weaker bases such as pyridine. Protonation of trialkylamine is not observed on rutile surfaces, the amine being adsorbed solely by coordination with the surface ions. Amines are frequently used for imparting oleophilicity. The adsorption of the amine can often be improved by impurities resulting from the manufacturing processes, particularly adsorbed chloride, sulphate, or bisulphate ions; or by pretreatments including removal of the adsorbed water, silica-alumina coated titanias, adsorption of hydrated Al^{3+} ions [Solomon, 1971; Hodgkin, 1974].

Higher alcohols having low volatility, such as trimethylolpropane or pentaerythritol can limit dust formation during mechanical milling of TiO_2 to prevent the reformation of strong aggregates. The polyols also act as wetting agents for dispersion of TiO_2 polar media.

2.3.3.2.2 Modification Involving Covalent Bond Formation

The O-H species on TiO_2 surface can be used as anchor groups for the attachment of covalently bound surface modifiers, “coupling agents” commonly being organosilanes, metal alkoxides, epoxides, and isocyanates

.

- **Reaction with Silanes**

Organofunctional silanes are often in the form of $RSiX_3$, where X represents a halide, alkoxide, acrylate, amino or alkyl group; and R an organofunctionality. They can act as a bridge between organic and inorganic layers. X is hydrolysable to react with TiO_2

surface hydroxylic species to form covalently bound siloxy derivative. Many of Organosilanes have three hydrolysable substituents on each silicon center which would enable the formation of a cross linked siloxane network of the condensation of adjacent adsorbed silantriols with each other as well as the O-H groups.

The functional groups R in the silanes generally possess one or more nonhydrolyzable alkyl or aryl groups which are used to provide compatibility with organic polymers. They may also contain substituent groups that can provide reactive centers for graft formation between a polymer and the TiO_2 surface. This reactive substituents can be tailored for specific applications and include vinyl, acrylate and methacrylate, chloro, amino, epoxy, and mercapto groups.

The chloro and alkoxy derivatives are two most frequently used types of organosilanes. The chlorosilane is considerably more readily reactive with TiO_2 surface hydroxylic species at ambient temperature because of being catalyzed by the byproduct, but yield hydrogen chloride as detrimental byproduct. Contrary, the alkoxysilane is less hazardous, but may be slowly hydrolyzed even if adsorbed water is also present. Reaction between the adsorbed alkoxysilane and surface silanol group does not occur at room temperature, unless catalyzed by co-adsorbed acidic or basic species.

- **Reaction with Metal Alkoxides**

Metal alkoxides, notably those of titanium and aluminum, are capable of condensation with adsorbed water or hydroxylic species on TiO_2 surface to form firmly bonded adducts. The principal difference between the silanes and the alkoxides lies in the type of bond between the metal and the functional organic substituents that interact with the organic polymer. With the exception of some specialized reagents derived from silicate esters, the functional organic moieties of the adsorbed silanes are attached by hydrolysis of Si-C bonds; but those of the common alkoxides contain hydrolysable Ti-O-C or Al-O-C bonds.

The reaction between alkoxytitanium derivatives and surface hydroxylic species is similar to that of the alkoxysilanes. However, the monomeric titanates are coordinately unsaturated and can form coordination complexes with Lewis bases, other hydroxylic species, ester, and acids. Adsorbed titanates can react rapidly with surface hydroxylic species at room temperature [Feld, 1965].

The titanate treatment of other fillers such as kaolins, alumina can result in significant improvement in the various properties of a diverse range of system. But TiO_2 and other white fillers which are treated with titanates have been reported to discolor through oxidation when incorporated in some polymers. The titanates can form highly colored compounds with some of the antioxidants used in polyolefins. Furthermore, the titanates are susceptible to hydrolysis, which is potentially deleterious, resulting in loss of interfacial adhesion [Solomon, 1983].

- **Reaction with Epoxides and Isocyanates**

The condensation reactions of epoxides and isocyanates with hydroxylic compounds are widely used for the manufacture of thermoset or cured resins. Epoxides such as propylene oxide can react with TiO_2 surface hydroxylic species to form grafted species (e.g. free polypropylene oxide (PPO)). This titania-epoxide adduct shows improved dispersibility in benzene, but it is susceptible to hydrolysis because the covalent bonding is similar to that of the alkoxides described earlier. Surface modification with epoxides has limited utility, and the polyol treatment may be the preferable alterative.

Alkyl and aryl isocyanates such as those used in the production of polyurethanes, are generally more reactive towards surface hydroxylic species than the epoxides. Examples involve treatment of TiO_2 with C_6-C_{18} alkyl monoisocyanates, followed by heating at 100 to 160^{o}C to form hydrophobic fillers [Eastes, 1957]; and treatment with alkyl or aryl diisocyanates, or with vinylic or allylic isocyanates, to obtain oleophilic materials which can serve to be a reactive reinforcing filler for incorporation in plastics and elastomers.

2.3.3.2.3 Modification by the Adsorption of Polymers

In contract to small molecular modifiers only resulting in the thin adsorbed layers, some polymers are capable of forming thick, solvatable, adsorbed layers on TiO_2 surface. Depending on their structures, the adsorbed polymers may act as dispersants, dispersion stabilizers, or as processing aids.

The silicone oils such as polydimethylsiloxanes or derivatives containing polar hydroxyl or amino substituents can bond to TiO_2 surface. The adsorbed silicones reduce moisture adsorption and aid in preventing agglomeration of TiO_2. The chemisorption of the silicone on the titania or silica-alumina coated titania occurs largely by hydrogen bond formation, although acid-catalyzed condensation between surface hydroxyls and the cleaved siloxane polymers may also occur on heating the silicone-treated TiO_2. Maximum adsorption of the silicones form solution is obtained by predrying of the TiO_2 or by use of nonpolar solvent. Such silicone treatment can enhance the dispersion of TiO_2 in the nonpolar polymers such as polyolefins and improve their durability [Ashmead, 1971]. However, the silicones may hinder the dispersion of TiO_2 in polar polymer such as polyesters, which instead are often modified by transesterfication with oxidizing vegetable oils [Solomon, 1967].

Rutile modified by the polyesters with unsaturated center, e.g. those prepared from a 2-ethylhexanoic acid/maleic anhydride/phthalic acid and 1,2,6-hexantriol mixture, has been claimed to show improved dispersibility in polyvinyl chloride, thus leading to the improvement of its tensile and impact strengths as well as elongation-at-break point [Plueddemann, 1978].

Another number of strongly bonded polymers have been reported for improvement of dispersibility of titanias, probably as processing aids rather than dispersants. These include styrene-maleic anhydride copolymers, for dispersion in alkyd media; polyethylene imine, or its reaction products with acrylonitrile or oxiranes, for dispersion in polar polymers such as polyesters [Barksdale, 1969]; polymeric aluminum or zinc salts derived form partially hydrolyzed acrylic copolymers, for dispersion in nonpolar

polymers [Sugiyama,1972]; carboxylate-terminated polycaprolactone, for dispersion in polyethylene or polystyrene; and polyvinyl pyrrolidone, for dispersion in polyurethane formulations [Wolf, 1974].

2.4 Polymer TiO_2 Nanocomposites

2.4.1 Introduction

Titanium dioxide is a widely applied filler to PVC, polyolefins, PS, ABS, and many other polymers to prepare composites due to their improved physical and mechanical properties induced by TiO_2 while without loss of ease processing, light weight, and often ductile nature of neat polymer. Traditionally, the polymer composites were reinforced with micron-sized TiO_2. Recently, processing techniques have been developed to allow the size of TiO_2 to go down to nanoscale. Experiments have shown that nanoscale reinforcement brings new optical, electrical, physiochemical phenomena, which contribute to material properties and correspondingly extended applications. In this section, the review interest was in experimental procedures of preparing polymer TiO_2 nanocomposites and their properties that are available to-date.

2.4.2 Preparation Procedures

Like many other polymer nanopowder composites synthesis, direct mixing, sol-gel processing, and in situ grafting polymerization are the three mostly common processing techniques many researchers have tried to make a polymer TiO_2 nanocomposite. We have discussed the general principles and advantages/disadvantages of each synthesis method in Section 2.1.2.3, which are also suitable for the polymer TiO_2 nano-system. The following only illustrates some examples of detailed experimental conditions and parameters for processing this system in literature.

Carotenuto et al. produced a good nanocomposite film by directly dispersing dehydrated nano-TiO_2 into a poly-3-hydroxy-2,3-dimethylacrylic acid (PDAA) solution. For achieving well disperse, TiO_2 nanopowders were thoroughly dehydrated by washing with

ethanol to remove water and rinsing twice with propylene glycol methyl ether acetate (PGMA) to remove the alcohol; then dispersed in PGMA in an ultrasonic bath, followed by mixing with a PDAA/PGMA solution containing 50 wt% polymer. The excess solvent was evaporated in vacuum under stirring at room temperature until the desired viscosity was achieved. This mixture was then poured over cleaned glass plates to make a nanocomposite film using a spin coater and subsequently dried under vacuum at 70^{o}C for 5 min. To avoid agglomeration, the powders were kept wet during the entire process [Carotenuto, 1996].

Ma et al. were able to make nanocomposites with low-density polyethylene (LDPE) matrix and TiO_2 nanoparticles (23 nm on average) through melt mixing of the components. TiO_2 nanoparticles with three surface conditions: as-received (hydrophilic), dried (less hydrophilic), and polar silane treated (more hydrophilic), were used in this work. Drying of the nanoparticles was carried out at 195°C in vacuum for 24 h. Dried particles were used immediately either for composite processing or in the coating process. Coating of the nanoparticles was performed by using N-(2-aminoethyl) 3-aminopropyl-trimethoxysilane (AEAPS) in a dry toluene reflux method. Next, 5% (by mass) of TiO_2 particles were mixed into LDPE at 130°C in a Haake System 90 Buchler mixer with 50 rpm screw speeding for 10 min. The size of the nanoparticle aggregates were on the microscale in the AEAPS-TiO_2/LDPE, whereas nanoparticle aggregates were not even observable in the dried TiO_2/LDPE in atom force microscopy (AFM) [Ma, 2005].

Polystyrene or polycarbonate rutile nanocomposites have been synthesized by Nussbaumer et al. by first modified the rutile with dodecylbenzenesulfonic acid (DBSA). Polystyrene or polycarbonate was dispersed in dichloromethane solvent and stirred at room temperature for 40 min. Then modified rutile (2 nm average particle size) was added, the mixture was stirred in 15 min and poured in a petri dish. Upon evaporation of the solvent at ambient conditions, the nanocomposites were obtained [Nussbaumer, 2002]. Solution mixing has also been found to prepare TiO_2 poly-D,L lactic acid

(PDLLA) [Boccaccini, 2005]; carbowax; polyvinyl chloride (PVC), polyethylene glycol (PEG), and polyethylene oxide (PEO) [Xiao-e, 2004] nanocomposites.

In nanocomposites made by direct mixing above, the interactions between the hosting matrix and the entrapped TiO_2 are relatively weak and based on hydrogen bonds and van der Waals forces. Re-aggregation of nano-TiO_2 particles stemming from their high surface energy is a perennial problem that undermines their efficacy. To avoid re-aggregation, a few researchers have already used in-situ grafting polymerization technique to produce steadier polymer TiO_2 nanocomposites. For example, Rong et al. synthesized nanocomposites in high yield by in situ grafting and polymerizing styrene in the presence of nano TiO_2 surface. Firstly, nano TiO_2 was modified with a coupling agent at room temperature for 48 h. In the next step, ethanol suspension free radical copolymerization of styrene with the functional group at the modified nano-TiO_2 surface was irritated at 65°C into a flask fitted with a condenser and a thermometer under the nitrogen atmosphere and allowed to proceed for 22 h. This technique produced strong chemically bonded interface between organic-inorganic phases [Rong, 2005].

Sol gel processing is another frequently used technique to build stronger chemical bond between polymer and TiO_2 components in nanocomposites. Wang et al synthesized good polystyrene maleic anhydride (PSMA)/TiO_2 nanocomposites via the hydrolysis and condensation reactions of multi-component sol since the PSMA have functional groups which can anchor TiO_2 and prevent them aggregating. They first dissolved the PSMA in tetrahydrofuran (THF) with stirring at 40°C for 12 h and added dionized water and acetylacetone, which played a role in reducing the hydrolyzing rate of tetrabutyl titanate ($Ti(OBu\text{-}n)_4$) into the polymer solution. The pH of the mixture was adjusted to about 1.7. After stirring 20 min, the precursor $Ti(OBu\text{-}n)_4$ dissolved in THF was dropped into the mixture and then heated to 60°C and stirred for 4h. Finally, the homogeneous mixture was sealed in an oven and kept at room temperature for 4 days to obtain transparent nanosamples [Wang, 1999B].

In a study of Liu et al., the synthesis of PEO/TiO_2 nanocomposite electrolytes was also carried out by sol gel approach. First, the dried PEO and lithium tetrafluoroborate ($LiBF_4$) were dissolved in acetonitrile and stirred at 40°C for 3 h to obtain a homogeneous solution. The concentration of PEO in acetonitrile was maintained at 5% and ratio of EO: Li was fixed at 20: 1 for all solutions. A calculated amount of titanium ethoxide was added into the solution under continuous stirring. The residual water in acetonitrile was adequate for hydrolysis, and no water was deliberately added to the mixture. After complete hydrolysis and condensation reactions of titanium ethoxide, the mixture was transferred to a Teflon petri dish to allow the solvents to evaporate, further dried at 50°C under vacuum for 2 days. This process resulted in homogeneous, freestanding, and flexible nanocomposite membranes [Liu, 2003B]. Other researchers have also used this method to make TiO_2 poly-*p*-phenylenevinylene (PPV) [Yang, 2004], PI [Chiang, 2003, 2004], polymethyl methacrylate (PMMA) [Chen, 1999; Lee, 2001], polyarylene ether ketone/sulfone (PEK/PSF) [Wang, 1991] nanocomposites.

Yoshida et al. combined so-gel and solution mixing approaches to prepare transparent PI/TiO2 nanocomposites. In the first step, the nano-TiO_2 particles were produced through reverse micelles using the sol–gel method. The reverse micellar solution was prepared by dissolving sodium bis(2-ethyl hexyl) sulphosuccinate (AOT) in isooctane and the resulting solution was filtered, followed by the addition of required amount of distilled water. Then titanium iso-propoxide (TIP) diluted with isopropanol was injected into the reverse micellar solution with mild stirring. After the hydrolysis reaction, TiO_2 particles were then extracted form micellar solution by the addition of N-methyl pyrrolidinone (NMP). In the second step, to this NMP solution containing TiO_2, the fluorinated polyimide solution was added under stirring. The mixture was coated on a glass substrate, and a PI/TiO_2 nanocomposite (4 wt% TiO_2 concentration) was successfully produced after the heat treatment [Yoshida, 1997].

Zhu et al. synthesized polyamide 6 (PA6) TiO_2 nanocomposites via a combination of grafting polymerization and compounding. Firstly, the TiO_2 particles were dried first to remove any water absorbed on the surface and reacted with a silane coupling agent in

ethanol solvent. After completed reaction, modified TiO_2 were mixed with the vinyl dianhydride (VDA) monomer and acetone solvent. This mixture was then initiated by benzoyl peroxide (BPO) at 60°C for 5 h to prepare the anchoring polymerization modified TiO_2 and the solvent was removed. Nano-samples were then made by adding PA6, mixing, compounding and spinning. This technique produced samples without aggregation and increased the TiO_2 polymer matrix interfacial interaction [Zhu, 2004].

Thus, in general, there is no single procedure that is followed for making polymer TiO_2 nanocomposites. A combination of two- or multi-methods may be applied. As seen from the above mentioned summary the most important factor to consider in deciding between different processing techniques is the requirement of good TiO_2 dispersion in the polymer matrix. This dispersion will play a major role in the results reviewed below.

2.4.3 Properties

Although there is not yet to be a consensus on how nano-sized TiO_2 affect material properties partly due to the novelty of the area, and the challenges in processing of nanocomposites, lack of systematic experimental results, and scarcity of theoretical studies, some properties of the nanocomposites have been studied in-depth, leaving gaps in the knowledge on nanocomposite behavior. The focus of this summary will be on how thermomechanical, morphologic, optical, electrical behaviors of the polymers are altered by introducing nano-sized TiO_2 reinforcement, and what therein applications contribute to the material response of nanocomposites.

2.4.3.1 Thermomechanical Properties

TiO_2 has relatively high elasticity modulus, which can be frequently combined into various polymers to obtain the mechanical gain of the nanocomposites. Chiang et al. preformed a series of tests on the mechanical properties (elastic modulus, elongation, strength, yield stress, thermal stability, and glass temperature T_g) of PI/TiO_2 nanocomposites with various contents of titania and three different PI systems

(Pyromellitic dianhydride (PMDA) series; 3,3′,4,4′-biphenyl tetracarboxylic dianhydride (BPDA) series; and 3′,4,4′-benzophenonetetracarboxylic acid dianhydride (BTDA) series. They found that the TiO_2 nanoparticles, formed via sol–gel process, would uniformly disperse in PI matrix and result in enhanced mechanical properties. For all three series of systems the elastic modulus increased with increasing volume fraction of TiO_2 additions. For 9% TiO_2 additions, the increase in effective elastic modulus was around 30% over that of the pure PI. The reverse effect was found to elongation coefficient. Interestingly, there was a little initial increase in yield stress followed by a steady drop as filler content increased, with a peak occurred at about 1%. It was also observed that the color of the hybrids became darker with increase of titania. For flexibility, in the series of PMDA/ODA, the hybrids containing titania of 5 wt% or more were brittle. However, the hybrids of BPDA and BTDA series were still flexible with titania content up to 5 wt% or more. The results implied that the flexibility of hybrid films have an order of BTDA>BPDA >PMDA. For all systems, the storage modulus (E') of hybrids improved with increasing TiO_2 amount at lower and elevated temperatures. But their loss modulus (E'') decreased with the increasing amount of TiO_2. Hence, Tg, defined as the peak tan $\delta(E''/E')$, shifted to higher temperatures with added increasing amounts of TiO_2 which is much stiffer than the pure PI. However, due to oxidatively degradable ability of titania, their introduction caused a little decrease in thermal stability of hybrids which still possess good thermal property for the practical application. There was also a marked lowering of the coefficient of thermal expansion (CTE) in hybrids with small amount of titania because TiO_2 not only had lower CTE values and but also served as cross-link points resulting in a decrease in the segmental mobility of the PI chain [Chiang, 2004].

Another study centered on polybenzoxazine (PBa)-titania hybrids. The improvement of viscoelastic properties was obviously indicated by incorporation of titania into the PBa matrix. For example, the storage moduli of the hybrids at room temperature increased with the increase of the titania content and maintained constant up to relatively higher temperature in comparison with the neat PBa resin. These increments in the storage moduli of the hybrid materials in comparison with the neat resin indicated that the micro-Brownian motion of PBa segments is restricted by the homogeneous dispersion of titania

into the matrix, leading to reinforced PBa network. In addition, the T_g of the neat PBa(151°C) is shifted to 161, 171 and 179°C with inclusion of 3, 5 and 7% of titania, respectively. In sharp contract to PI/TiO_2 studied by Chiang, higher thermal stability was obtained by the addition of only very small amount of TiO_2 nanoparticles possibly because of their thermal insulation effect which protects the underlying PBa matrix. The decomposition behaviour of the hybrids was also studied by thermogravimetric analysis (TGA). Char yield at 800°C was 31% for PBa-0, 42% for PBa-3, 49% for PBa-5, 55% for PBa-7, 59% for PBa-10, and 63% for PBa-20, thus confirming that the hybridization with nano-TiO_2 improved greatly the flame retardance of the hybrid [Agag, 2004].

Zhu et al. also investigated that the PA6/TiO_2 nanocomposites had improved spinnability and mechanical properties. It was found that tenacity at break and the initial modulus of PA6 with modified nano-TiO_2 composites were improved by about 10%, 20%, respectively, as compared to the pure PA6 [Zhu, 2004].

2.4.3.2 Morphologic Study

Given the evidence in the literature, the degree of crystallinity of semi-crystalline polymers determines many their macroscopic properties. It is important to evaluate the effect of TiO_2 surface chemistry on the crystallization process in nanocomposites. Ma et al studied the impact of TiO_2 nanoparticles with different degrees of aggregates on crystalline structure of LDPE in TiO_2/LDPE. It was found that the size of the TiO_2 nanoparticles, corresponding to the three different surface conditions investigated, did not significantly affect the degree of LDPE crystallinity, the unit cell dimensions, the average lamellar thickness, or the average spherulite size. The peak crystallization temperature was observed at appropriately the same position with the addition of the TiO_2 inclusions. However, the nanoparticles did affect the internal arrangement of intraspherulitic crystalline aggregates by decreasing the relative optic axis orientation of these crystals, usually referred to as internal spherulite disorder. The LDPE filled with the TiO_2 treated with a polar silane AEAPS, whose TiO_2 aggregate was at microscale comparable to the spherulite size, showed the highest internal spherulitic disorder and exhibited the most poorly developed spherulite structure. The large agglomerate size in AEAPS sample was

quite possibly due to the enhanced surface hydrophilicity and the resulting poor interfacial compatibility between AEAPS treated TiO_2 and LDPE matrix [Ma, 2005].

On the other hand, Chiang et al. reported that the introduction of TiO_2 nanoparticles disrupted the intermolecular regularity of polyimide, thereby causing the disappearance of a highly ordered crystalline phase [Chiang, 2003]. The decrease in crystallinity with the presence of nanoscale fillers has also been reported for other nanocomposites [Wang, 2002; Ogata, 1997].

The homogeneity of the organic-inorganic phases is another important morphology. Agag et al. indicated that the uniform PBa-TiO_2 hybrid material and the dispersion of fine titania particles of size less than 100 nm were formed at 2%of TiO_2 loading. With the increasing TiO_2 content, the presence of large aggregates was observed [Agag, 2004]. Zhu et al. also found that the TiO_2 particles after surface modification of the grafted polymer were dispersed in PA6 matrix homogenously and their average size was less than 50 nm, while some big agglomerates and black holes were visible when unmodified TiO_2 was added [Zhu, 2004].

The impact of TiO_2 nanoparticles on polymer morphology is quite possibly dominated by the interaction between the nanoparticle surface and the surrounding polymer. The region around the filler can exhibit altered polymer chain dynamics. With the large surface area of nanofillers, the enhancement or restriction of chain mobility near the particle surface could significantly affect morphology in their formed nanocomposites [Ma, 2005].

2.4.3.3 Optical Properties

In addition to their highest refractive index, strong UV adsorption up to visual wavelength, and transparency at the visible wavelength, nano-TiO_2 particles (especially rutile) are optically active and do not scatter light significantly, which render nanocomposites attractive for making optical materials. As mentioned earlier, Yoshida et al. prepared a novel PI/TiO_2 hybrid via a combination of sol gel processing and solution

mixing for optical waveguide application. They measured and calculated the optical propagation loss of the nanoTiO_2-dispersed PI hybrid (containing 4% TiO_2) to be 1.41 db/cm, the same number as that of pure PI. The impregnation of nano-TiO_2 did not show any significant adsorption increase leading to the discoloration of the material. For comparison, they also made a traditional microsized TiO_2 filled composite by sample mixing, as a result of discolored yellow system because large TiO2 particles scatter light at their surface and light can not penetrate them. Furthermore, the refractive index of 4% nanoTiO_2-dispersed PI sample was also calculated from the prism coupling angles, and was 1.560, a little higher than that of pure PI [Yoshida, 1997].

Chiang et al. also confirmed that the PI/TiO_2 nanocomposites had fair good optical transparency, even with TiO_2 content up to 40 wt%. The TiO_2 nanocrystalline was well dispersed in the PI matrix with 10–40 nm in diameter when the TiO_2 content is from 5 to 30 wt%. Absorbance band is observed below 400 nm for pure PI. The spectrum of PI/TiO_2-5 wt% hybrid film is almost the same as pure PI. When the content of TiO_2 is equal to or more than 10 wt%, a relatively stronger absorbance can be seen at $\lambda \geq 450$ nm wavelength. Based on the UV–visible results, the low TiO_2 content is expected to produce more transparent films than those prepared from higher TiO_2 content. Another interesting observation was the drastically increase of the absorbance curve between 5 and 10 wt%. This result might be attributed to the aggregation of metal oxide thereby causing growth of particle size and hence led to large scattering. However, the particle size of TiO_2 is still in the nanosized region [Chiang, 2003].

Visual transparency was also observed for PVAL-based nanocomposites up to TiO_2 contents of 35 wt% (10.5 vol%), although some scattering in visible wavelength was evident in the samples containing 31-35%. Strong UV adsorption of the nanocomposites was indicated due to the incorporated TiO_2, which showed an absorption maximum at 225nm and a full width at half maximum of 45nm. At relatively high TiO_2 contents (>24 wt%), UV radiation was virtually completely absorbed from the instrumental limit of 180 to 360 nm; these samples thus could serve as efficiently transparent UV filters. The refractive index of the PVAL-TiO_2 nanocomposites rose linearly form 1.521 for neat

PVAL to 1.609 at 10.5 vol% TiO_2, showing that the refractive index of the nanocomposites can be readily controlled by the TiO_2 content [Nussbaumer, 2003].

Transparency, an increase in refractive index, and other optical gains resulting from the inclusion of nano-TiO_2 were also investigated into nanocomposites with the polymer matrices including PMMA [Chen, 1999; Lee, 2001], PEK/PSF [Wang, 1991], PBa [Agag, 2004], PDAA [Carotenuto, 1996], PPV [Yang, 2004], PSMA [Wang, 2001] pyromellitic dianhydride (PMDA) [Chang, 2001].

2.4.3.4 Electrical Properties

With a high dielectric constant in bulk and size-dependent discrete electric properties, nano-TiO_2 can be incorporated into a polymer matrix to prepare nanocomposites for electrical applications. Chiang et al. pointed out that the dielectric constants of nanoTiO_2-dispersed polyimide hybrids (in the range of 3.2–3.9) increased with the increasing titania content while the surface and volume resistivities displays the reverse trend. This electrical property can be tailored to other non-conductive or low-conductivity polymers to extensively be applied as conductive space and industry films [Chiang, 2004].

The electrical breakdown strength (defined as electric-field intensity that causes the "insulator to conductor" transition in a material) of nanoTiO_2-filled low-density polyethylene (LDPE) nanocomposites was investigated by Ma et al. It was found that the surface water on the nanoparticles and the size of particles played a very important role in determining the breakdown strength. The breakdown strength at 63.2% cumulative failure probability (E_0) for the composites filled with dried nanoscale TiO_2 was similar to that of neat LDPE and 50% higher than that for the samples filled with as-received nanoscale TiO_2, which were observed some larger agglomerates. This increase was due to a better dispersion, a better interface, and a morphology change of the matrix. It was also found that surface modification of nanoscale TiO_2 had a significant influence on the breakdown strength. N-(2-aminoethyl) 3-aminopropyl-trimethoxysilane (AEAPS)-coated TiO_2 filled samples showed about 40% higher E_0 than that of uncoated, as received TiO_2-

filled samples. This was mainly due to enhanced electron scattering because of the presence of polar groups in AEAPS [Ma, 2004].

Liu et al. studied the electrochemical properties of interest to battery high-voltage lithium application such as ionic conductivity, Li^+ transference number, and electrochemical stability window in PEO/TiO_2 nanocomposite electrolytes with lithium tetrafluoroborate ($LiBF_4$) as the lithium salt. TiO_2 had two opposing effects in ionic conductivity; one was the enlargement of the polymer amorphous phasewhich increased conductivity and the other the increase in phase discontinuity which decreased conductivity. A maximum value of ionic conductivity was obtained at 10% nano-TiO_2 loading with a conductivity of 7×10^{-7} S/cm, which was over an order of magnitude higher than that of the electrolytes without TiO_2, also higher than that of microsized-TiO_2 filled electrolytes. Li^+ transference number (indicative of high cationic mobility) was improved by the inclusion of TiO_2, which gave rise to an enhanced lithium ion transport in the polymer, as a result of increased interactions between Li^+ ions, anions, ether oxygen atoms, and the surface of the TiO_2. The 10 wt% TiO_2/PEO nanocomposite electrolyte was also found to be electrochemically stable up to 4.5 V versus Li+/Li via cyclic voltammetric (CV) measurement [Liu, 2003B]. Similar results were also observed by other researchers [Yu, 2004; Karlsson, 2003].

2.5 Appendix

2.5.1 Methods in Characterization of Modified TiO_2 Surface

Modern methods for the characterization of chemically modified TiO_2 surface with respect to its geometrical structure, particle size& size distribution, and adsorbed chemical compositions make use of the interaction of electromagnetic radiation, electrical fields, neutral or charged particles with its surfaces. Among enormous surface analysis techniques, the most frequently used in the experiments are scanning electron microscopy (SEM), X-ray diffraction (XRD), proton nuclear magnetic resonance (^{1}H-NMR) spectroscopy and Fourier transform infrared (FT-IR) spectroscopy.

2.5.1.1 Scanning Electron Microscopy (SEM)

The SEM is the prime tool for providing visual image of materials at the micron and in some case of the submicron level of resolution. One primary reason for the SEM's usefulness is the high resolution which can be obtained; its magnification reaches up to 300,000 times and maximum resolution is about 2.5 nm. Another feature of SEM images is the three-dimensional appearance of the specimen. So, the SEM is particularly powerful in characterizing crystallographic, magnetic, electrical characteristics of the specimen and in determining if any change of the particle morphology has occurred when the specimen surface is modified by other molecules.

The basic components of the SEM are the lens system, electron gun, electron collector, visual and recording cathode ray tubes (CRT) and the electronics associated with them. A finely focused electron beam produced by electron gun and lenses is scanned across and then impinges the specimen surface in a 'raster' or pattern of parallel lines. By electron impact, the emission of secondary electrons with energies of a few tens eV and re-emission of the high-energy backscattered electrons from the primary electron beam are gathered by electron collector into the electron current which is in turn amplified to be transformed by the amplifier and CRT into forming the images. The angle at which the electron beam impinges the specimen surface determines the intensity of both emissions

and then emitted electron current. The brightness of the trace of the CRT being scanned is proportional to the magnitude of the resulting signal strength, which is determined by the amount of current. Through this mechanism, we can obtain clear topographical features on the specimen surface [Goldstein, 1975].

2.5.1.2 X-Ray Diffraction (XRD)

The XRD, also known as θ-2θ Scans, has the potential to provide information on an atomic scale especially for crystalline species. Its basic constitutions are the x-ray source and the x-ray detector which lie on the circumference of a circle (focusing circle) with the specimen. The x-ray source is one which generates x-rays by directing an electron beam of high voltage at a metal target anode inside an evacuated x-ray tube. The detector is capable of counting the number of x-ray protons of a particular energy for each angle 2θ which is a proportional reflection of the peak intensity.

As shown in Figure 11 [Huber, 2003], X-ray diffraction anatase pattern is the general feature independent of the specimen. The pattern consists of a series of peaks. To identify an unknown specimen, we start by matching the strongest peak, then the next strongest, and up to eighth strongest peak between in experiment and in handbook (e.g. Powder Diffraction File). The positions of the peaks in the pattern also depend on the crystal structure, more specially the shape and size of the unit cell. The width of an individual peak, often defined as the full width at half the maximum height, can be used to determine crystallite size and the presence of lattice strain in the crystal [Suryanarayana, 1998].

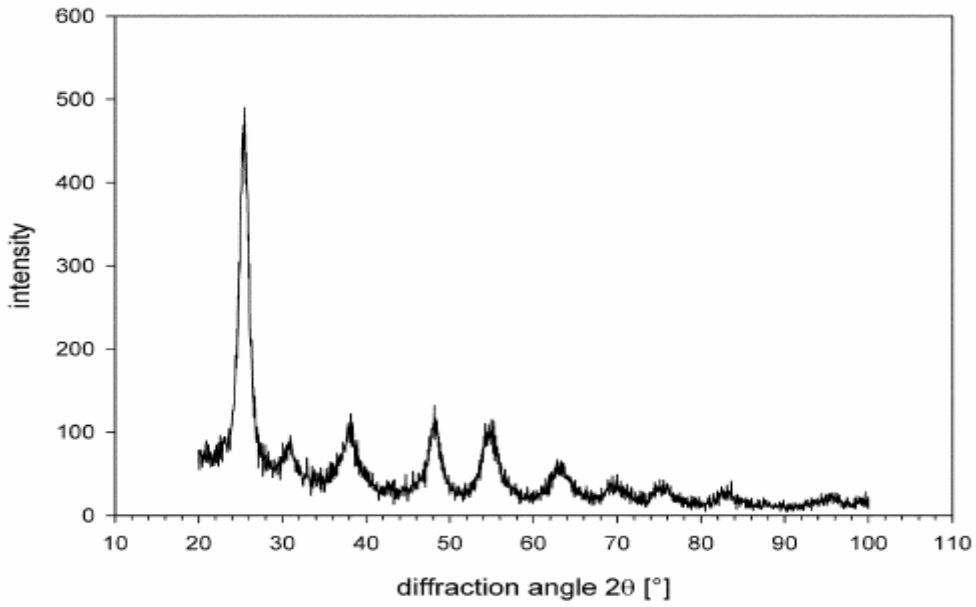

Figure 11 XRD intensity of a anatase sample (6-nm particle size) versus the diffraction angle 2θ [Huber,2003]

2.5.1.3 Proton Nuclear Magnetic Resonance (^{1}H-NMR) Spectroscopy

Highest sensitivity of the proton yielding sharp signals make the ^{1}H-NMR one of the most common NMR absorption spectrometry, which is widely used for the structural and compositional determinations of organic moiety adsorbed on the oxide surface. According to the electromagnetic theory, a molecule containing certain amounts of nuclei has intrinsic characteristics of absorbing electromagnetic radiation in the radio frequency (RF) region corresponding to its frequencies upon an applied magnetic field. Generally, the adsorption frequency is indirectly measured from compared to a suitable reference compound (e.g., tetramethylsilane (TMS)). The difference of the adsorption positions between the specimen and the reference is defined as chemical shift δ (dimensionless unit in ppm). A plot of the chemical shift δ versus absorption peak intensities constitutes a ^{1}H-NMR spectrum.

The chemical shift δ is only a function of the nuclei and their environments. The number of nuclei of each type of a pure specimen can be obtained directly from the integrals of each peak multiplet in the ^{1}H-NMR spectrum provided that there is no overlap from the

residual solvent signals and no undergoing conformational exchange of the molecule. The ^{1}H-NMR spectrum also yields information about the molecular environment. The orientation of neighboring nuclei affecting the effective magnetic field can cause splitting of the signal for each type of nucleus into two or more lines. These spin-spin couplings are transmitted through chemical bonds to yield the information. In addition to homonuclear couplings, the multiplets may be split by other nuclei. If such heteronuclear couplings are undesirable they may be decoupled. The best pulse sequence in such a case is that for inverse gated decoupling in order to minimize the change in sensitivity while maintaining decoupling. To determine the multiplicity, one may measure the coupling constant, which gives an indication of the distance between the protons [Lambert, 2004]

2.5.1.4 Fourier Transform Infrared (FT-IR) Spectroscopy

The FT-IR spectroscopy is another useful adsorption spectroscopy in IR frequency regions (about 13,000 to 10 cm^{-1} wavenumbers, of which 400 - 4000 cm^{-1} is of particular interest) for monitoring qualitative and quantitative information on specific functional group and the bonding of organic moieties to oxide surface. A plot of the frequency of the incident radiation versus radiation intensity absorbed is the IR spectrum of the compound.

It is possible to obtain an IR spectrum from samples in many different forms. However, many solids are opaque to IR radiation and must be dissolved or diluted in an IR-transparent solvent in order to obtain spectra. The conventional IR-transparent solvents are carbon tetrachloride for the region between 4000 and 1330 cm^{-1} and carbon disulfide for between 1330 and 625 cm^{-1}, which are quite toxic and should be carefully handled. Recently, carbon tetrachloride is replaced with the less-toxic tetrachloroethylene or methylene chloride and carbon disulfide with n-hexane or n-heptane. Water is seldom used because water protons dominate the spectrum and obscure useful information about the specimen.

Typically, solutions of 5% to 10% in concentration are handled in 0.1 to 1 mm thick IR cells which consist of metal frame plates, IR transmitting windows and gaskets. Salt

plates (e.g. NaCl) is used for semivolatile or nonvolatile liquid, while disposable IR cards containing polytetrafluoroethylene or polyethylene substrate for volatile solvent. Pellets are used for solid samples that are difficult to melt or dissolve in any suitable IR-transmitting solvents. Suitable KBr disks or pellets can often be made using a simpler device such as a Mini-Press.

After the above possible treatment, the IR radiation is directed toward the specimen surface in a cup and the scattered light from the surface is collected. The spectrum is acquired from an interferometer so that the signal must be transformed by a Fourier function. In general a few hundred scans are needed to signal average in order to obtain a good spectrum [Garton, 1992].

2.6 References

Adams, R.; *Focus on Pigm.*, 2005, 1, 1

Agag, T.; Tsuchiya, H.; Takeichi, T.; *Polymer*, 2004, 45, 7903

Akita,H.; Hattori, T.; *J. Polym. Sci. B: Polym. Phys.,* 1999, 37, 189

Alexandre, M.; Dubois, P.; *Mater. Sci. Eng. R : Rep.,* 2000, 28, 1

Ajayan, P. M.; Schadler, L. S..; Braun, P.V.; *Nanocomposites. Sciece and Technology*, Wiley-VCH, 2003

Ashmead, B. V.; Bowrey, M.; Owen, M. J.; *J. Oil Colour Chem. Assoc.,* 1971, 54, 403

Baetzold, R. C.; *Inorg. Chem.,* 1982, 21, 2189

Baetzold, R. C.; *J. Am. Chem. Soc*., 1981, 103, 6116

Bahr, J. L.; Tour, J. M.; *Chem. Mater.,* 2001A, 13, 3823

Bahr, J. L.; Yang, J.; Tour, J. M.; *J. Am. Chem. Soc.,* 2001B, 123, 6536

Barksdale, J.; Coker, W. P.; *U.S. Patent 2425855*, 1969

Banfield, J. F.; Navrotsky, A.; *Nanoparticles and the Environment*, Mineralogical Society of America, Washington, D.C., 2001

Beck, R. D.; St. John, P.; Whetten, R.L.; *Science,* 1991, 253, 879

Bennett, R. A.; Stone, P.; Bowker, M.; *Catal. Lett.,* 1999, 59, 99

Bhimaray, P.; Burris, D. L.; Schadler, L. S.; *Wear,* 2005, 258, 1437

Biener, J.; Wang, J.; Madix, R. J.; *Surf. Sci.,* 1999, 442**,** 47

Bissett, D. E.; *the Printing Ink Manual,* Northwood, London, 1979

Boccaccini, A. R.; Gerhardt, L. C.; Blaker, J. J.; *Composites:Part A,* 2005, 36, 721

Boccuzzi, F.; Chiorino, A.; Haruta, M.; *J. Phys. Chem*., 1996, 100, 3625

Bondzie, V. A.; Parker S. C.; Campbell C. T.; *Catal. Lett.,* 1999, 63, 14

Bonhote, P.; Gogniat, E.; Ashrit, P.V.; *Thin Solid Films*, 1999, 350, 269

Boul, P. J.; Liu, J.; Smalley, R. E.; *Chem. Phy. Lett*., 1999, 310, 367

Bourgeois, S.; Jomard, F.; Perdereau, M.; *Surf. Sci.,* 1992, 279, 349

Braun, J. H.; Baidins, A.; Marganski, R. E.; *Prog. Org. Coat.,* 1992, 20, 105

Breiner, J. M.; Mark, J. E.; Beavcage, G.; *J. Polym. Sci.(B):Polym. Phys.,* 1999, 37, 1421

Brinkley, D.; Dietrich, M.; Szuchmacher, A.; *Surf. Sci.,* 1998, 395 292

Brinker, C.; Scherer, G.; *Physics and Chemistry of Sol-Gel Science Processing*, Academic Press, Toronto, 1990

Brookes, I. M.; Muryn C. A.; Thornton G.; *Phys. Rev. Lett.,* 2001, 87, 266103

Buffat, P.; Borel, J. P.; *Phys. Rev. A*: *Atom. Molecl. Opti. Phys*., 1976, 13, 2287

Burda, C.; Chen, X.; El-Sayed, M.A.; *Chem. Rev*., 2005, 105, 1025

Burnside, S. D.; Giannelis, E. P.; *Chem. of Mater*., 1995, 7, 1598

Cai, R.; Hashimoto, K.; Fujishima, A.; *Bull. Chem.Soc. JPN*., 1991, 64, 1268

Campbell, S. A.; Kim, H.-S.; Gladfelter W. L.; *IBM J. Res. Devlop*., 1999, 43, 383

Carotenuto, C.; Her, Y.-S.; Matijevic, E.; *Ind. Eng Chem. Res.,* 1996, 35, 2929

Chang, C. C.; Chen, W. C.; *J. Polym. Sci,* 2001, 39, 3419

Chang, Y.C.; Frank, C.W.; *Langmuir,* 1998, 14, 326

Chen,G.; Chen, X.; Yao,K.; *J. Mater. Sci. Lett.* 1999, 18, 1761

Chen, J.; Hamon,M. A;. Haddon, R. C.; *Science,* 1998A, 282, 95

Chen, R. J.; Zhang, Y.; Dai, H.; *J. Am. Chem. Soc.,* 2001, 123, 3838

Chen, T. K.; Tien, Y. I.; Wei, K. H.; *Polymer,* 2000, 41, 1345

Chen, Y.; Haddon, R. C.; Smally, R. E.; *J. Mater. Res.* 1998B, 13, 2423

Chen, W. C.; Lee, S. J.; Liu, J. L.; *J Mater. Chem.,* 1999, 9, 2999

Chiang, P. C.; Whang, W. T.; *Polymer,* 2003, 44, 2249

Chiang, P. C.; Whang, W. T.; Tsai, M. H.; Wu, S. C.; *Thin solid film*, 2004, 447-448, 359

Coombes, C. J.; *J. Phys. F.,* 1972, 2, 441

Crivello, J. V.; Song, K. Y.; Ghoshal, R.; *Chem. Mater.,* 2001, 13, 1932

Curran, S. A.; Ajayan, P. M.; Strevens, A.; *Adv. Mater.,* 1998, 10, 1091

Cushing, B. L.; Kolesnichenko,V. L.; O'Connor, C. J.; *Chem.Rev.,* 2004, 104, 3893

Dalton, A.B.; Stephan, C.; Byrne, H. J.; *J. Phys. Chem. B*, 2000, 104, 10012

Diebold, U.; *Surf. Sci. Rep.,* 2003, 48, 53

Dietsche, F.; Thomann, Y.; Mulhaupt, R.; *J. Appl. Polym. Sci.* 2000, 75, 396

Dulub, O.; Hebenstreit, W; Diebold, U.; *Phys. Rev. Lett.*, 2000, 84, 3646

Eastes, J. W.; Cooke, T. F.; *Chem. Abs.,* 1957, 51, 10925

Edmondson, S.; Osborne, V. L.; Huck, W. T. S.; *Chem. Soc. Rev.,* 2004, 33, 14

Eklund, P. C.; Pradhan, B. K.; Smith, M. W.; *Nano. Lett.,* 2002, 2, No.6 561

Ercolessi, F.; Andrecni, W.; Tosatti, E.; *Phys. Rev. Lett*.,1991, 66, 911

Fahmi, A.; Minot, C.; *Surf. Sci.,* 1994**,** 304, 343

Feld, R.; Cowe, P. L.; *Organic Chemistry of Titanium,* Butterworth, London, 1965

Feng, W.; Bai, X.D.; Yoshino, K.; *Carbon,* 2003, 41, 1551

Ferris, K. F.; Wang, L. Q.; *J. Vac. Sci. Technol. A*, 1998, 16, 956

Fitzgerald, J. J.; Landry, C. J. T.; Pochan, J. M.; *Macromolecules,* 1992, 25, 3715

Fu, X.; Qutubuddin, S.; *Mater. Lett.,* 2000, 42, 12

Fujishima, A.; Honda, K.*; Nature,*1972, 238, pp37

Garcia, M.; Vliet, G. V.; Blank, D. H. A.; *Polym. Adv. Technol*., 2004, 15, 164

Garton, A.; *Infrared Spectroscopy of Polymer Blends, Composites and Surfaces,* Hanser Publishers, New York, 1992

Goldstein, A. N.; Echer, C. M.; Alivisatos, A. P.; *Science,* 1992, 256, 5062

Goldstein, J. K.; Yakowitz, H.; *Practical Scanning Electron Microscopy: Electron and Ion Microprobe Analysis*, Plenum Press, New York, 1975

Gomez-Romero, P.; *Adv. Mater*., 2001, 13, 163

Gong, X.; Liu, J.; Young, J. S.; *Chem. Mater.,* 2002, 12, 1049

Gopakumar, T. A.; Lee, J.A.; Parent, J. S.; *Polymer,* 2002, 43, 5483

Grunze, M.; *Chem. Phys. Lett.*, 1978, 58, 409

Guo, Q.; Lee, S.; Goodman D. W.; *Surf. Sci.,* 1999, 437, 38

Gupta, D. C.; Brown, G. A.; *Gate Dielectric Integrity,* ASTM, 2000

Grieve, K.; Mulvaney, P.; Grieser, F.; *Cur. Opin. Colloid Interf. Sci.,* 2000, 5, 168

Hahn, H.; *Nanostruct. Mater.*, 1997, 9, 3

Hasegawa, N.; Kawasumi, M.; Okada, A.; *J. Appl. Polym. Sci.,* 1998, 67, 87

Henderson, M. A.; *Surf. Sci.,* 1994, 319, 315

Henderson, M. A. *Langmuir,* 1996A, 12, 5093

Henderson, M. A.; *Surf. Sci.,* 1996B, 355, 151

Henrich, V.E.; Cox, P. A.; *The Surface Science of Metal Oxides,* Cambridge, University Press, Cambridge, 1994

Heiz, U.; Sanchez, A.; Schneider, W. D.; *J. Am. Chem. Soc.,* 1999, 121, 3214

Herman, G. S.; Dohnalek, Z.; Diebold, U; *J. Phys. Chem. B,* 2003, 107, 2788

Herrmann, W. A.; Stumpf, A. W.; Basset, J. M.; *Angew. Chem. Int. Ed.,* 1996, 108, 2976

Hewitt, J.; *Cosmet. Toiletries*, 1999, 114, 59.

Hodgkin, J. H.; Solomon, D. H.; *J. Macromol. Sci. Chem.,* 1974, 8, 621

Holzinger, M.; Vostrowsky, O.; Jellen, F.; *Angew. Chem. Int. Ed.,* 2001, 40, 4002

Hong, J. I.; Cho, K. S.; Siegel, R. W.; *J. Mater. Res.*, 2002, 17, 940

Huber, B.; Gnaser, H.; Ziegler, C.; *Anal. Bioanal. Chem.,* 2003, 375, 917

Hugenschmidt, M. B.; Gamble, L.; Campbell, C. T.; *Surf. Sci.,* 1994, 302, 329

Hsiue, G. H.; Kuo, W. J.; Jeng, R. J.; *Polymer,* 2000A, 41, 2813

Hsiue, G. H.; Chen, J. K.; Liu, Y. L.; *J. Appl. Polym. Sci.*, 2000B, 76, 1609

Iijima, S.; *Nature,* 1991, 354, 56

Jia, Z.; Wang, Z.; Zhu, S.; *Mater. Sci. Eng. A,* 1999, 271, 395

Johnson, D. C.; Benfield, R. E.; Vargas, M. D.; *Nature,* 1985, 314, 231

Jordan, J.; Jacob, K. I.; Jasink, I.; *Materi. Sci. Eng. A,,* 2005, 393, 1

Jordan, R.; West, N.; Nuyken, O.; *Macromolecules,* 2001, 34, 1606

Kammler,H. K.; Madler, L.; Pratsinis, S. E.; *Chem. Eng. Technol.,* 2001, 24, 583

Karlsson, C.; Best, A. S.; Borjesson, L.; *J. Chem. Phys.,* 2003, 118, 4206

Kato, M.; Usuki, A.; Okada, A.; *J. Appl. Polym. Sci*., 1997, 66, 1781

Kichelbick, G.; *Prog. Polym. Sci.*, 2003, 28, 83

Kim, S. B.; Hong, S. C.; *App;. Catal. B: Environ.*, 2002, 35, 305

Kirner, U.; Schierbaum, K. D.; Chu, W. F.; *Sens. Actuators B,* 1990, 1, 103

Kojima, Y.; Usuki, A.; Kamigito, O.; *J. Mater. Res.,* 1992, 8, 1185

Kruis, F. E.; Fissan, H.; Peled, A.; *J. Aerosol. Sci.,* 1998, 29, 511

Kuo, S.; Huang, W.; Chang, F.; *Polymer*, 2003, 44, 7709

Kurokawa, Y.; Yasuda, H.; Oyo, A.; *J. Mater. Sci. Lett.*, 1997, 16, 1670

Kurtz, R. L.; Stockbauer, R.; Segovia, J. L.; De Segovia, J.; *Surf. Sci.,* 1989, 218, 178

Lambert, J.B.; Mazzola, E.P., *Nuclear Magnetic Resonance Spectroscopy:* an introduction to principles, applications, and experimental methods, Pearson Education Inc., Upper Saddle River, N.J. , 2004

Lan, T.; Kaviratna, P. D.; Pinnavaia, T. J.; *Chem. Mater.*, 1994, 6, 573

Langel, W.; *Surf. Sci.,* 2002, 496, 141

Laus, M.; Francescangeli, O.; Sandrolini, F.; *J. Mater. Res.,* 1997, 12, 3134

Lee, L. H.; Chen, W. C.; *Chem. Mater.,* 2001, 13, 1137

Li, X.; Wu, B.; Li, H.; *Letter to the Editor/Carbon,* 2002, 411, 1645

Lindan, P. J. D.; Harrison, N. M.; Gillan, M. J.; *Chem. Phys. Lett.,* 1996, 261, 246

Lindan, P. J. D.; Harrison, N. M.; Gillan, M. J. *Phys. Rev. Lett.,* 1998, 80**,** 762

Liu, J.; Smallley, R, E.; *Science*, 1998, 280, 1253

Liu, T.; Lim, K. P.; Chen, Z. K.; *Polymer,* 2003A, 44, 3529

Liu, X.; Wu, Q.; *Macromol. Mater. Eng.*, 2002, 287, 180

Liu, Y.; Lee, J. Y.; *J. Appl. Polym. Sci.,* 2003B, 89, 2815

Ma, D.; Akpalu, Y. A.; Schadler, L. S.; *J. Polym. Sci B,* 2005, 43, 488

Ma, D.; Biegel, R.W.; Schadler, L.S.; *J. Mater. Res.,* 2004, 19, 857

Ma, J.; Qi, Z.; Hu, Y.; *J. Appl. Polym. Sci.,* 2001, 82, 3611

Maness, P. C.; Smolinski, S.; Jacoby, W. A.; *Appl. Envir. Microbiol.,* 1999, 65, 4094

Mao, Y.; Fung, B. M.; *Chem. Mater.,* 1998, 10, 509

Martin, C.; Rives, V.; Sanchez-Escribano, V.; *Surf. Sci.,* 1991, 251-252, 825

Martin, T. P.; Naeher, U.; Zimmermann, U.; *J. Chem. Phys.,* 1994, 100, 2322

Mark, J. E.; Eisenberg, A.; Graessley, W.W.; Mandelkern, L.; Koenig, J. L.; *Physical Properties of Polymers*, American Chemical Society, Washington, D.C. ,1984

Mark, J. E.; *Polym. Eng. Sci.,* 1996, 36, 24

Maser, W. K.; Benito, A. M.; Biro', L. P.; *Mater. Sci. Eng. C,* 2003, 23, 87

Mason, T. J.; *Sonochemistry: The use of Ultrasound in Chemistry*, Royal Society of Chemistry, Cambridge, 1990

Matsumoto, Y.; Shono, T.; Koinuma, H.; *Science,* 2001, 291 854.

Mauritz, K. A.; Warren, R. M.; *Macromolecules,* 1989, 22, 1730

Mccarthy, D. W.; Mark, J. E.; Schaefer, D. W.; *J. Polym. Sci. B: Polym. Phys.,* 1998, 36, 1167

McNamara, J. P.; Tresadern, G.; Hillier, I.H.; *Chem. Phys. Lett.,* 1999, 310, 265

Mickelson, E. T.; Chiang, I. W.; Margrave, J. L.; *J. Phys. Chem. B: Polym. Phys.,* 1999, 103, 4318

Mills, A.; Davies, R. H.; Worsley, D.; *Chem. Soc. Rev.,* 1993, 22, 417

Murray, C. B.; Kagan, C. R.; Bawendi, M. G.; *Annual Rev. Mater. Sci.,* 2000, 30, 545

Muryn, C. A.; Hardman, P. J.; Law, D. S. L.; *Surf. Sci.,* 1991, 251–252**,** 747

Nalewajski, R. F.; Koester, A. M.; Jug, K.; *J. Mol. Catal.*, 1993, 82**,** 407

Nollen,K.; Kaden,V.; Hamann,K.; *Angew. Macromol. Chem.*, 1969, 6, 1

Nunes, S. P.; Peinemann, K.V.; Pires, A. T. N.; *J. Membr. Sci.*, 1999, 157, 219

Nussbaumer, R. J.; Caseri, W. R.; Smith, P.; Tervoort, T.; *Macromol. Mater. Eng.,* 2003, 288, 44

Nussbaumer, R. J.; Caseri, W. R.; Tervoort, T.; Smith, P.; *J. Nanoparticle Res.,* 2002, 4, 319

Ogata, N.; Kawakage, S.; Ogihara, T.; *Polymer,* 1997,38, 5115

Ohno, T.; Masaki, Y.; Matsumura, M.; *J. Catal.*, 2001, 204, 163

O'lonnell, M. J.; Boul, D.; Smalley, R. E.; *Chem. Phy. Lett.,* 2001, 342, 265

Okamoto, M.; Morita, S.; Tateyama, H.; *Polymer,* 2000, 41, 3887

Pan, J. M.; Madey, T. E.; *Catal. Lett*., 1993, 20, 269

Paz, Y.; Luo, Z.; Rabenbery, L.; Heller, A.; *J. Mater. Chem.,* 1995, 10, 2848

Peral, J.; Domenech, X.; Ollis, D. F.; *Biotechnology,* 1997, 70, 117

Park, C.; Ounaies, Z.; Clair, T. L.; St. Clair, T. L.; *Chem. Phys. Lett.,* 2002, 364, 303

Park, C. I.; Park, O. O.; Kim, H. J.; *Polymer,* 2001, 42, 7465

Park, S. J.; Cho, M. S.; Jhon, M. S.; *Macromol. Rapid Commun.,* 2003, 24, 1070

Pennewiss, J.; Hoffmam, B.; *Mater. Lett.,* 1990, 40, 219

Perruchot, C.; Khan, M. A.; Pattten, T. E.; *Langmuir,* 2001, 17, 4479

Pesty, F.; Steinrück, H. P.; Madey, T.E.; *Surf. Sci.,* 1995, 339**,** 83

Petrovicova, E.; Knight, R.; Twardowski, T. E.; *J. Appl. Polym. Sci.*, 2000, 77, 1684

Phang, Y.; Liu, T.; Hu, X.; *Polym. Int.,* 2005, 54, 456

Phillips, L. G.; Barbano, D. M.; *J. Dairy Sci.,* 1997, 80, 2726

Pillai, U. R.; Sahle-Demessie, E.; *J. Catal.*, 2002, 211, 434

Plueddemann, E. P.; Stark, G. L.; Seymour, R. B.; *Additives for Plastics,* Academic Press, New York, 1978

Poulios, I.; Spathis, P.; Tsoumparis, P.; *J. Envir. Sci. Health A,* 1999, 34, 1455

Preuss, H. P.; *Pigments in Paint*, Noyes Data Corp., Park Ridge, N. J., 1974

Prucker, O.; Ruhe, J.; *Macromolecules,* 1998, 3, 602

Qu, L.; Peng, Z. A.; Peng, X.; *Nano Lett.,* 2001,1, 333

Rademann, K.; Even, U.; Hensel, F.; *Phys. Rev. Lett.,* 1992, 69, 3208

Rao,C. N. R.; Santra, A. K.; Prins, M. W. J.; *Angew. Chem. Int .Ed. Engl.,* 1992, 31, 1062

Ray, S.; Galgali, G.; Sivaram, S.; *J. Polym. Sci. Part A: Poly Chem.*, 2005, 43, 304

Riggs, J. E.; Guo, Z.; Sun, Y. P.; *J. Am. Chem. Soc.,* 2000, 122, 5879

Rong, M. Z.; Ji, Q. L.; Friedrich, K.; *Europ. Polym. J.,* 2002, 38, 1573

Rong, M. Z.; Zhang, M. Q.; Friedrich, K.; *Polymer,* 2001A, 42, 167

Rong, M. Z.; Zhang, M. Q.; Friedrich, K.; *Polymer,* 2001B, 42, 3301

Rong, Y.; Chen, H. Z.; Wang, M.; *Mater. Chem. Phys.,* 2005, 91, 370

Safadi, B.; Andrews, R.; Grulke, E. A.; *J. Appl. Polym. Sci.*, 2002, 84, 2660

Sambi, M.; Sangiovanni, G.; Parmigiani, F.; *Phys. Rev. B,* 1996, 54, 13464

Satterfield, C. N.; *Heterogeneous Catalysis in Industrial Practice*, McGraw-Hill, New York, 1991

Sedjo, R. A.; Mirous, B. K.; Brittain, W. J.; *Macromolecules,*.2000, 33, 1492

Selhofer, H.; Muller, R.; *Thin Solid Films,* 1999, 351, 180

Sengupta, R.; Bandyopadhyay, A.; Bhowmick, A. K.; *Polymer,* 2005, 46, 3343

Schaub, R.; Thostrup, P.; Besenbacher, F.; *Phys. Rev. Lett.,* 2001, 87, 266104

Schmid, G., *Nanoparticle: From Theory to Application,* Wiley VCH, Weinheim, 2004

Shin, S.Y. A.; Simon, L. C.; Scholz, G.; *Polymer,* 2003, 44, 5317

Silveira, K. F.; Yoshida, I. V. P.; Nunes, S. P.; *Polymer*, 1995, 36, 1425

Sittig, C.; Textor, M.; Spencer, N. D.; Vallotton, P. H.; *J. Mater. Sci.,* 1999, 10, 35

Solomon, D. H.; Hawthorne, D. G.; *Chemistry of Pigments and Fillers,* John Wiley&Sons, Inc., New York, 1983

Solomon, D. H.; Swift, J. D.; Murphy, A. J.; *J. Macromol. Sci. Chem.,* 1971, 5, 587

Solomon, D.H.; *Chemistry of Organic Film Formers*, Krieger, New York, 1967

Star, A.; Stoddart, J. F.; Heath, J. R.; *Angew. Chem. Int. Ed*., 2001, 40, 1721

Stefanithis, I. D.; Mauritz, K. A.; *Macromolecules,* 1990, 23, 2397

Sugiyama, I.; Tomozuka, H.; *U.S.Patent 3642510*, 1972

Sun, Y.; Wilson, S. R.; Schuster, D. I.; *J. Am. Chem. Soc.* 2001, 123, 5348

Suryanarayana, C.; Norton, M. G.; *X-Ray Diffraction: A Practical Approach,* Plenum Press, New York, 1998

Suzuki, F.; Onozato, K.; *J. Appl. Polym. Sci.,* 1990, 39, 371

Suzuki, S.; Onishi, H.; Sasaki, T.; Iwasawa, Y.; *Stud. Surf. Sci. Catal.*, 2001, 132, 753.

Swihart, M. T.; *Cur. Opin. Colloid Interf. Sci.,* 2003, 8, 127

Te Grotenhuis, T. A.; *Chem. Abs.,* 1957, 51, 9183

Theng, B. K.G.; *Formation and Properties of Clay-Polymer Complexes*, Elsevier Scientific Pub. Co., New York, 1986

Trindade, T.; O'Brien, P.; Pickett, N. L.; *Chem. Mater.,* 2001, 13, 3843

Tsubokawa, N.; Yoshihara, T.; Sone, Y.; *Colloi. Polym. Sci.,* 1991, 269, 324

Tyan, H.; Liu, Y.; Wei,K.; *Chem. Mater.*, 1999A, 11, 1942

Tyan, H.; Liu, Y.; Wei, K.; *Polymer,* 1999B, 40, 4877

Usuki, A.; Kawasumi, N.; Kamigaito, O.; *J. Mater. Res.,* 1992A, 8, 1174

Usuki, A.; Kojima, Y.; Kamigaito, O.; *J. Mater. Res.,* 1992B, 8, 1179

Usuki, A.; Kato, M.; Kurauchi, T.; *J. Appl. Polym. Sci.,* 1997, 63, 137

Vaia, R. A.; Price, G.; Lichtenhan, *J.; Appl. Clay Sci.*,1999, 15, 67

Valden, M.; Lai, X.; Goodman, D. W.; *Science,* 1998, 281,1647

Velasco, S. C.; Martlnez, H. A. L.; Castano,V.M.; *Nanotech.*, 2002, 13, 495

Vijayakrishnan, V.; Chainani, A.; Rao, C. N. R.; *J. Phys. Chem.,* 1992, 96, 8679

Vittadini, A.; Selloni, A ; Grätzel, M.; *Phys. Rev. Lett.,* 1998, 81**,** 2954

Volokitin, Y.; Sinzig, J.; Moiseeo, I. I.; *Nature,* 1996, 384, 621

Wagner, H. D.; Lourie, O.; Tenne, R.; *Appl. Phys. Lett.,* 1998, 72, 188

Wang, B.; Wilkes, G. L.; McGrath, J. E.; *Macromolecules,* 1991, 24, 3449

Wang, K. H.; Choi, M. H.; Song, H. H.; *J. Polym. Sci B,* 2002, 40, 1454

Wang, L. Q.; Skiba, P. X.; Engelhard, M. H; *Mater. Res. Soc. Symp. Proc.,* 1997A**,** 432**,** 45

Wang, M.S.; Pinnavaia, T. J.; *Chem. Mater.,* 1994, 6, 468

Wang, R.; Hashimoto, K.; Watanabe, T.; *Nature*, 1997B, 388, 431

Wang, R.; Sakai, N.; Hashimoto, K.; *J. Phys. Chem. B*, 1999A, 103, 2188

Wang, S. X.; Wang , M.; Zhang, L. D.; *J. Mater. Sci. Lett.,* 1999B, 18, 2009

Wang, S. X.; Zhang, L. D.; Guo, T.; *Phys Lett.* 2001, 281, 59

Wang, Z.; Pinnavaia, T. J.; *Chem. Mater.*, 1998, 10, 1820

Wang, Z.; Pinnavaia, T. J.; *Chem. Mater.*, 1998, 10, 3769

Wei, Y.; Yang, D.; Tang, L.; *J.Mater. Res.,* 1992, 8, 1143

Weme, T. V.; Patten, T. E.; *J. Am. Chem. Soc.,* 1999, 121, 7409

Wolf,K.; Preuss,M.; Mager,T.; *Chem. Abs.*, 81, 122980, 1974

Wong, S. S.; Wolley, A. T.; Joselevich, E.; Cheung, C. L.; Lieber, C. M.; *J. Am. Chem. Soc.,* 1998, 120, 8557

Xiao-e, L.; Green, A. N. M.; Durrant, J. R.; *J. Photochem. Photobio. A,* 2004, 162, 253

Xu, Y.; Yao, K.; Cao, Q.; *Sens. Actuators B,* 1993, 13–14, 492

Yang, B. D.; Yoon, K. H.; *Synth. Metals,* 2004, 142, 21

Yang, Y.; Zhu, Z.; Qi, Z.; *Polymer*, 1999, 40, 4407

Yano, K.; Usuki, A.; Okada, A.; *J. Polym. Sci. A: Polym Chem.* 1997, 35, 2289

Yoshida, M.; Lal, M.; Deepark-Kumar, N.; Prasad, P. N.; *J. Mater. Sci.,* 1997, 32, 4047

Yu, X.; Xie, J.; Wang, K.; *J. Powder Sources,* 2004, 132, 181

Yu, W.W.; Qu, L.; Peng, X.; *Chem. Mater.,* 2003, 15, 2854

Zhang, H.; Banfield, J. F.; *J. Phys. Chem. B:,* 2000, 104, 3481

Zhang, J.; Jiang, D. D.; Wilkie, C. A.; *Thermochimica Acta,* 2005, 430, 107

Zhang, Z.; Henrich, V. E.; *Surf. Sci.,* 1992, 277, 263

Zhao, B.; Brittain, W. J.; *Macromolecules,* 2000, 33, 342

Zhou, Q.; Wang, S.; Mays, J.; *Langmuir,* 2002, 18, 3324

Zhou, Q.; Wang, S.; Hadjichristides, N.; *Polym. Preprints,* 2001, 42, 59

Zhu, M.; Xing, Q.; Adler, H.-J.; *Macromol. Symp.,* 2004, 210, 251

Zhu, Z.; Yang, Y.; Qi, Z.; *J. Appl. Polym. Sci.,* 1999, 73, 2063

Chapter 3 Preparation and Characterization of Modified TiO_2

3.1 Introduction

Because of their hydrophilic surface characteristics, titanium dioxide (TiO_2) particles as received (shown in Figure 12 and Figure 13) are extremely sensitive to atmospheric conditions such as moisture, insufficiently dispersed in nonpolar solvents and incompatible with hydrophobic polymers. Furthermore, TiO_2 nanoparticles have tendency to agglomerate caused by very high surface energy, by which dispersion of polymer is hindered. In addition, TiO_2 is strongly photoactive when exposed to sunlight or UV, especially in presence of moisture, which makes polymers oxidatively degrade and result in embrittlement and chalking. Hence some form of modification is first necessary step implemented in order to reduce the surface photoactivity, to alter their hydrophobic/hydrophilic character and improve their dispersibility in various media, to introduce new functional groups which can react with organic molecules and enhance their compatibility with hydrophobic polymers. The modification surfactants used widely are C_{10} to C_{18} organoacids, trialkylamine, trimethylolpropane, organosilanes, metal alkoxides, epoxides, and isocyanates.

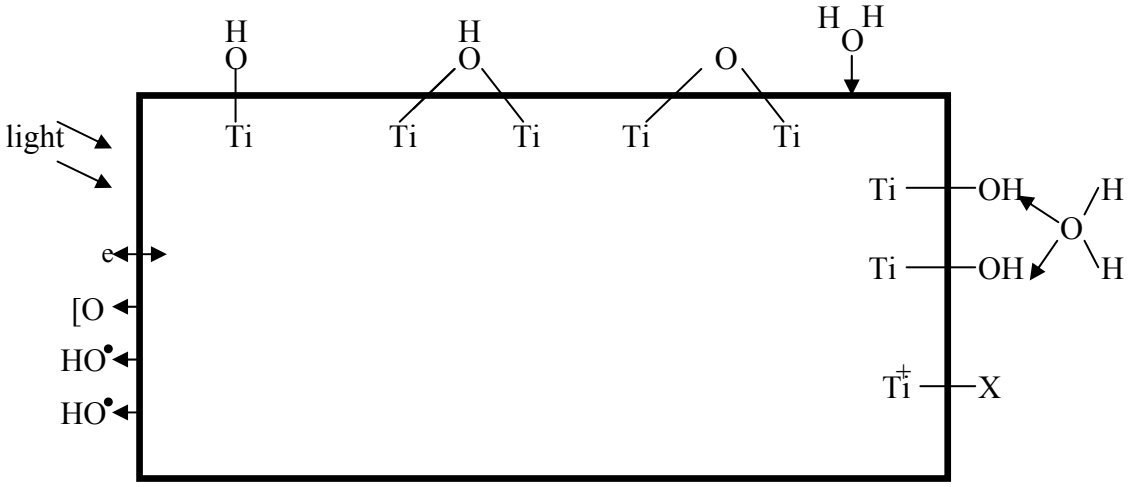

Figure 12: The principal surface features of a TiO_2 particle

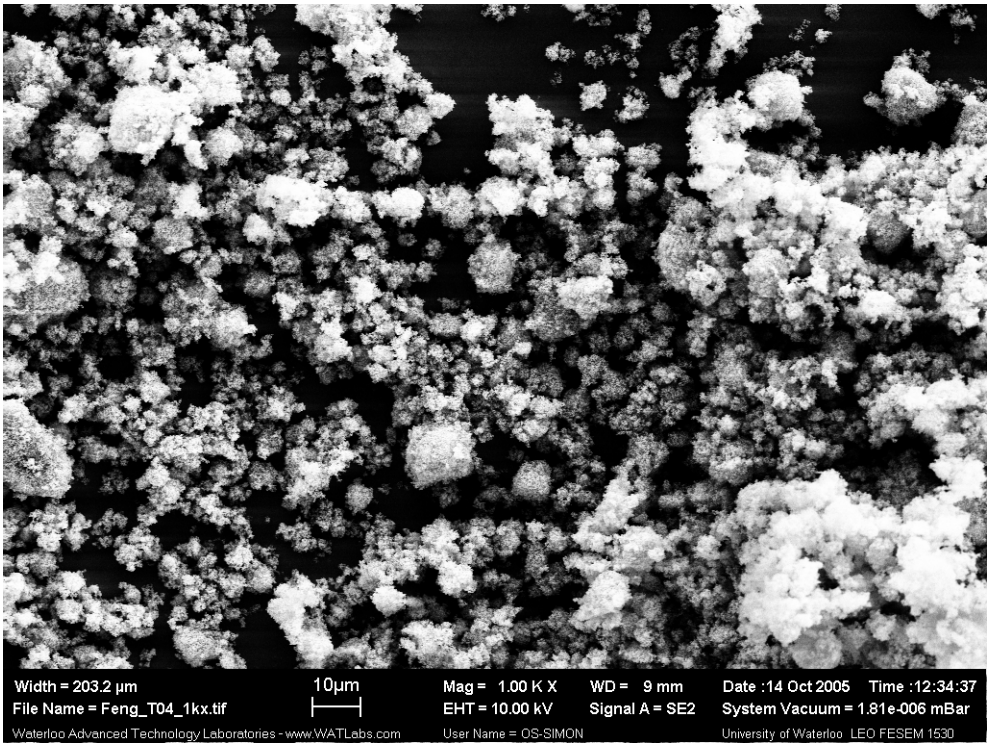

Figure 13: SEM micrograph of as-received Titanium dioxide nanopowders

In this chapter, we describe the preparation and characterization of a novel type of modified TiO_2 with increased stable dispersion in "intermediate" medium such as ethanol and weakly polar solvents such as toluene (weak Lewis base). We have used the silane coupling agent 3-trimethoxysilyl propylmethacrylate (MPS) for the modification of TiO_2. In Section 3.2 we briefly discuss the materials being used including unmodified TiO_2 and the coupling agent and describe modification and characterization experiments in details. Results are discussed in Section 3.3 and we summarize our findings in Section 3.4.

3.2 Experimental

3.2.1 Materials

Titanium dioxide nanopowder (Hydrophilic Fumed, P25) was obtained by AEROSIL and its physicochemical data are listed in Table 1. Coupling agent 3-trimethoxysilyl

propylmethacrylate (MPS) with 98% purity was purchased from Aldrich. Solvents ethanol (85%), toluene (98%), and ammonia (25%) were used as received from VWR.

Table 1: Physico-chemical data of the applied TiO_2 nanopowder

Propertites	Unit	Typical Value
Average primary particle size	nm	21
Specific surface area (BET)	m^2/g	50+/-15
Content of titanium dioxide	wt%	≥99.5%
Density	g/ml	3.9
Tapped density	g/ml	0.13
Moisture (after 2hrs at 105°C)	wt%	≤ 1.5
Ignition loss (2hrs at 1000 °C)	wt%	≤ 2.0
pH (in 4% dispersion)		3.5-4.5
Residue of sieve of 45 μm mesh	wt%	≤ 0.05

3.2.2 TiO_2 modification process

Modification of the surface of TiO_2 was carried out in a Schlenk tube connected under a condenser shown in Figure 14. The process started with dispersing of certain amount of TiO_2 as received in the solvent ethanol under 20 min ultrasonication, into which distilled water, ammonia and the coupling agent MPS were added. The mixture was then mechanically stirred at room temperature with 500 rpm for one hour. During this period MPS hydrolyzes under the influence of ammonia and water; oligomers formed are absorbed on the particle surface. Next, the mixture was heated at around 75°C for 3 h to promote the condensation reaction. After reaction the dispersion was purified from free MPS and water or ammonia by several cycles of sedimentation and redispersion of the sediment in ethanol solvent. The solvent was removed by evaporation in air overnight and then modified TiO_2 was dried at 60 °C under vacuum for 6 h.

A list of the experiments are listed in Table 2, whose label starts with the concentration of TiO_2 (T1=50 g/l, T2=20 g/l), concentration of MPS (M1=0.02 mol/l, M2=0.04 mol/l,

M3=0.08 mol/l, M4=0.16 mol/l). Other factors keep constant, volume ratio of ammonia or water to ethanol solvent is equal to 2%.

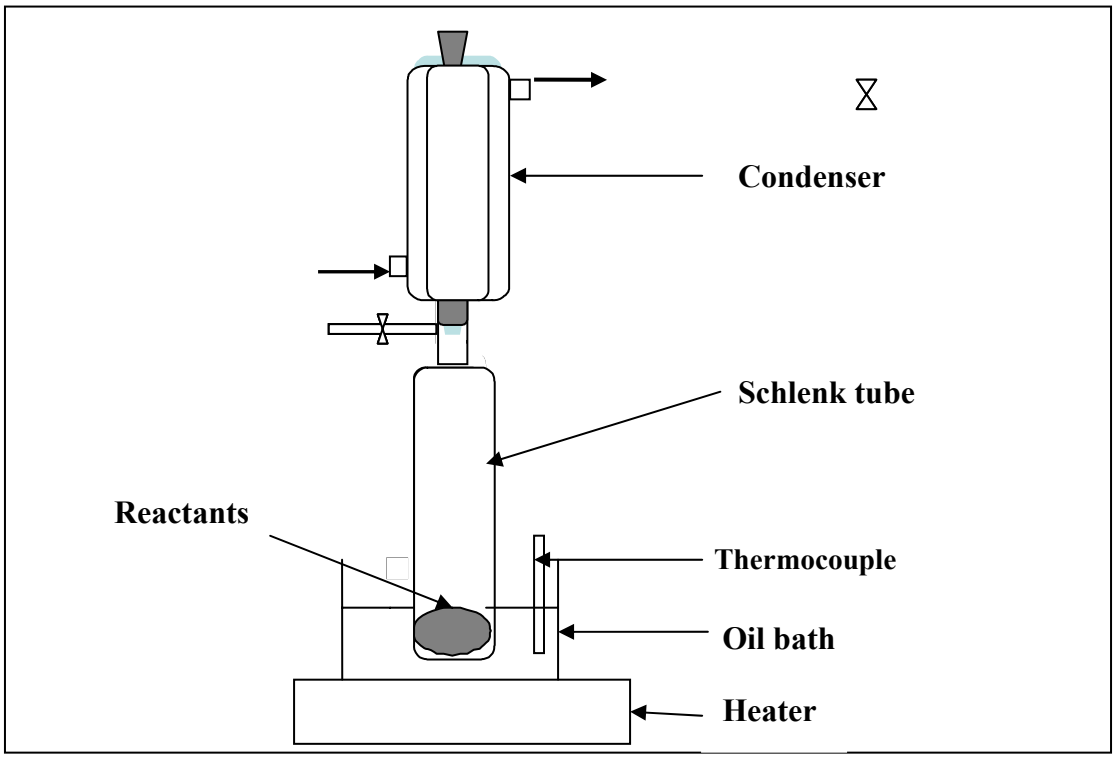

Figure 14: Experimental setup of the modification process of TiO_2

Table 2: Experimental condition for each modification run

Experiment Name	TiO_2 Concentration (g/l)	MPS Concentration (mol/l)	Temperature (^oC)	NH_4OH Content (vol%)	H_2O Content (vol%)	Label
Exp. 2	50	0.02	75	2	2	T1M1
Exp. 3	50	0.04	75	2	2	T1M2
Exp. 4	50	0.08	75	2	2	T1M3
Exp. 5	50	0.16	75	2	2	T1M4
Exp. 6	20	0.02	75	2	2	T2M1
Exp.7	20	0.04	75	2	2	T2M2
Exp. 8	20	0.08	75	2	2	T2M3
Exp. 9	20	0.16	75	2	2	T2M4

3.2.3 Physicochemical Properties and Characterization

3.2.3.1 Fourier Transform Infrared (FT-IR) Spectroscopy

It was important to verify if MPS molecules were effectively grafted at the surface of TiO_2. This was done by FT-IR measurements using a model Tesor 27 Broker spectrometer. The sample was prepared using KBr. A small amount (approximately 200 milligrams) of dried TiO_2 sample was ground separately and finely in a flat agate mortar and then intimately mixed with KBr, after which it is ground as little as possible to achieve good mixing. Adsorbed water was minimized by drying the KBr in oven at 120^oC for at least 24 h and carefully grinding it. The mixture produced in this way was introduced into a hydraulic pressing tool and pressed into pellets with 2 min holding under a pressure of 3000 psi. The spectra in transmission mode were recorded in the range from 400 to 4000 cm^{-1}, after 32 scans, with resolution of 4 cm^{-1}. Calibration of the wavenumber was automatically done by the instrument with using an internal polystyrene film. Spectra reported here were compensated from a background spectrum obtained with a blank KBr pellet.

3.2.3.2 ^{1}H-Nuclear Magnetic Resonance (^{1}H-NMR)

The quantitative grafting of MPS on the TiO_2 particles was determined by ^{1}H-NMR analysis. The measurement was conducted in a Bruker AVANCE 300 NMR spectrometer at room temperature with 16 scans by using a well-cleaned 5mm NMR tube. The sample was taken from the supernatant of two-hour, 3000 rpm centrifuging sedimentation of the suspension after modification. Dibromomethane was added as internal standard of quantification, deuterated chloroform as lock solvent and tetramethylsilane (TMS) as peak calibration reference.

3.2.3.3 Disc Centrifuge Photosedimentometer (DCP) Particle Sizer

During the preparation of modified TiO_2, The particle size distributions of the aggregates in ethanol suspensions were estimated by Disc Centrifuge Photosedimentometer (DCP) Size Analyser (Brookhaven Instruments Corporation). The TiO_2 suspension in ethanol was prepared with 0.05 g unmodified or modified TiO_2 added in 10 ml ethanol dispersing for 30 min with an ultrasonic disintegrator. While the disc was spinning at a constant speed (typically 3000 rmp), a small volume (typically 0.2 ml) of the suspension was injected onto the surface of the spin fluid, which was injected previously into the disc cavity. In order to minimize hydrodynamic shock as particle sediments radically outward, the spin fluid was typically 15 ml with an additional 1 ml of a lighter buffer fluid. In this case, a 20-40 wt% sucrose solution was chosen as spin fluid and DI-H_2O as buffer fluid. A gradient between two layers was made and maintained by using either EG (by keeping syringe pointed down, the lighter buffer liquid rose up through the denser spin fluid to make partial mixing) or BLS (either accelerating or decelerating the disc for one half second after the buffer layer had been injected onto the spin fluid) technique. After the sample was injected and particles passed through the light beam from a tungsten /halogen lamp, the transmitted light intensity was extinguished and measured by a photodiode as a function of time. Respectively particle size distribution curve was calculated and generated by the computer.

3.2.3.4 Ultraviolet/Visible Spectroscopy (UV- Vis)

The dispersibility of modified TiO_2 in a hydrophobic monomer or polymer matrix was simulated by the sedimentation characteristics of modified TiO_2 in toluene as measured with the absorbance of the samples at different sedimentation times. The toluene suspension with TiO_2 was prepared in a 20 ml vial with 0.02 g unmodified or modified TiO_2 added in 10 ml toluene dispersing for 15 min with an ultrasonic disintegrator. The sedimentation of 8 TiO_2/toluene suspensions with the same concentration was done normally at 0, 0.5, 1, 1.5, 2, 2.5, 5, and 10 min, respectively. A small volume (typically 0.5 ml) of the sample was taken from the top supernatant in the suspension at each time and injected into a quartz cell window. The absorbance of the sample was detected by wavelength 550 nm of a model Genesys 2 UV-Vis spectrometer (Milton Roy). Data reported here were subtracted from baseline correction obtained with pure toluene.

3.2.3.5 Scanning Electron Microscopy (SEM)

Study on morphology was performed with a scanning electron microscopy (SEM) (LEO 1530, LEO Electron Microscopy, Ltd.) to obtain data on dispersion and particle agglomeration. The samples were prepared by placing a small dose of unmodified and modified TiO_2/toluene suspensions on the bottom of bottles, which were done by dispersing 20mg TiO_2 in 10 ml toluene under 1h ultrasonication, over a double face adhesive conductive tape on top of the aluminum stub. After solvent has been evaporated and dried, the samples were then gold coated for 5 min to produce a film of gold approximately 15-20 nm on the sample surface. The titania nanopowders as received were also directly analyzed to identify the particle size and the degree of agglomeration.

3.3 Results and Discussions

3.3.1 Reaction Mechanism

The general formula of a silane coupling agent (SCA) is $R_{(y-n)}Si\ X_n$, which includes at least two types of functionality, where X is a hydrolysable alkoxy group and R is a

nonhydrolyzable organic radical. The 3-trimethoxysilyl propylmethacrylate (MPS) is a typical representation of such a coupling agent, whose structure is shown in Figure 15.

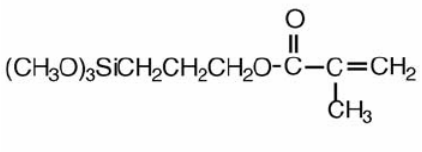

Figure 15: The structure of MPS

In addition, according to considerable pioneer works [Solomon, 1983], a metal oxide including TiO_2 has quite large amount of hydroxyl groups in its surface, with which alkoxy groups of an SCA have strong reactivity and can form covalent bonds. For this reason, the MPS coupling agent was employed to modify TiO_2 surface in this project. Figure 16 illustrates the reaction mechanism of the deposition of MPS on TiO_2 substrates as follows. First, the methoxyl groups of the MPS hydrolyze under the influence of a weak acid or base (ammonia in this case). Reactive silane triols are formed which readily associate and afterwards condense to oligomers. The oligomers adsorb rapidly and condense on the TiO_2 surface with hydroxyl groups to form Ti-O-Si covalent linkages. The actual structure formed at the surface of the nanoparticles at this stage is presently unknown. Because of the geometry and diffusion restriction, it was expected that there is only one bond form each silicon of MPS to TiO_2 surface, the remaining silanol groups are present either in condensed or free form although a distribution of species would be formed on the surface [Philipse, 1989].

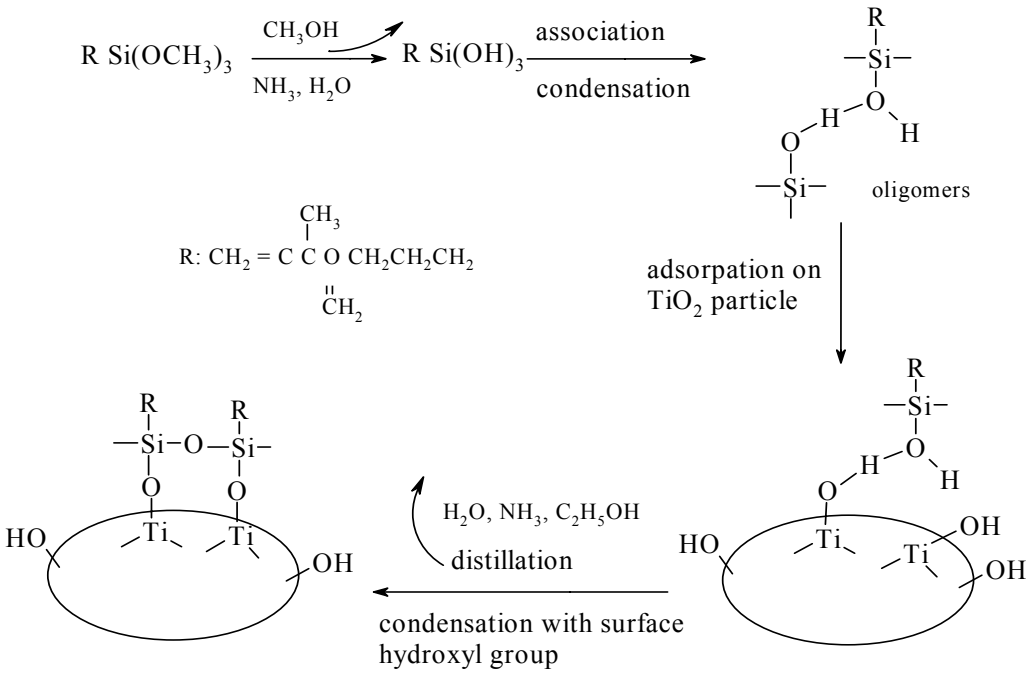

Figure 16: Deposition of MPS on a TiO_2 particle [Philipse, 1989]

We combined both the hydrolysis reaction at room temperature reported by Bourgeat-Lami [Bourgeat-Lami, 1998] and the condensation method as proposed by Philipse and Vrij [Philise, 1989] to modify the surface of nano TiO_2 particles by MPS coupling agent at elevated temperature and less reaction time in order to achieve a relatively high grafting efficiency and whereas to prevent the particles aggregation due to excess grafting density.

To keep the dispersion free from stiff white gel aggregates, we also follow and suggest the advice as follows according to our or pioneer experience of experiments. First, prolong and excessive heating which may led to MPS polymerization and the TiO_2 particles are then embedded into its matrix should be avoid and circumfluence condition could be applied. Second, very strong centrifuge force during separation procedures should also avoid since it can cause aggregation to take place in the sediment. We apply the "safe" sedimentation procedure pointed by Philipse et al. that the centrifugation speed should be controlled below 3000-4000 rpm for particles with a radius in the range 40-100 nm. Third, the change in the surface structure of modified TiO_2 leading to yellowish

discoloration may be occurred when it is exposed to rapid and long-time high temperature (especially 100^{o}C) during evaporation or drying period. Overnight air evaporation and vacuum solvent repelling under moderate temperature (60^{o}C) were employed in our operation.

3.3.2 Chemical Composition

To get evidence that MPS was chemically bonded to TiO_2 nanoparticles, FT-IR spectroscopy investigation was firstly used to identify the qualitative composition of modified TiO_2 and typical results are illustrated in Figure 17. Comparing with those of FT-IR spectra of pure TiO_2, MPS and MPS-modified TiO_2, we find that pure MPS peaks are indicated by C-H stretching bond between 2943 cm^{-1} and 2841 cm^{-1}, C=O vibration band at 1718 cm^{-1}. The Ti-O-Si transmittance peak at 1030 cm^{-1} and C=O vibration band at 1704 cm^{-1} are found for the modified TiO_2, implying the coupling agent was grafted onto TiO_2 surface by covalent chemical bonding. The shift of the C=O vibration band from 1718 to 1704 cm^{-1} comes from the formation of the hydrogen bond between the carbonyl group from MPS and the hydroxyl group on the surface of TiO_2. The peaks at 1630 cm^{-1} and 1379 cm^{-1} indicate the vinyl group which can act as the functional site for the further copolymerization [Rong, 2005; Zhu, 2004].

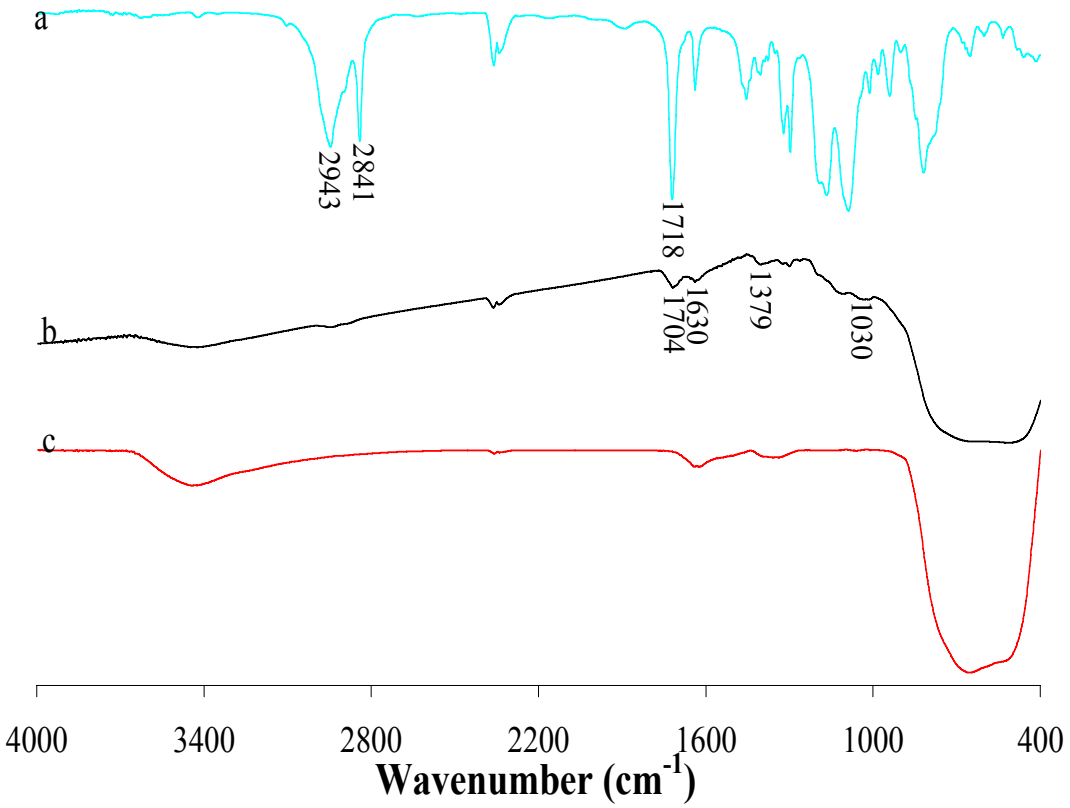

Figure 17: FTIR spectra of (a) pure MPS; (b) MPS-modified TiO_2; (c) pure TiO_2

3.3.3 Quantification of Grafting

In order to investigate the quantitative grafting of MPS on the TiO_2 surface, ^{1}H-NMR was employed to analyze the mole number of vinyl group (C=C) of MPS and sequentially to calculate the final unreacted mole number of MPS in the supernatant mixture after modification reaction. Dibromomethane was added as internal standard due to its chemical inertness and clearly distinguished chemical shift from others including MPS and solvents. One typical ^{1}H-NMR analysis spectrum is illustrated in Figure 18. The chemical shifts of Hs in the CH_2= group of MPS are located at the peaks 6.08 ppm and 5.55 ppm whereas the chemical shift of the protons in CH_2Br_2 is around 4.95 ppm.

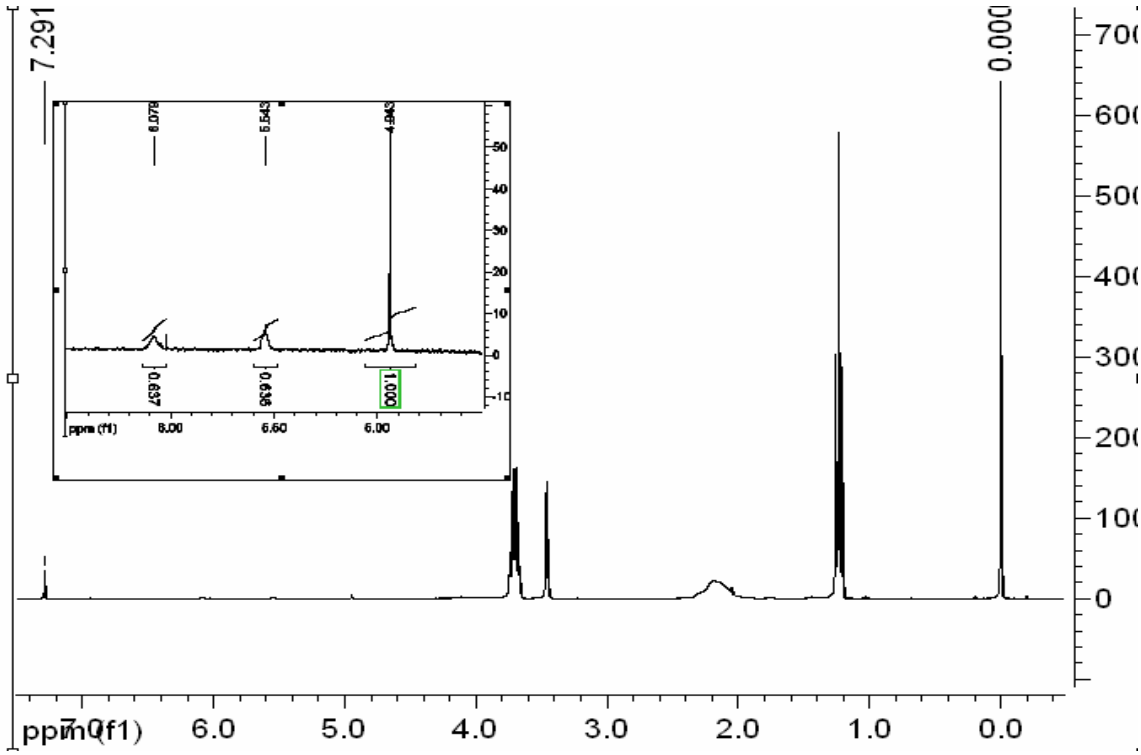

Figure 18: ^{1}H-NMR spectra of one supernatant after modification (Exp.4).

To represent the quantification of TiO_2 modification, two concepts are imported here, one of which is surface grafting density (SGD) while other surface grafting conversion (SGC). SGD is defined as the mole (molecule) number of silane coupling agent (MPS) reacted on unit square meter (or nanometer) of TiO_2 surface area, demonstrated by the following equation 3-1. SGC is defined as the percent of MPS that is added to the system that is grafted on the TiO_2 surface, expressed by equation 3-2.

$$\mathbf{SGD} = \frac{\text{Mole(or molecule)\_number\_of\_MPS\_reacted}}{\text{Area of } TiO_2 \text{ surface}}$$

$$= \frac{\text{Mole\_number\_of\_MPS\_ initial} - \text{Mole\_number\_of\_MPS\_final}}{\text{Weight of } TiO_2 \text{ used} \ * \ \text{Specific surface area of } TiO_2} \qquad \textbf{(3-1)}$$

$$\mathbf{SGC} = \frac{\text{Mole\_number\_of\_MPS\_reacted}}{\text{Mole\_number\_of MPS\_ initial}}$$

$$= \frac{\text{Mole\_number\_of\_MPS\_ initial} - \text{Mole\_number\_of\_MPS\_final}}{\text{Mole\_number\_of MPS\_ initial}} \quad \textbf{(3-2)}$$

To facilitate further calculations below, in the ^{1}H-NMR spectrum of the liquid mixture, the area under the peak around 6.1 ppm is defined as "a", the area under the peak around 5.5 ppm defined as "b", which are both correspondent to the protons of CH_2=; the area under the peak 4.95 ppm is defined as "c", which is correspondent to the protons of CH_2Br_2. The symbols representing other parameters are illustrated as follows,

W_T --------- Weight of TiO_2 used (g)

V_{M0} --------- Volume of MPS initial (ml)

V_E --------- Volume of ethanol initial (ml)

V_H --------- Volume of DI-H_2O initial (ml)

V_N --------- Volume of NH_4OH initial (ml)

V_O ---------- Volume of total liquids initial (=V_{Mo}+ V_E+ V_H+V_N)

V_S --------- Volume taken from the liquid phase after sedimentation (ml)

V_D --------- Volume of CH_2Br_2 added in V_S (ml)

ρ_D --------- Density of CH_2Br_2 (=2.477 g/ml)

ρ_M --------- Density of MPS (=1.045 g/ml)

M_{WD}--------- Molecular weight of CH_2Br_2 (=173.83 g/mol)

M_{WM}--------- Molecular weight of MPS (= 248.35 g/mol)

S_T --------- Specific surface area of TiO_2 (=50 m^2/g)

P_D --------- Number of protons in CH_2Br_2 (=2)

P_M --------- Number of protons in CH_2= (=2)

The equation 3-1 would be:

$$SGD = \frac{\left(\rho_M V_{M0} / M_{WM}\right) - \left(V_O / V_S\right)\left(P_D / P_M\right)\left((a+b)/c\right)\left(\rho_D V_D / M_{WD}\right)}{W_T S_T} 10^6\ \mu mol/m^2$$

$$= \frac{\left(\rho_M V_{M0} / M_{WM}\right) - \left(V_O / V_S\right)\left(P_D / P_M\right)\left((a+b)/c\right)\left(\rho_D V_D / M_{WD}\right)}{W_T S_T} 6.023*10^5\ \mu mol/m^2 \quad \textbf{(3-3)}$$

The Equation 3-2 would be:

$$SGC = \frac{\left(\rho_M V_{M0} / M_{WM}\right) - \left(V_O / V_S\right)\left(P_D / P_M\right)\left((a+b)/c\right)\left(\rho_D V_D / M_{WD}\right)}{\left(\rho_M V_{M0} / M_{WM}\right)} 100\% \quad \textbf{(3-4)}$$

The ^{1}H-NMR spectra were investigated at two concentrations of TiO_2 nanoparticles in ethanol: 50, 20 g/l; and four concentrations of MPS in ethanol: 0.02, 0.04, 0.08, 0.16mol/l twice individually, which are shown in Appendix A. According to equations 3-3 and 3-4, the surface grafting density and conversion of TiO_2 modified with MPS in ethanol were calculated and summarized in Table 3.

Table 3: SGD and SGC of modified TiO_2 with MPS for each experimental run

Run		W_T	V_{Mo}	V_O	V_S	V_D	a+b	c	SGD		SGC
		(g)	(ml)	(ml)	(ml)	(ml)			($\mu mol/m^2$)	($molecule/nm^2$)	(%)
	1st	0.5	0.05	10.45	5.225	0.005	1.187	1	1.65	0.994	19.6
2	2nd	0.5	0.05	10.45	5.225	0.01	0.643	1	1.08	0.654	12.9
	Ave.	0.5	0.05	10.45	5.225	0.0075	0.915	1	1.365	0.824	16.25
	1st	0.5	0.1	10.5	5.25	0.02	0.615	1	2.81	1.692	16.7
3	2nd	0.5	0.1	10.5	5.25	0.02	0.579	1	3.63	2.187	21.6
	Ave.	0.5	0.1	10.5	5.25	0.02	0597	1	3.22	1.939	19.15
	1st	0.5	0.2	10.6	5.3	0.02	1.283	1	4.41	2.657	13.1
4	2nd	0.5	0.2	10.6	5.3	0.02	1.273	1	4.64	2.79	13.8
	Ave.	0.5	0.2	10.6	5.3	0.02	1.278	1	4.525	2.724	13.45
	1st	0.5	0.4	10.8	5.4	0.02	2.737	1	4.92	2.965	7.3
5	2nd	0.5	0.4	10.8	5.4	0.02	2.743	1	4.78	2.883	7.1
	Ave.	0.5	0.4	10.8	5.4	0.02	2.74	1	4.85	2.928	7.2
	1st	0.2	0.05	10.45	5.225	0.01	0.669	1	1.97	1.188	9.4
6	2nd	0.2	0.05	10.45	5.225	0.01	0.686	1	1.49	0.897	7.1
	Ave.	0.2	0.05	10.45	5.225	0.01	0.678	1	1.73	1.042	8.25
	1st	0.2	0.1	10.5	5.25	0.02	0.683	1	3.15	1.896	7.5
7	2nd	0.2	0.1	10.5	5.25	0.02	0.675	1	3.60	2.171	8.6
	Ave.	0.2	0.1	10.5	5.25	0.02	0.679	1	3.375	2.034	8.05
	1st	0.2	0.2	10.6	5.3	0.02	1.398	1	4.47	2.693	5.3
8	2nd	0.2	0.2	10.6	5.3	0.02	1.393	1	4.76	2.865	5.7
	Ave.	0.2	0.2	10.6	5.3	0.02	1.395	1	4.635	2.779	5.5
	1st	0.2	0.4	10.8	5.4	0.02	2.871	1	4.67	2.81	2.8
9	2nd	0.2	0.4	10.8	5.4	0.02	2.859	1	5.35	3.224	3.2
	Ave.	0.2	0.4	10.8	5.4	0.02	2.865	1	5.01	3.017	3.0

The results from Table 3 clearly indicate that MPS coupling agent is indeed active in chemically grafting on nano-TiO_2 surface to some extent, which is in agreement with those of FT-IR spectra, even though the grafting rate is relatively low and different among every different experiment run condition depending on concentration change of two reactants. Corresponding to Table 3, SGD as function of concentration of MPS was illustrated in Figure 19 and SGC as function of concentration of MPS in Figure 20 respectively.

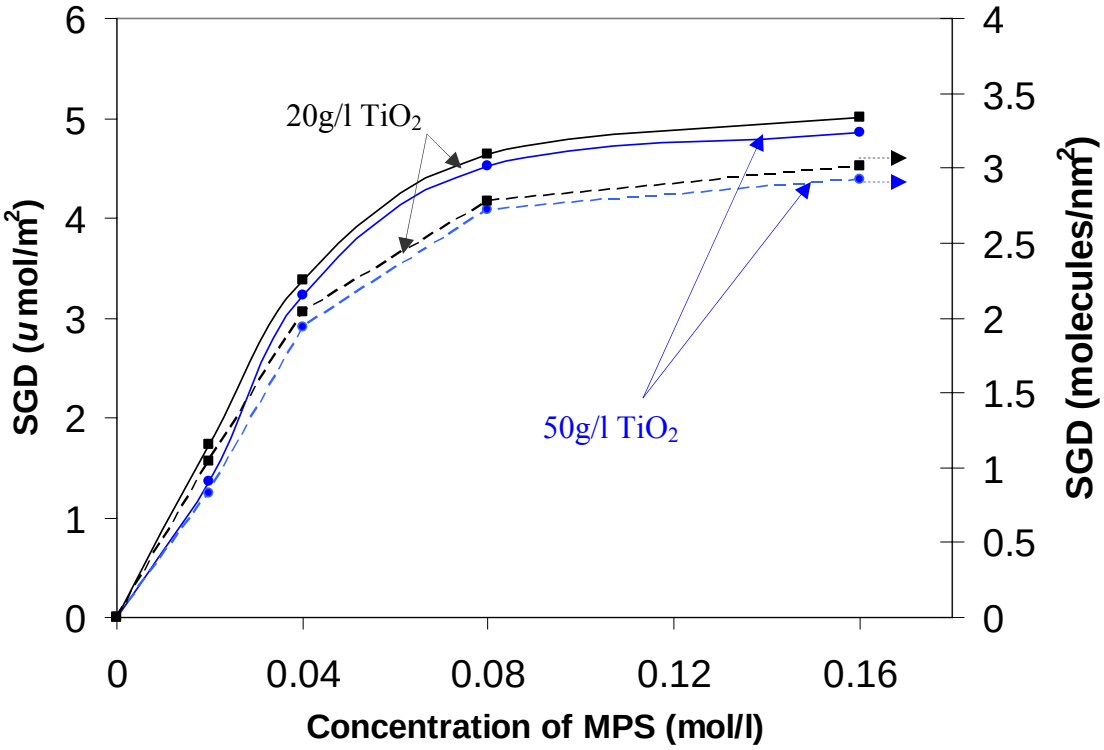

Figure 19: Surface grafting density vs Concentration of MPS in ethanol

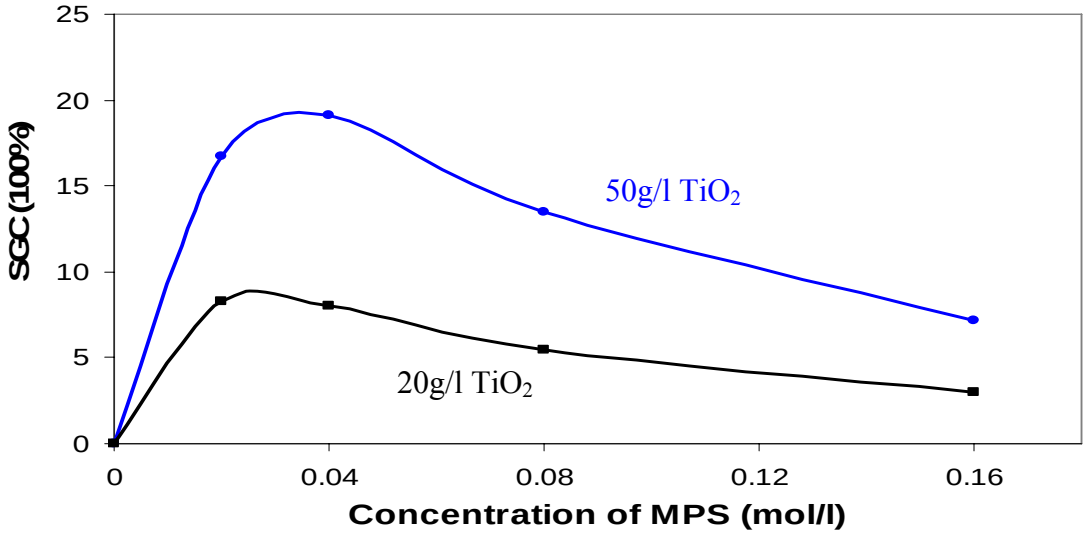

Figure 20: Surface grafting conversion vs Concentration of MPS in ethanol

At a closer look, the reaction kinetics in this system is not quite simple and the effect of concentrations of two reactants is mutual but nonequal on the grafting density and efficiency. Let us first only consider the relationship of concentration of MPS and the grafting quantification analysis. From the curves in Figure 19, regardless of what concentration of TiO_2, the surface grafting density increases with increasing concentration of MPS but level off when it reach 0.08 M in ethanol. For example, at the curves of 20 g/l TiO_2, the SGD is 4.635μmol/m^2 or 2.779 molecules/nm^2 with MPS concentration at 0.08 M; very little increase to 5.01 μmol/m^2 or 3.017 molecules/nm^2 when MPS concentration is double to 0.16 M. These phenomena may suggest that MPS concentration at 0.08 M is near to the most optimal reaction concentration and the increase in MPS concentration does not affect significantly the improvement of the SGD.

On the other hand, if we look at the curves in Figure 20, the grafting conversion first increases at low MPS concentration, then reaches its maximum value with MPS concentration at between 0.02 M and 0.04 M, finally decreases at higher concentration of MPS, which also demonstrates that this grafting reaction is not complete but equilibrium with relatively low conversion and increased free MPS does not really take part in grafting with increasing MPS addition.

The effect of TiO_2 concentration on the surface grafting efficiency was also invesitaged. SGD and SGC as function of concentration of TiO_2 are illustrated in Figure 21 and in Figure 22 respectively.

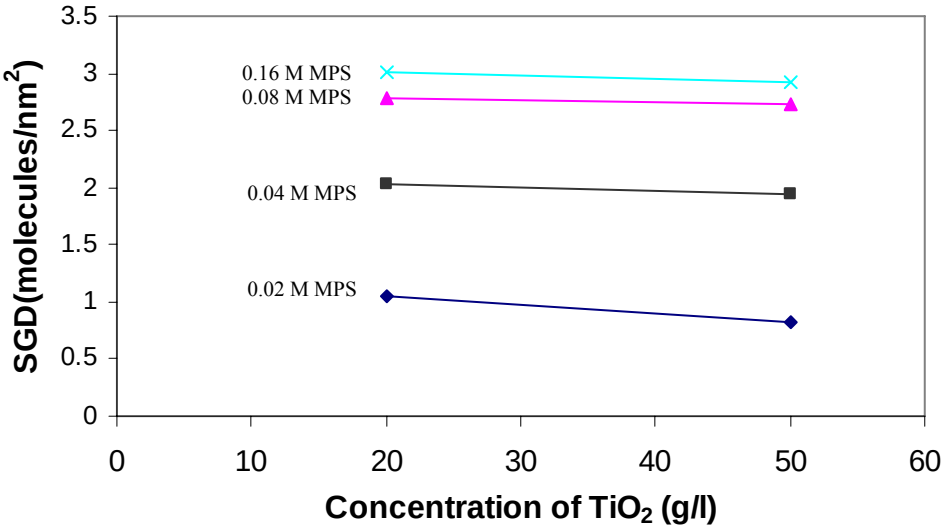

Figure 21: Surface grafting density vs Concentration of TiO_2 in ethanol

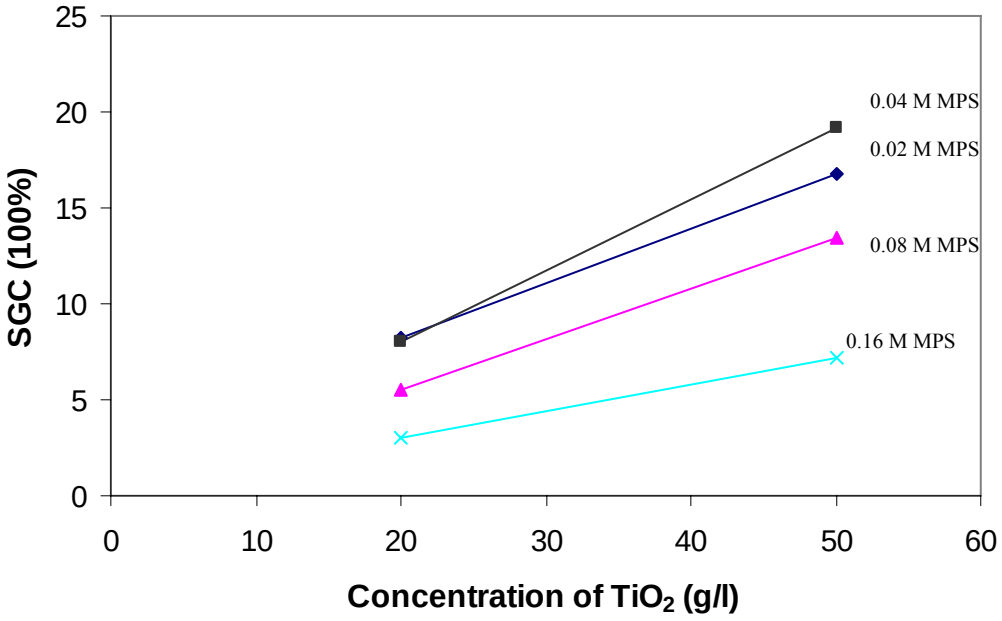

Figure 22: Surface grafting conversion vs Concentration of TiO_2 in ethanol

According to the curves in Figure 21, we find that the SGD slightly decreases with the increasing TiO_2 concentration in ethanol, in all the range of concentrations of MPS. However, the surface grafting conversion somehow increases when the concentration of TiO_2 becomes greater in the solvent, regarding to the curves in Figure 22.

Furthermore, it is also possible find out a suitable reaction concentration of both reactants from the following SGD or SGC curves as function of their weight ratio displayed respectively in Figure 23 and Figure 24. The weight ratio represented here is the weight of MPS over the weight of TiO_2 in the system.

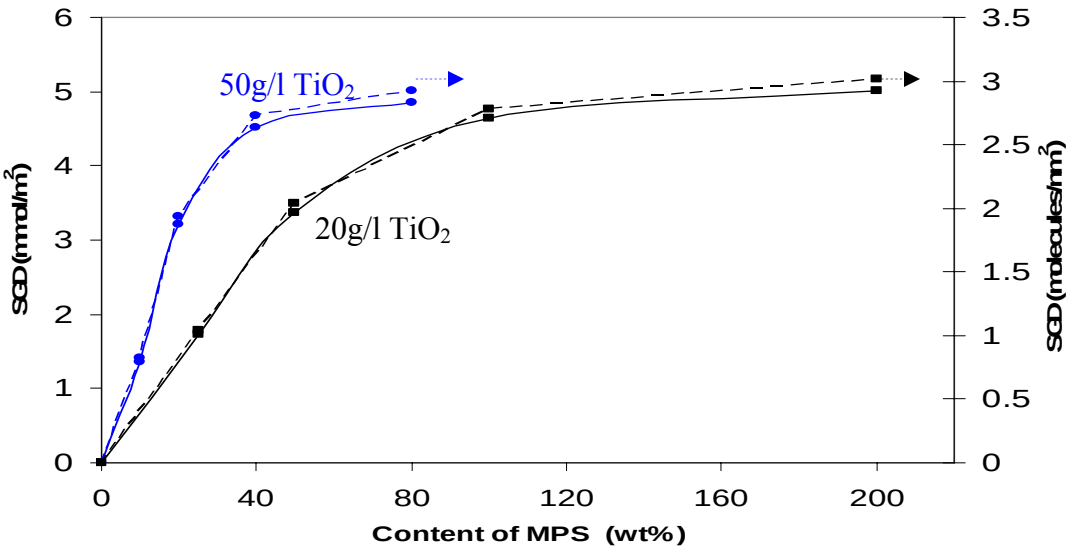

Figure 23: Surface grafting density vs Weight ratio of MPS over TiO_2

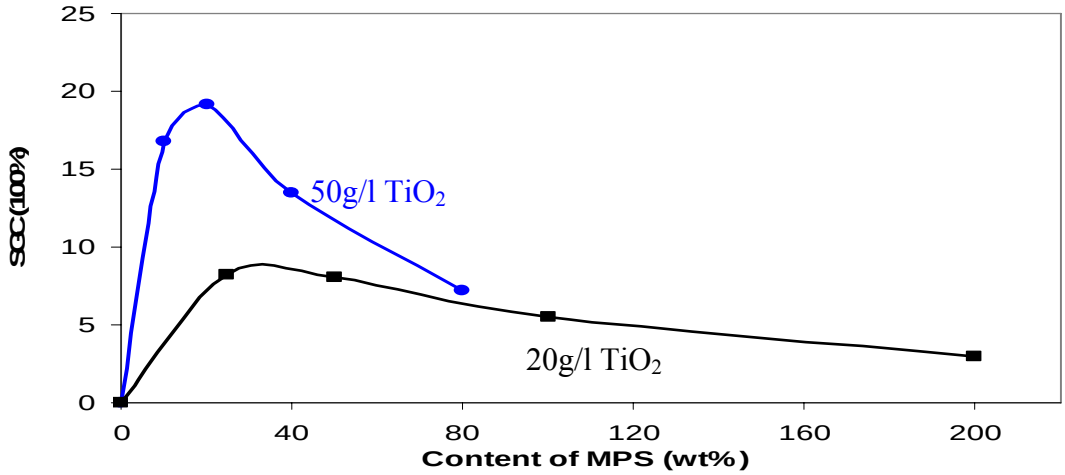

Figure 24: Surface grafting conversion vs Weight ratio of MPS over TiO_2

It is clear that the curves for 50 g/l TiO_2 have steeper slops than those for 20 g/l TiO_2 and either SGD or SGC for the curve of 50 g/l is higher than that for 20 g/l at the same weight ratio of MPS over TiO_2. At the curve of 50 g/l TiO_2 in Figure 23, the SGD is first increased at relatively steeper slop to 4.525 μmol/m^2 or 2.724 molecules/m^2 with the increasing weight ratio of MPS over TiO_2 up to 40 % (i.e. MPS concentration at 0.08 M), then much slightly increased to 4.85 μmol/m^2 or 2.928 molecules/m^2 when MPS weight percent is multiplied to 80%. Whereas, from the of 50 g/l TiO_2 in Figure 24, the SGC become greater at low weight ratios, reaches the maximum value at 20 wt% (i.e. MPS concentration at 0.04 M), then reduces at high weight ratio of MPS over TiO_2 . From the view of considering the economic cost, these results could demonstrate that TiO_2 concentration at 50 g/l and MPS concentration at 0.08 M (Exp. 4) in ethanol are close to the most appropriate reaction concentration for the highest SGD, and TiO_2 concentration at 50 g/l and MPS concentration at 0.04 M (Exp. 3) in the solvent are nearly the most appropriate for the highest SGC.

3.3.4 Particle Size Distributions

As mentioned earlier, titanium dioxide nanopowder as received is hydrophilic and has strong tendency to form the state of agglomeration in nonaquous media. The size of these agglomerated particles is larger than the nanoscale. In order to improve dispersion ability of TiO_2 nanoparticles in the polymer matrix, it is important to reduce the particle size as much as possible before polymerization. It is also commercially significant to stabilize this suspension of nanomers in a nonaquous solvent. It was expected that the grafted coupling agent MPS formed an organic layer on the inorganic TiO_2 nanoparticle surface which could serve as the compatibilizer for an intermediate medium such as ethanol or a weakly polar medium. To get these evidences we used BI-DCP particle sizer to measure and compare the particle size distributions of unmodified TiO_2 and modified TiO_2 with above different experimental run conditions only in ethanol solvent due to instrumental limitations.

Figure 25 represents typical examples of unmodified and modified TiO_2 particle size distribution analyzing curves measured by BI-DCP. It is possible to find that TiO_2 as received has much broader and bigger size distribution in ethanol than modified TiO_2. Sizes of unmodified TiO_2 in ethanol with certain amount of fraction ranging from 200 nm to 2.5 μm while 90% of modified TiO_2 particles are distributed in the narrower size range of 500 nm to 100nm.

In order to demonstrate how the initial concentration of two reactants affects the average size of modified TiO_2, we investigated the weight average size of the aggregates in suspension for two concentrations of TiO_2, five concentrations of MPS (0, 0.02, 0.04, 0.08, 0.16 mol/l) by BI-DCP, for three different times. The data are being read from the BI-DCP curves in Appendix B and summed in Table 4. In addition, Figure 26 shows the resulting two curves (50 g/l or 20 g/l TiO_2) correlating average particle size as a function of concentration of MPS.

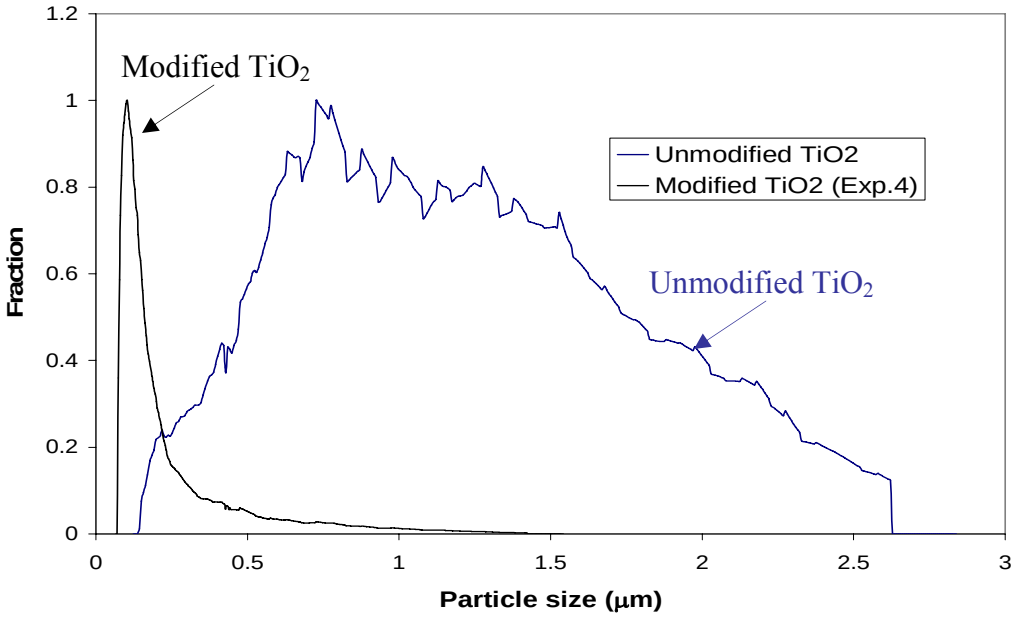

Figure 25：Typical size distribution curves of unmodified and modified TiO_2

Table 4: Weight average size of aggregates in ethanol suspension at different concentrations of MPS and TiO_2

MPS : TiO_2 (mol/l): (g/l)	Weigth Ratio	Ave. D. (nm)	Mean D. (nm)	St. Dev. (nm)
0	0	1248 1236 1234	1239	8
0.02: 50	1:10	359 429 440	409	44
0.04: 50	2:10	388 349 328	355	30
0.08:50	4:10	225 248 269	247	22
0.16:50	8:10	239 253 247	246	7
0.02: 20	2.5:10	275 349 357	327	45
0.04:20	5:10	256 270 309	278	27
0.08: 20	10: 10	258 259 264	260	3
0.16:20	20:10	194 192 192	193	1

Ave. D.: Weight average diameter of the particles measured from BI-DCP;
Mean D.: Mean diameter by calculation from the samples with repeated experiments
St. Dev.: Standard deviation of mean. D.

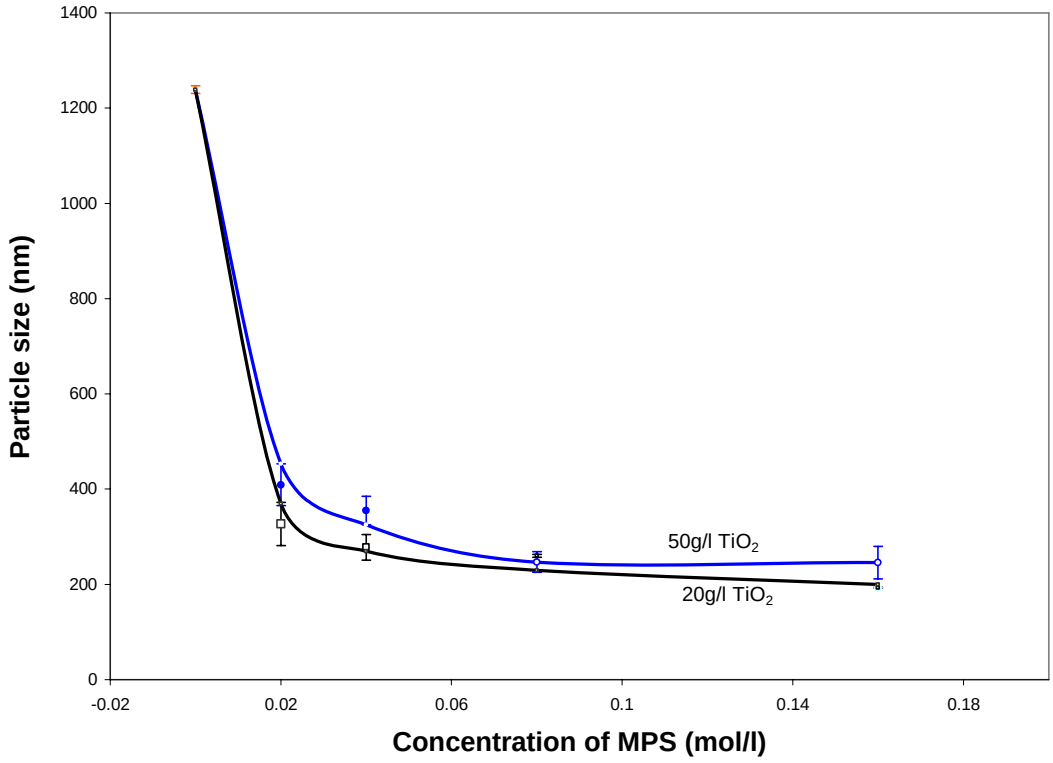

Figure 26: Weight average size of modified TiO_2 vs concentration of MPS

According to the curves in Figure 26, regardless of 50 g/l or 20 g/l of TiO_2, the weight average size of modified TiO_2 decreases dramatically at first when small amount of concentration of MPS is added to react with them. Small changes in particle size are observed with increasing concentration of MPS in ethanol. Taking the curve of 20g/l TiO_2 for example, compared with the 1239 (+/-8) nm average size of unmodified TiO_2, the size of modified TiO_2 with initial MPS concentration at 0.02 M is significantly reduced to 327(+/-45) nm; very little decreased to 278(+/-27) nm, 260(+/-3) nm, 193(+/-1) nm when MPS concentration is double to 0.04, 0.08, 0.16 M each time. This may point out that even at low concentrations MPS is active in decreasing the size of modified TiO_2 in the solvent ethanol.

From these curves we can also see that the initial concentration of TiO_2 has a small effect on average size of the aggregates in ethanol suspension. When the MPS concentration is fixed, the size of modified TiO_2 slightly decreases with decreasing initial concentration of

the TiO_2 reactant. For instance, at the same 0.02 M concentration of MPS, the size of modified TiO_2 is 409(+/-44) nm at 50 g/l initial concentration of TiO_2, while its size being 327(+/-45) nm at 20 g/l.

Similarly, we can draw the average size of unmodified and modified TiO_2 particles in ethanol as function of weight ratio of MPS over TiO_2 initially, which is shown in Figure 27. As result of this curve, we find out that TiO_2 concentration at 50 g/l and MPS concentration at 0.08 M in ethanol (Exp. 4) are adequete reaction concentration for obtainieng the smallest average size of the aggregate, implying the best dispersibility in the intermediate media such as ethanol.

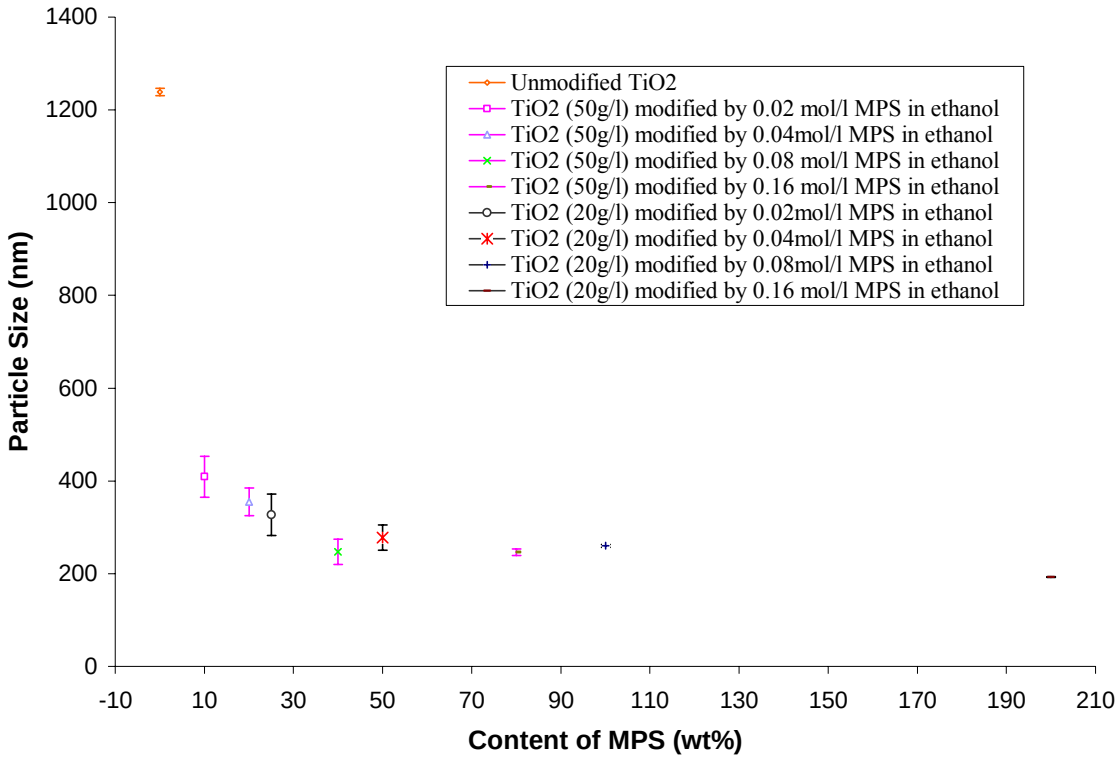

Figure 27: Weight average size vs Weight ratio of MPS over TiO_2

If we correlate between the particle size of the aggregates in ethanol and the surface grafting density of MPS on TiO_2, represented in Table 5, we could see that the size of modified TiO_2 in ethanol is inversely proportional to the SGD. When the SGD increases, the particle size of modified TiO_2 in suspension (ethanol) decreases. This also means that

the dispersibility of modified TiO_2 increases with increasing SGD of MPS on TiO_2 surface.

Table 5: Correlation between weight average size of aggregates in ethanol suspension and the surface grafting density of MPS on TiO_2

Particle Size (nm)	SGD (molecules/nm^2)
1293 +/-8	0
409 +/- 44	0.824
327 +/- 45	1.042
355 +/- 30	1.939
278 +/- 27	2.034
247 +/- 22	2.724
260 +/- 3	2.779
246 +/-7	2.928
193 +/-1	3.017

3.3.5 Dispersibility Test

The dispersion of nanoparticles within a nonpolar organic monomer or polymer matrix is relatively difficult and costly to obtain. In order to simulate the dispersibility of TiO_2 in a monomer or polymer, the sedimentation of TiO_2 in toluene was introduced by using toluene as the substitute of styrene monomer or polystyrene. Some basic properties of toluene, styrene and polystyrene are shown in Table 6.

Table 6: The basic properties of toluene, styrene and polystyrene at 25^{o}C [Zhu, 2004]

Property	Toluene	Styrene	Polystyrene
Polarity (Snyder)	2.4	~2.5	2.2-2.6
Density (g*cm^{-3})	0.865	0.909	~1.05
Rheological behavior	Mucous (liquid)	Mucous (liquid)	Viscous (melt)

To establish whether the MPS-modified TiO_2 was more stable in toluene we firstly used visual inspection to observe and compare the stability of the unmodified and modified titania suspension in toluene. The toluene solutions of both (a) as-received and (b) MPS-modified TiO_2 nanoparticles in Experiment run 4 were treated in an ultrasonic bath for 1 hr. A photograph of vials with both materials is shown in Figure 28: (a) unmodified TiO_2 in toluene; (b) modified TiO_2 by MPS in toluene. The unmodified TiO_2 particles did not form a suspension stable in toluene (Figure 28-a) and precipitated quite quickly (less than a few seconds) even after the vial had been exposed for 1 h ultrasonication. A homogeneous suspension was observed in the modified TiO_2 nanoparticles (see vials in Figure 28-b) for a longer time (tens of minutes). But compared with the modified TiO_2 in ethanol which did not sediment noticeably within several hours, the titania in toluene settled into a gel like layer which could be redispersed upon shaking.

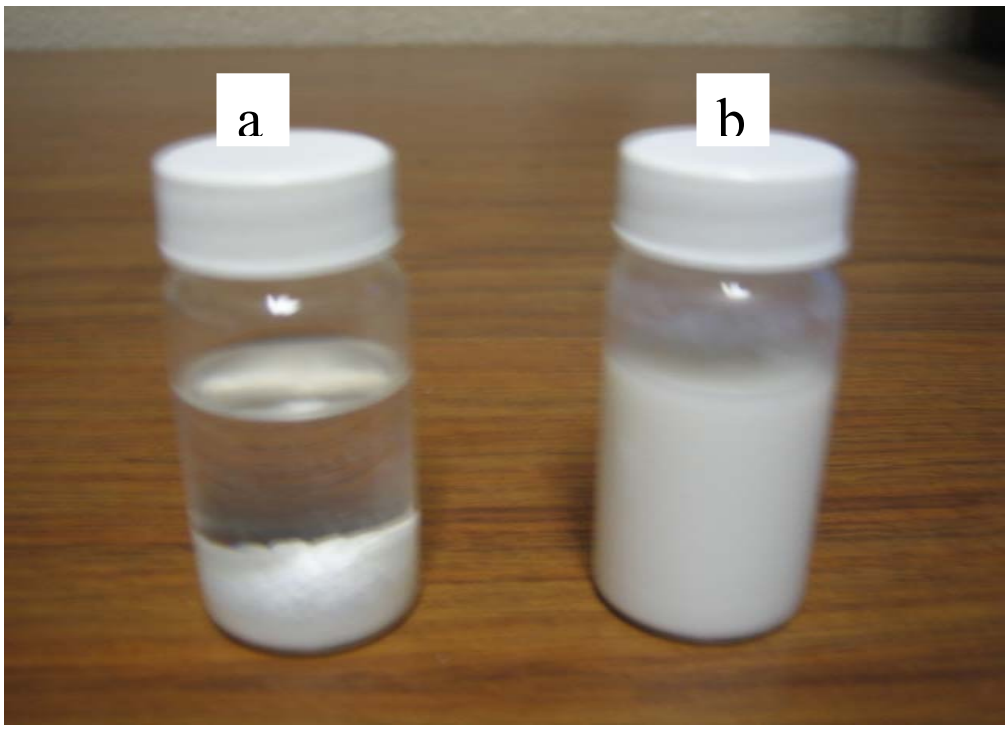

Figure 28: (a) unmodified TiO_2 in toluene; (b) modified TiO_2 by MPS in toluene

All pictures were taken right after 1hr ultrasonic

The morphology of unmodified and modified TiO_2 particles dispersed in toluene was observed by SEM. The unmodified TiO_2 particle agglomerated severely in toluene as shown in Figure 29(a) and separate particles cannot be distinguished. However, the modified TiO_2 particles shown in Figure 29(b) showed different degree of agglomeration; within the agglomerated areas, clear contours are visible between the TiO_2 particles. This indicates that the modified TiO_2 particles are easier to disperse in the weakly polar media.

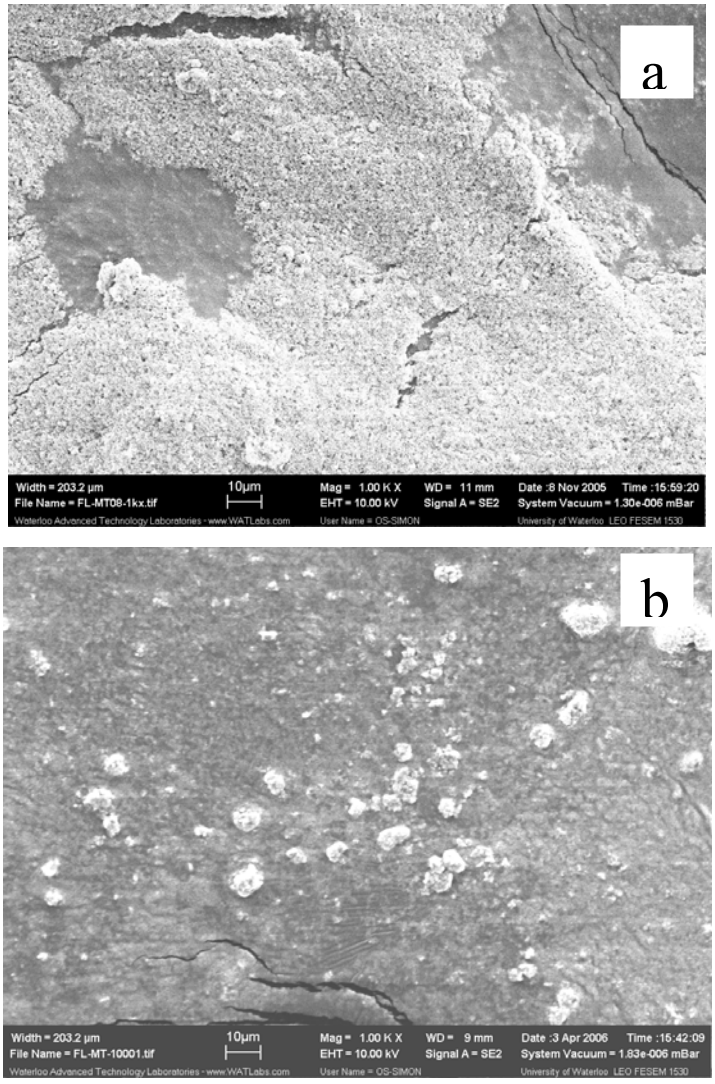

Figure 29: SEM images of (a) unmodified TiO_2; (b) modified TiO_2 (Exp.4) in toluene

In addition, in order to quantify these observations, UV-Vis spectroscopy was also employed to detect the absorbance reduction in the single wavelength 550 nm. Figure 30

shows the absorbance of the TiO_2/toluene suspension as function of the sedimentation time. As the lower the sedimentation speed (as the slower the absorbance reduction), the better the TiO_2 are dispersed in the toluene solvent [Zhu, 2004].

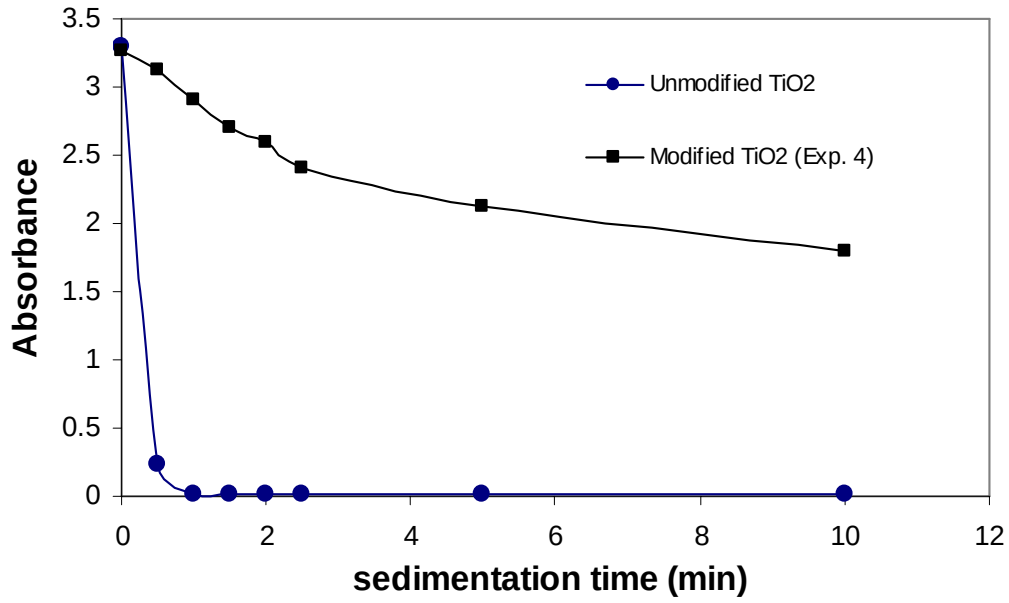

Figure 30: Absorbance of 550nm vs sedimentation time of the suspension

3.4 Summary

We have developed an adequate procedure for the modification of TiO_2 with a silane coupling agent 3-trimethoxysilyl propylmethacrylate in a weak base alcohol at elevated temperature. The grafting of vinyl groups was based on the hydrolysis and condensation reactions between methoxyl groups of the coupling agent and hydroxyl groups on TiO_2 surface to form chemically-bonded Ti-O-Si linkage. This surface grafting reaction was also quantified and it could be seen that initial TiO_2 concentration at 50 g/l and MPS concentration at 0.08 M in ethanol are close to the most adequate reaction concentration for the highest surface grafting density, and TiO_2 concentration at 50 g/l and MPS concentration at 0.04 M in the solvent are nearly the most adequate for the highest grafting conversion.

We also found out that the grafting of the silane coupling agent was effective to modify the surface properties of TiO_2 nanoparticles from hydrophilic to hydrophobic character with decreased average aggregate size in the suspension of ethanol and improved dispersibility in the weakly polar media. The average size of modified TiO_2 in ethanol was decreased to the range of 200 nm to 400 nm depending on the density of the silane grafting on the surface, in comparison with more than 1200 nm average of unmodified TiO_2. In addition, the "severe agglomeration" state of compactly assembled unmodified TiO_2 particles in nonpolar media was replaced by a "light agglomeration" of TiO_2 particles. However, the average aggregate size (~ 200 nm) of modified TiO_2 even in the most optimal condition was still considerably larger than the size of individual TiO_2 nanopowders (~ 21 nm), implying that only an aggregate of nanopowders was obtained at this stage.

3.5 References

Baurgeat-Lami, E. B.; Lang, J.; *J. Colloid Interf. Sci.*, 1998, 197, 293

Philipse, A. P.; Vrij, A.; *J. Colloid Interf. Sci*., 1989, 128, 121

Rong, Y.; Chen, H. Z.; Wu, G.; Wang, M.; *Mater. Chem. Phys*., 2005, 91, 370

Solomon, D.H.; *Chemistry of Organic Film Formers*, Krieger, New York, 1967

Zhu, M.; Xing, Q.; He, H.; Zhang, Y.; Chen, Y.; Potschke, P.; Adler, H.-J.; *Macromol. Symp.*, 2004, 210, 251

3.6 Appendix

3.6.1 ^{1}H-NMR Spectra

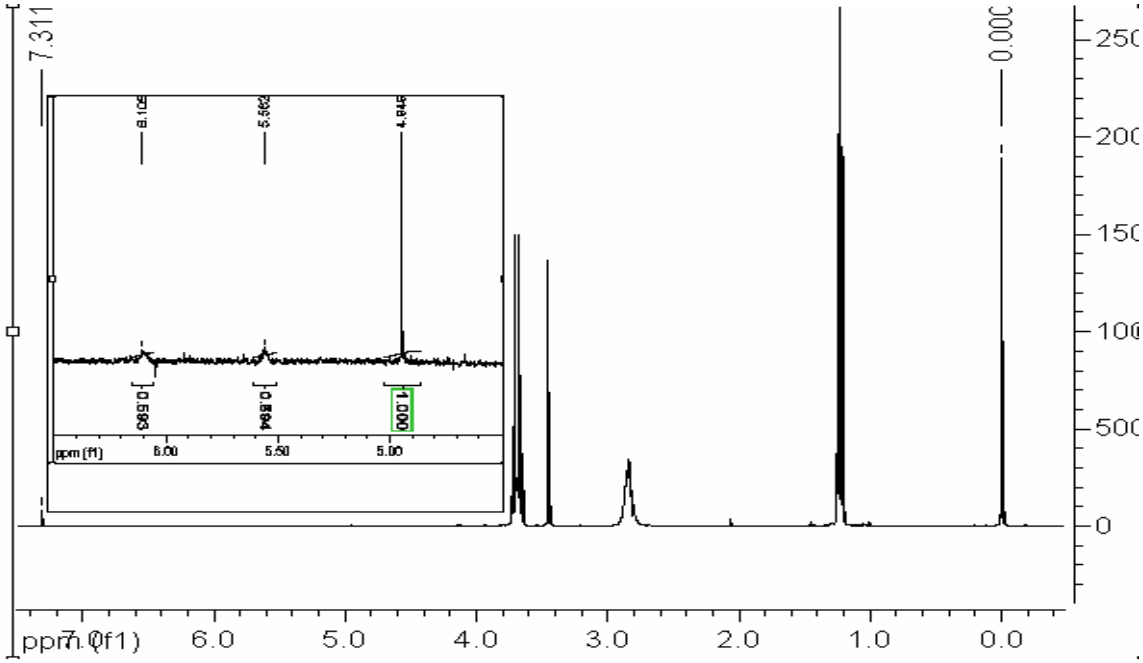

Figure 31: 0.5g TiO_2 modified by 0.05ml MPS (1st Exp. 2), 0.005ml CH_2Br_2

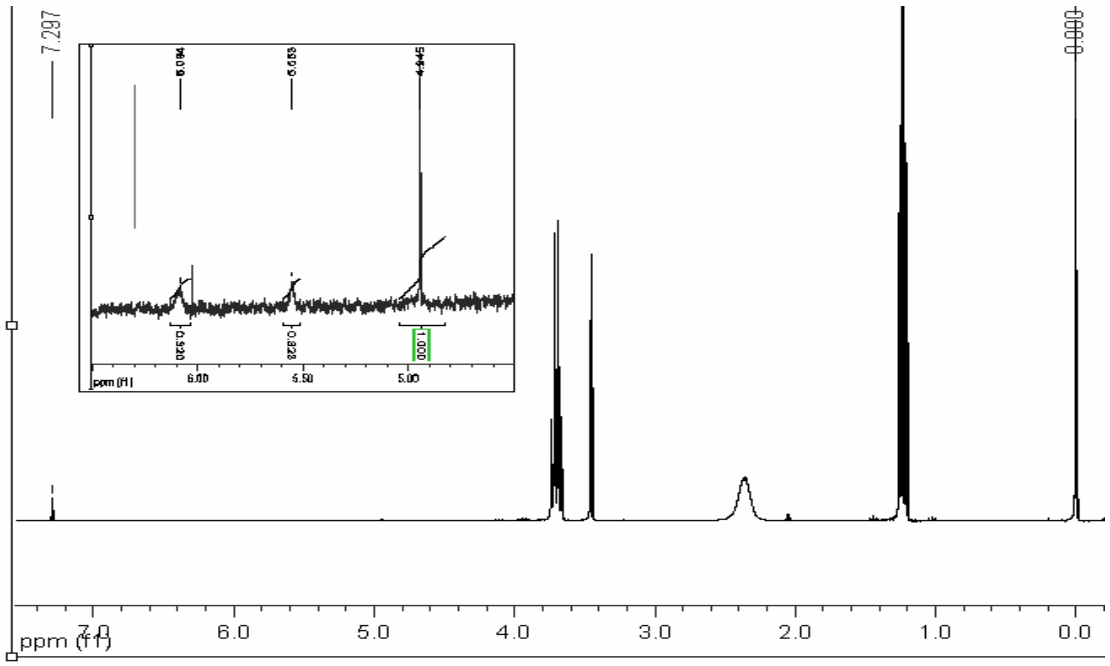

Figure 32: 0.5g TiO_2 modified by 0.05ml MPS (2nd Exp. 2), 0.01ml CH_2Br_2

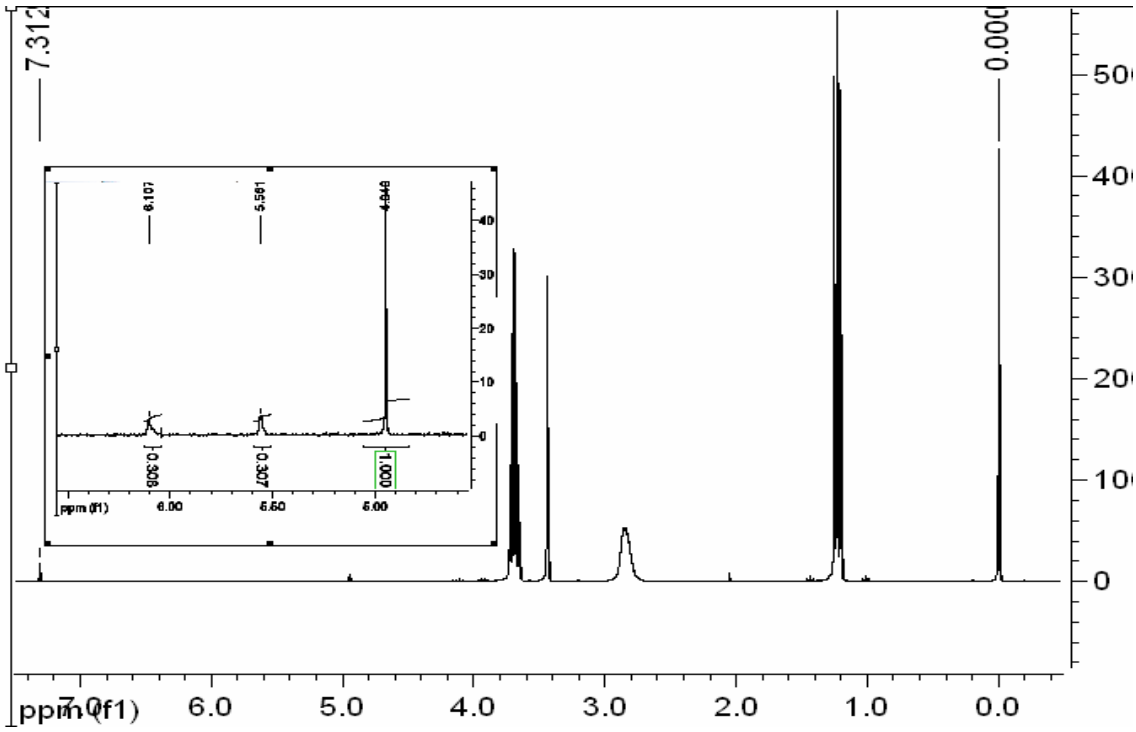

Figure 33: 0.5g TiO_2 modified by 0.1ml MPS (1st Exp. 3), 0.02ml CH_2Br_2

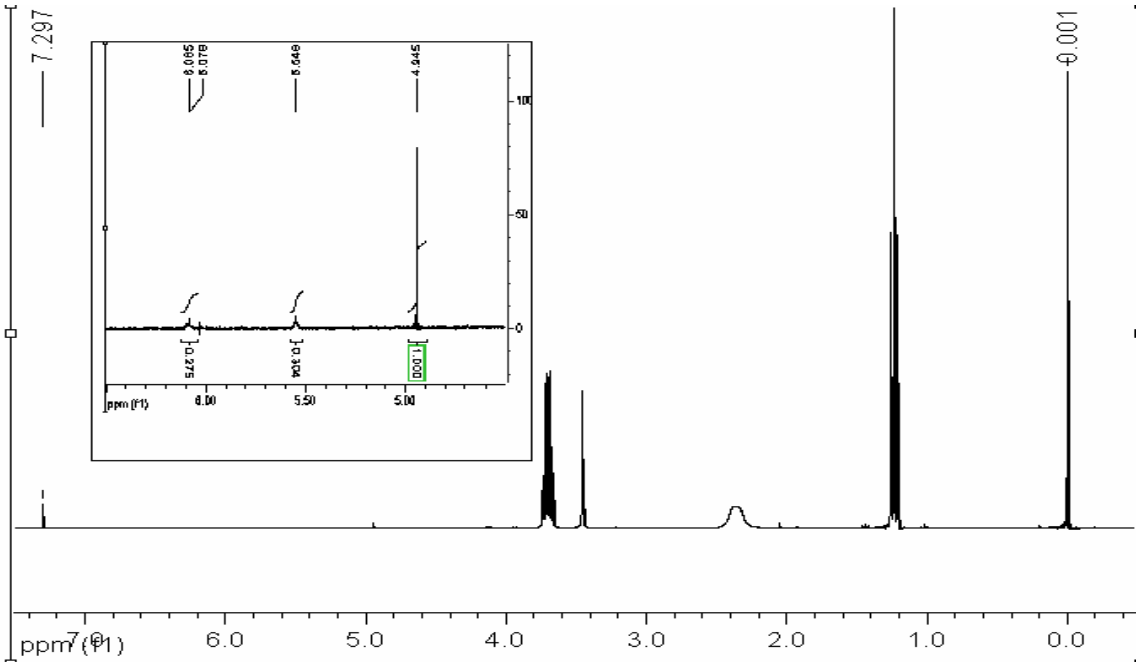

Figure 34: 0.5g TiO_2 modified by 0.1ml MPS (2nd Exp. 3), 0.02ml CH_2Br_2

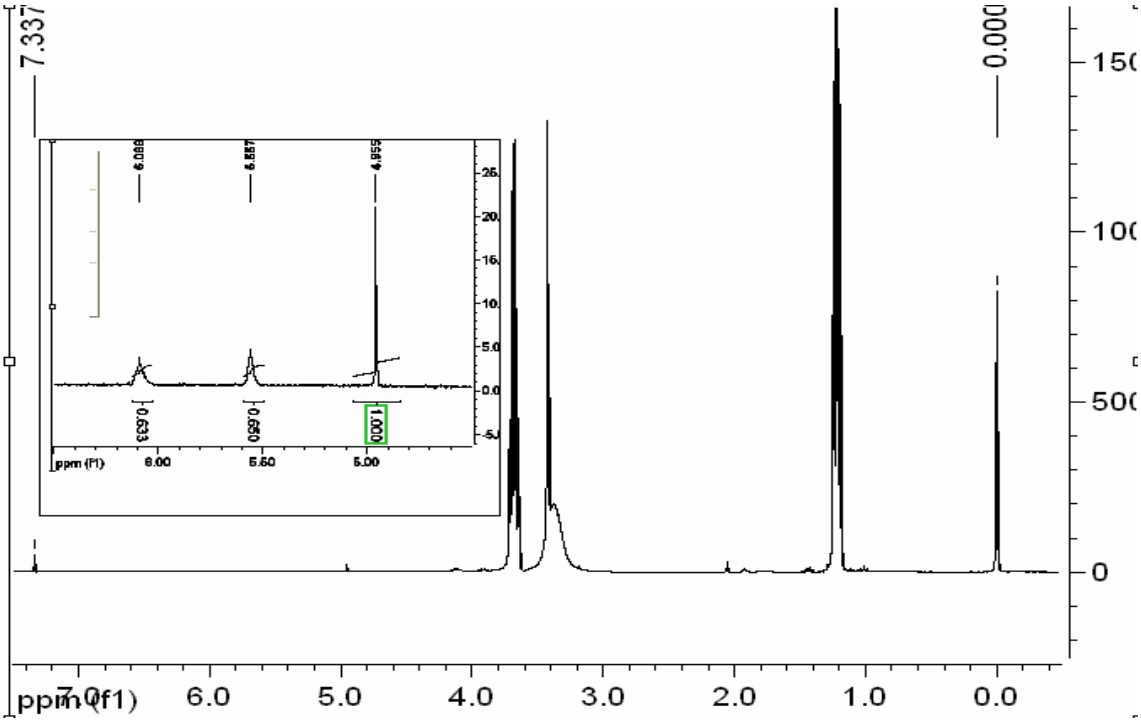

Figure 35: 0.5g TiO_2 modified by 0.2ml MPS (1st Exp. 4), 0.02ml CH_2Br_2

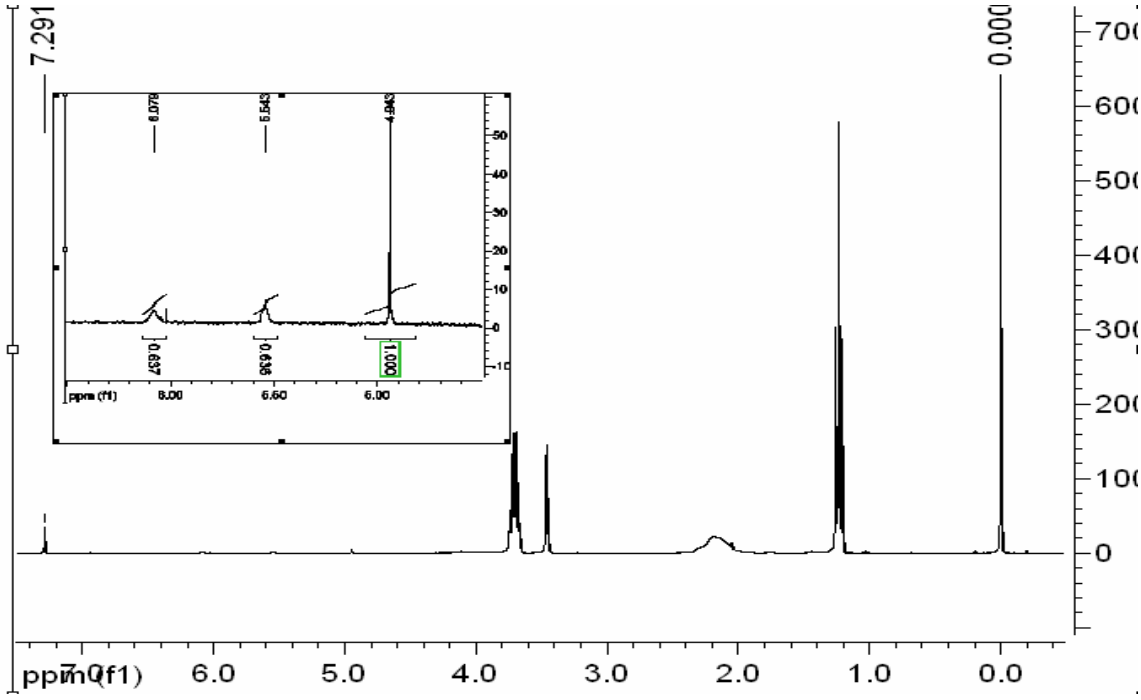

Figure 36: 0.5g TiO_2 modified by 0.2ml MPS (2nd Exp. 4), 0.02ml CH_2Br_2

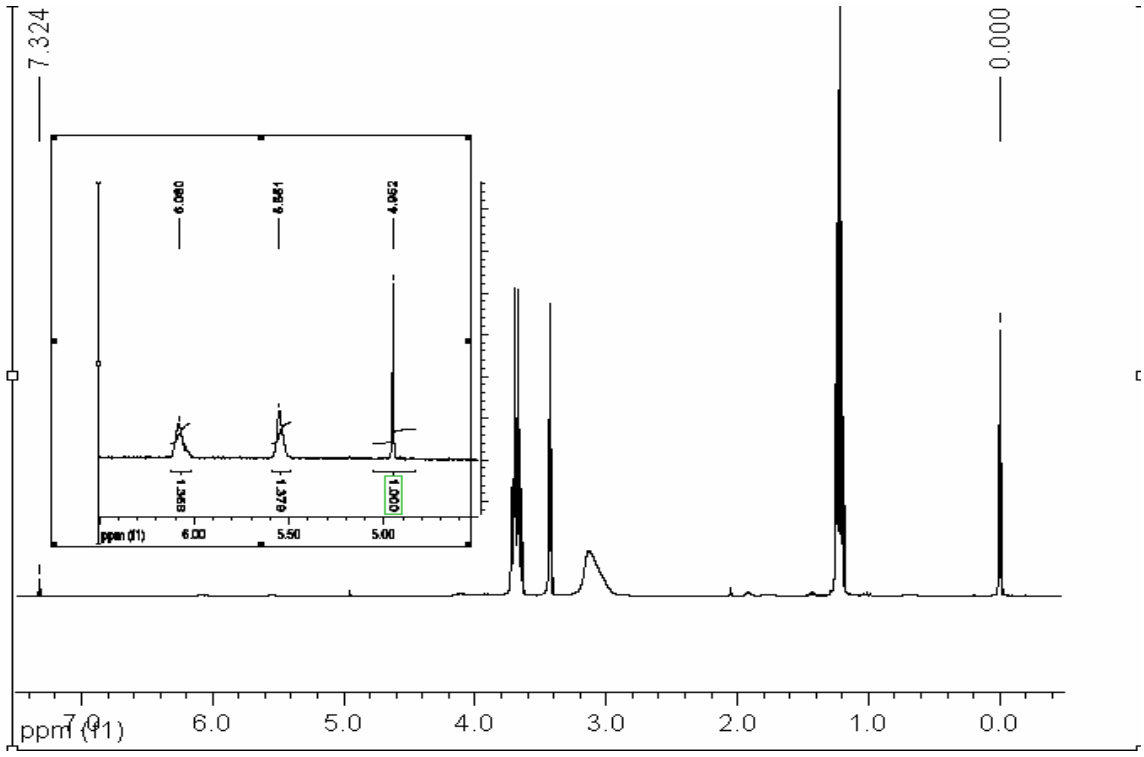

Figure 37: 0.5g TiO_2 modified by 0.4ml MPS (1st Exp. 5), 0.02ml CH_2Br_2

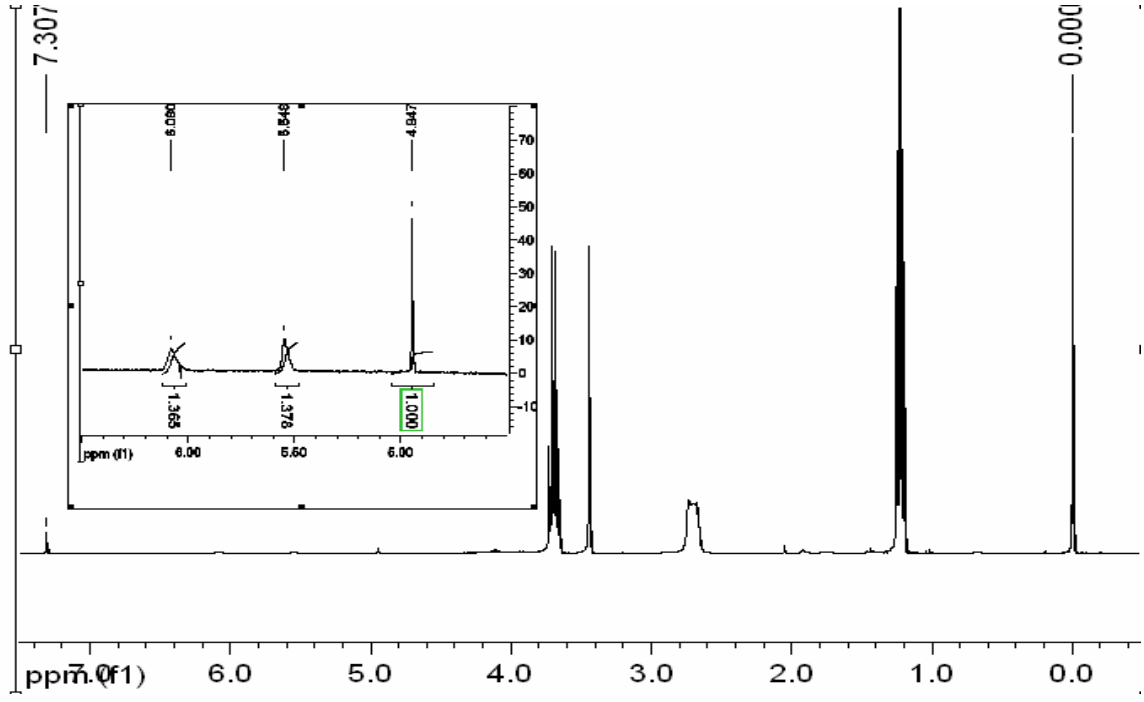

Figure 38: 0.5g TiO_2 modified by 0.4ml MPS (2nd Exp. 5), 0.02ml CH_2Br_2

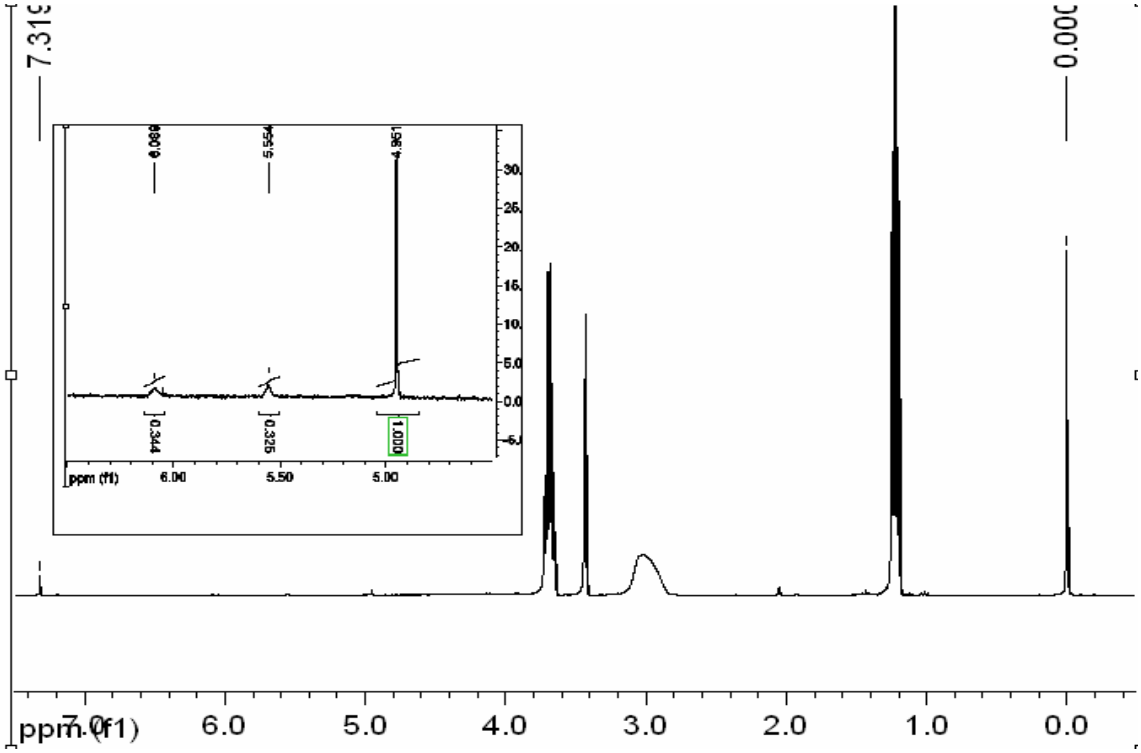

Figure 39: 0.2g TiO_2 modified by 0.05ml MPS (1st Exp. 6), 0.01ml CH_2Br_2

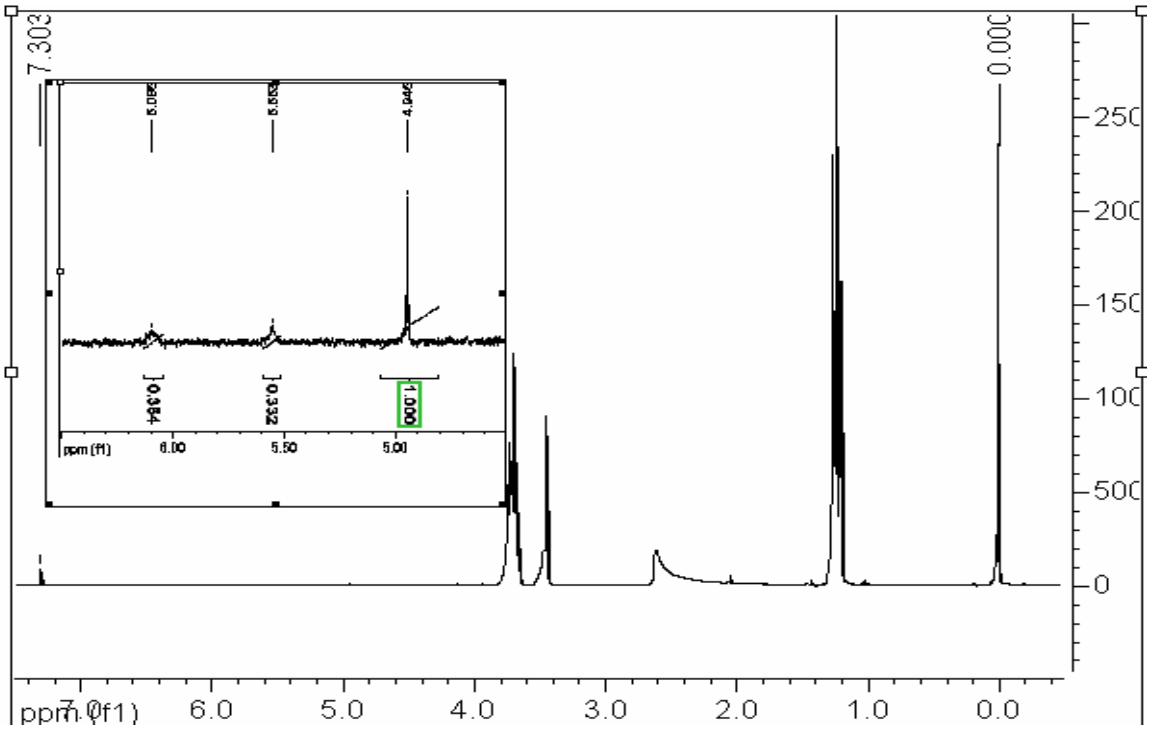

Figure 40: 0.2g TiO_2 modified by 0.05ml MPS (2nd Exp. 6), 0.01ml CH_2Br_2

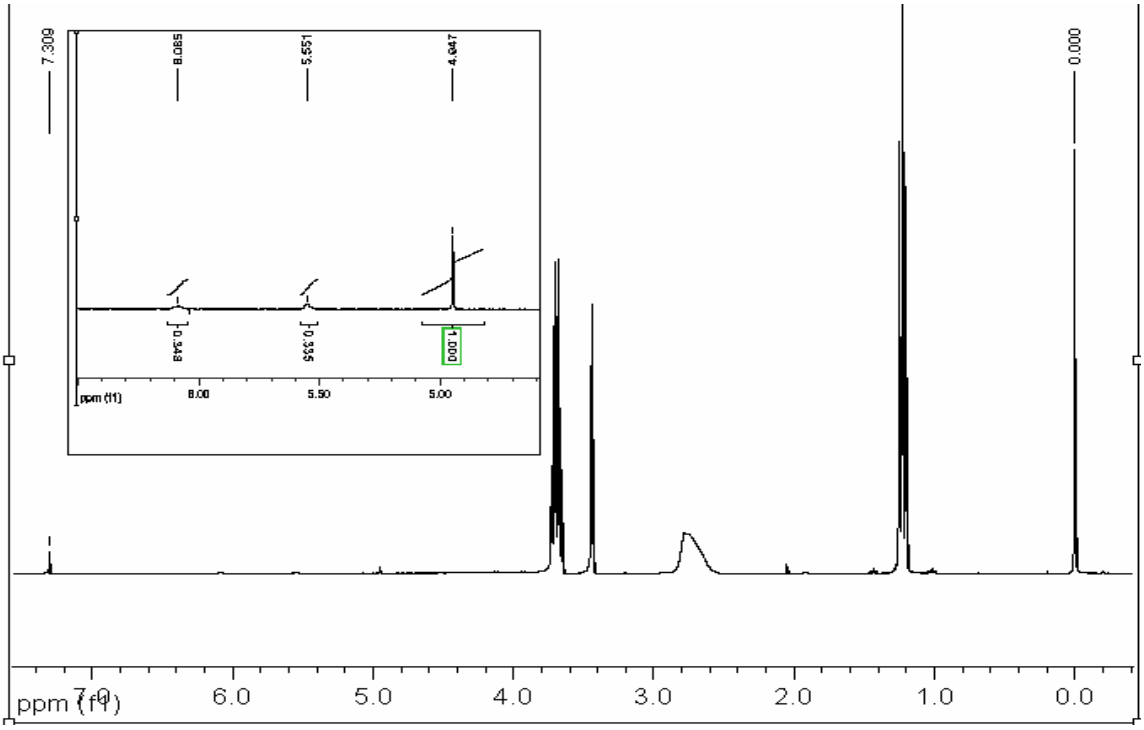

Figure 41: 0.2g TiO_2 modified by 0.1ml MPS (1st Exp. 7), 0.02ml CH_2Br_2

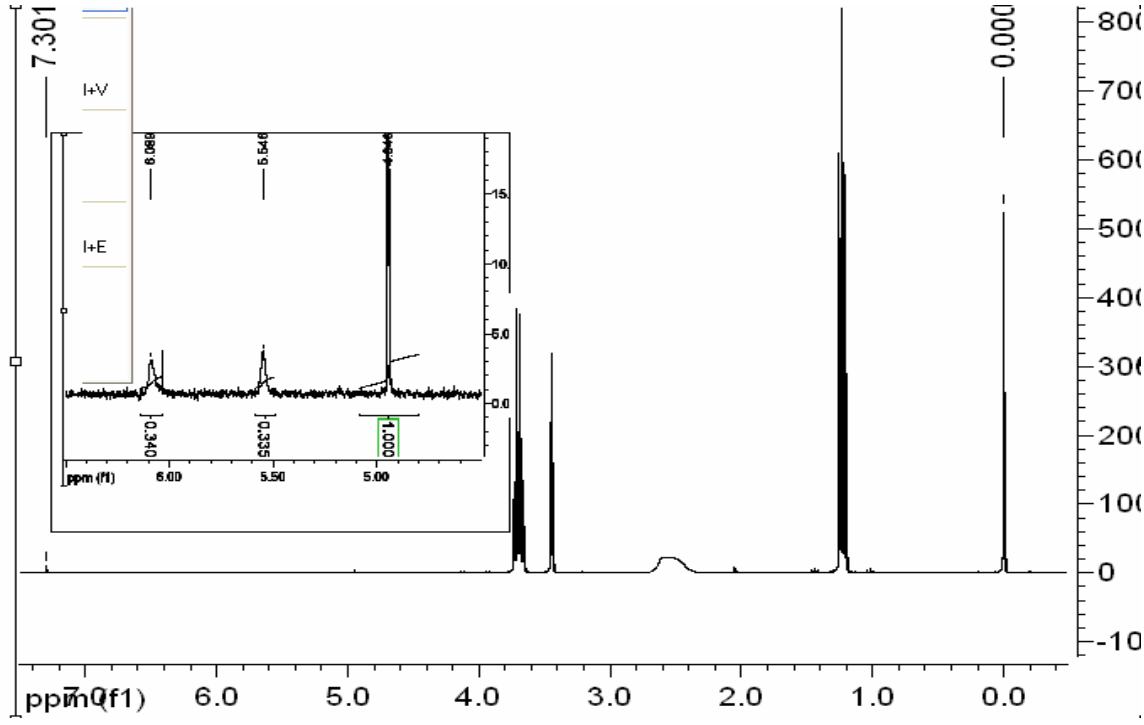

Figure 42: 0.2g TiO_2 modified by 0.1ml MPS (2nd Exp. 7), 0.02ml CH_2Br_2

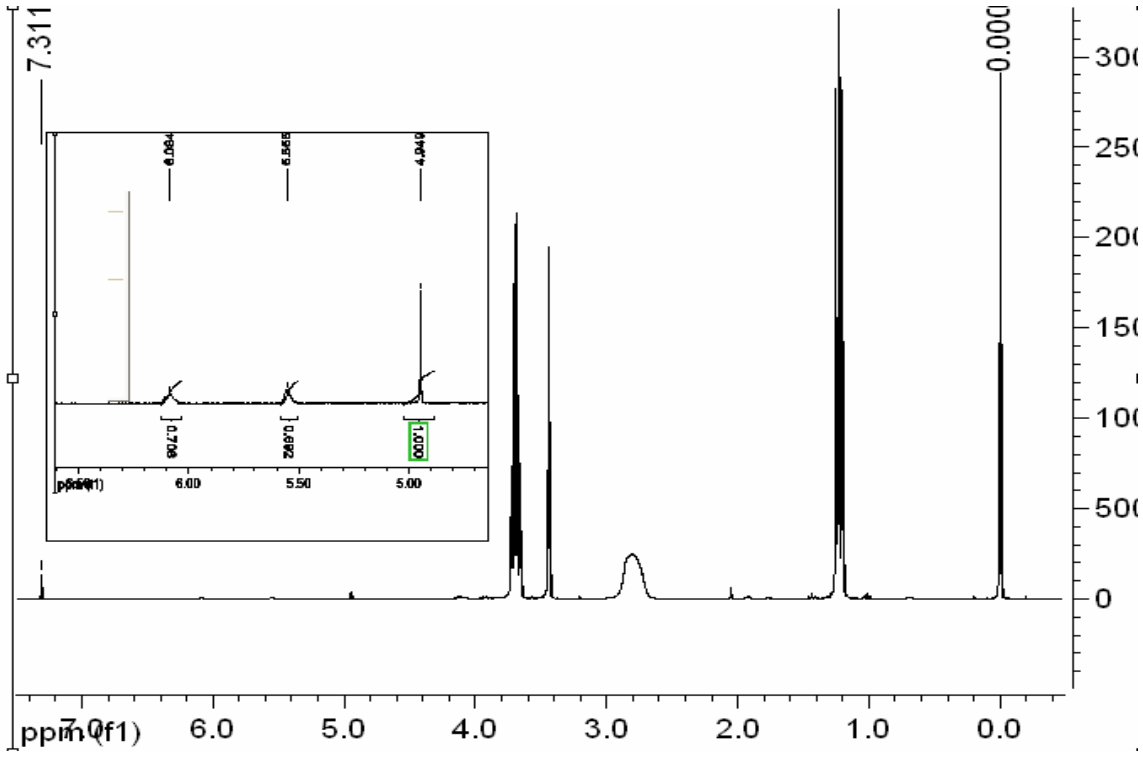

Figure 43: 0.2g TiO_2 modified by 0.2ml MPS (1st Exp. 8), 0.02ml CH_2Br_2

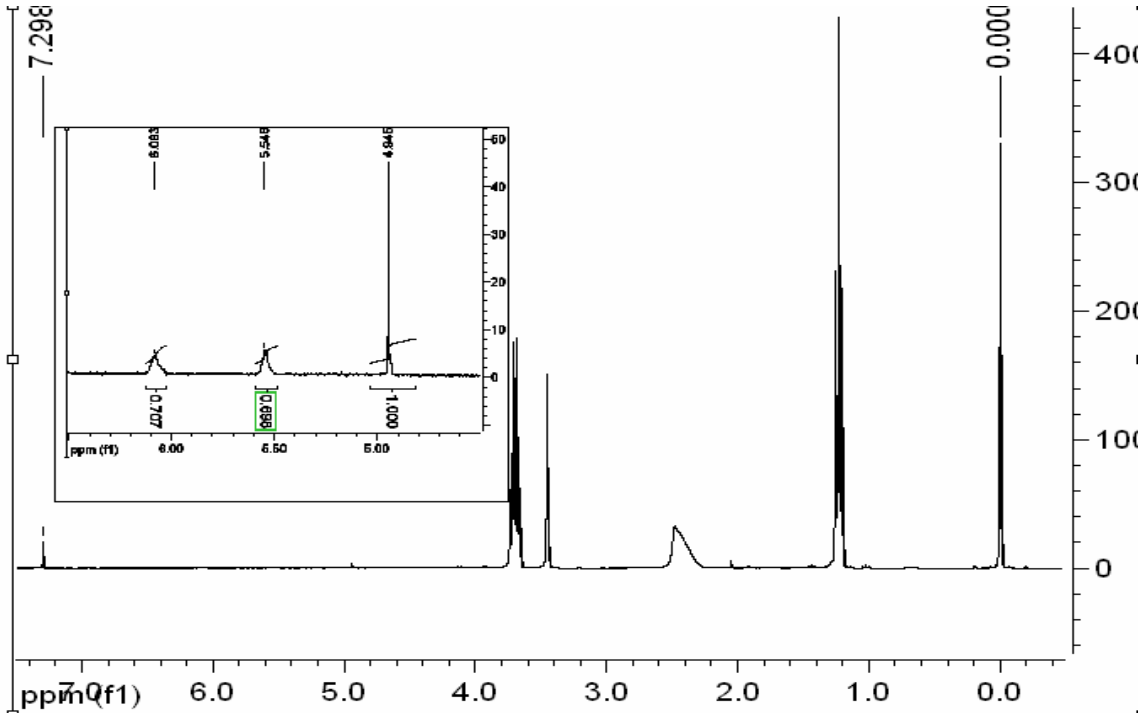

Figure 44: 0.2g TiO_2 modified by 0.2ml MPS (2nd Exp. 8), 0.02ml CH_2Br_2

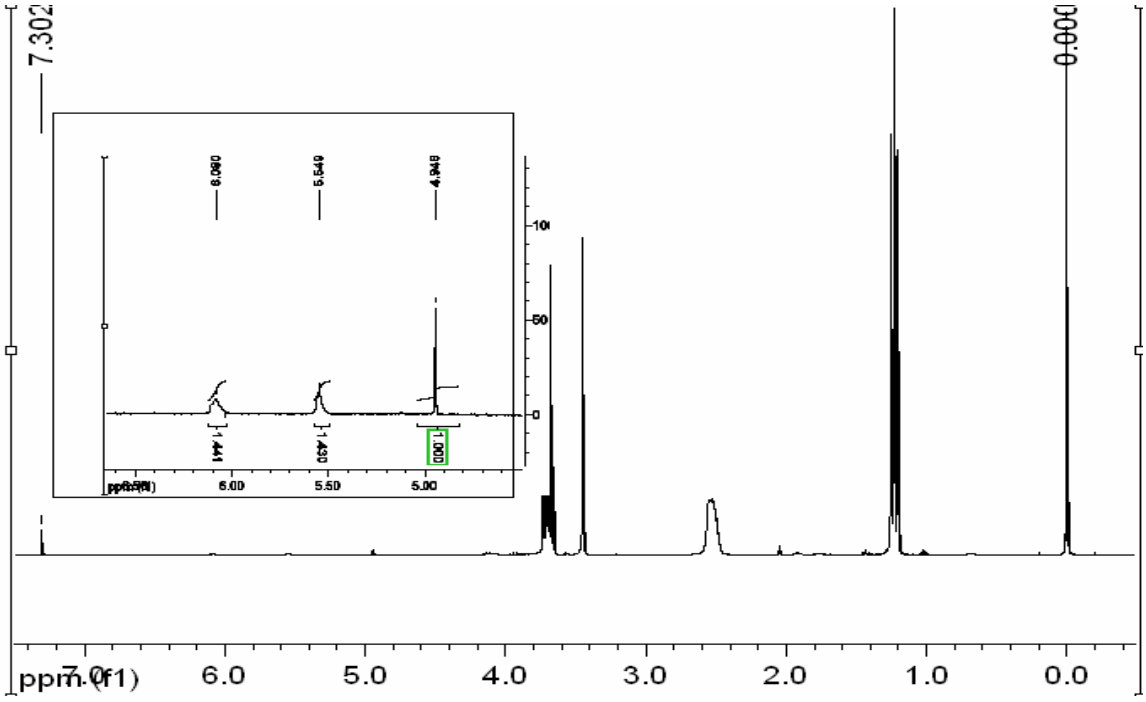

Figure 45: 0.2g TiO_2 modified by 0.4ml MPS (1st Exp. 9), 0.02ml CH_2Br_2

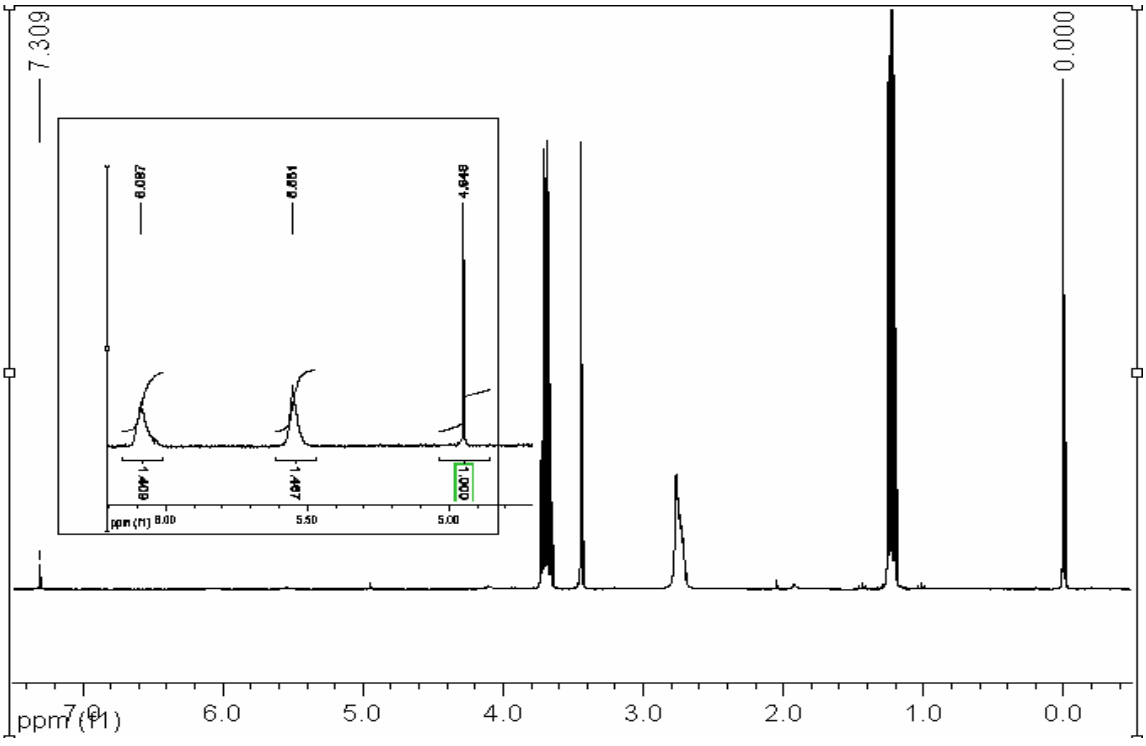

Figure 46: 0.2g TiO_2 modified by 0.4ml MPS (2nd Exp. 9), 0.02ml CH_2Br_2

3.6.2 Particle Size Distributions

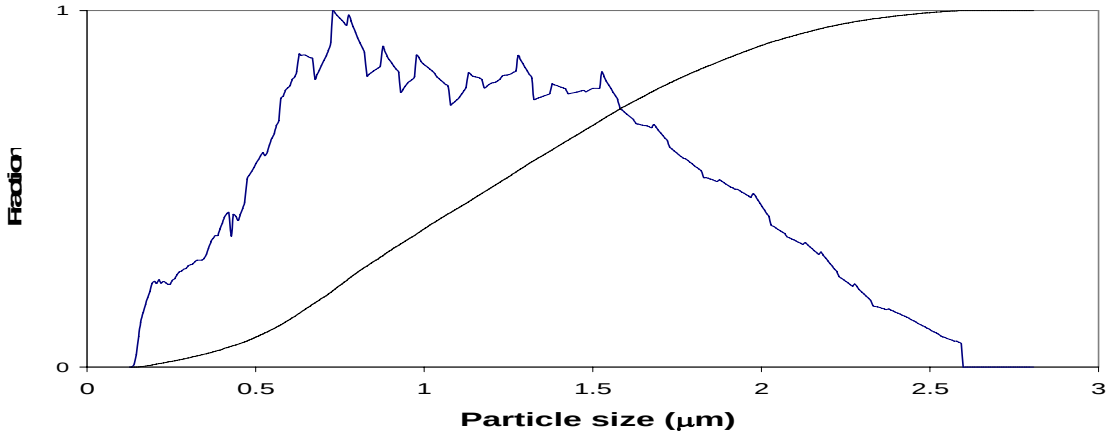

Figure 47: Averge size: 1.248µm (1st Exp. 1: unmodified)

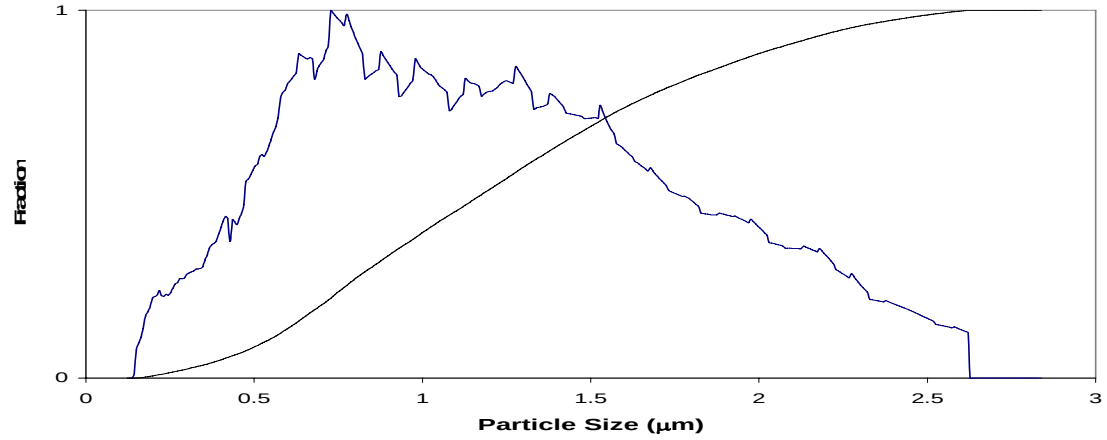

Figure 48: Averge size: 1.236µm (2nd Exp. 1: unmodified)

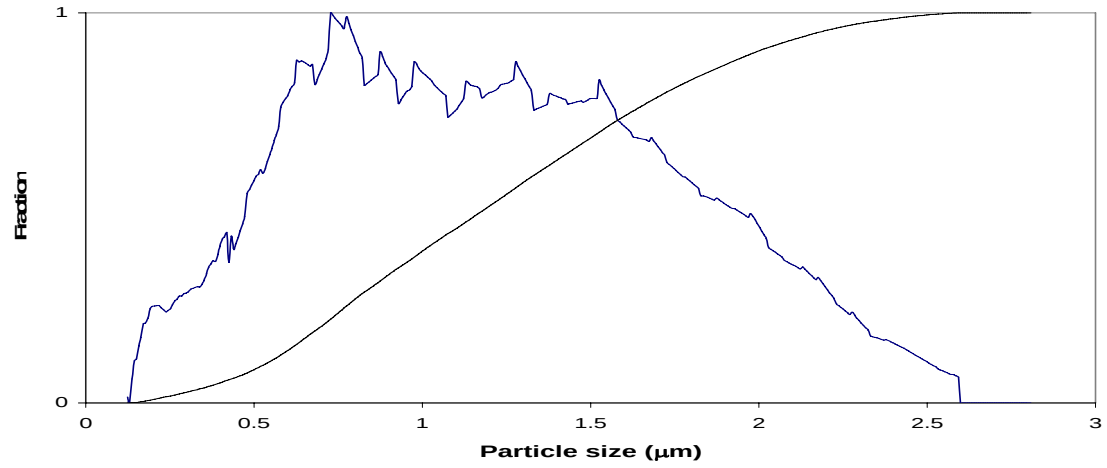

Figure 49: Averge size: 1.234µm (3rd Exp. 1: unmodified)

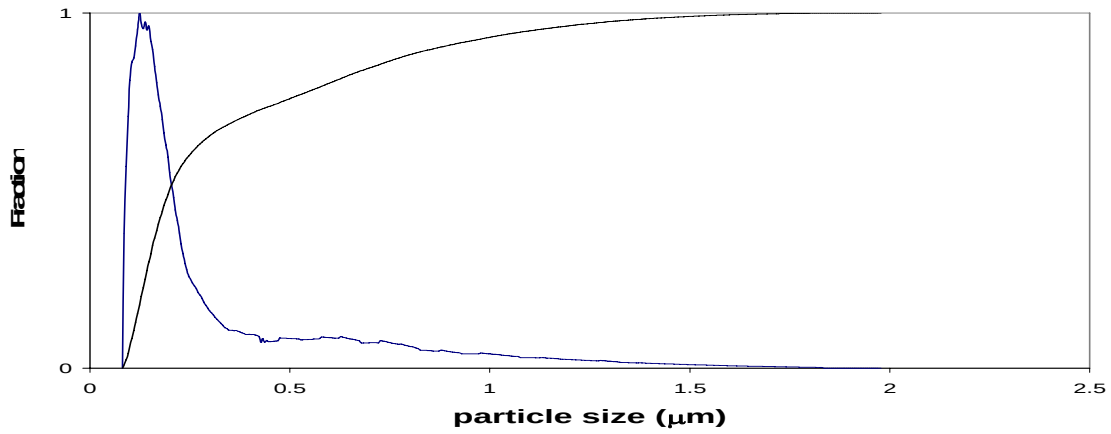

Figure 50: Averge size: 0.359μm (1st Exp. 2)

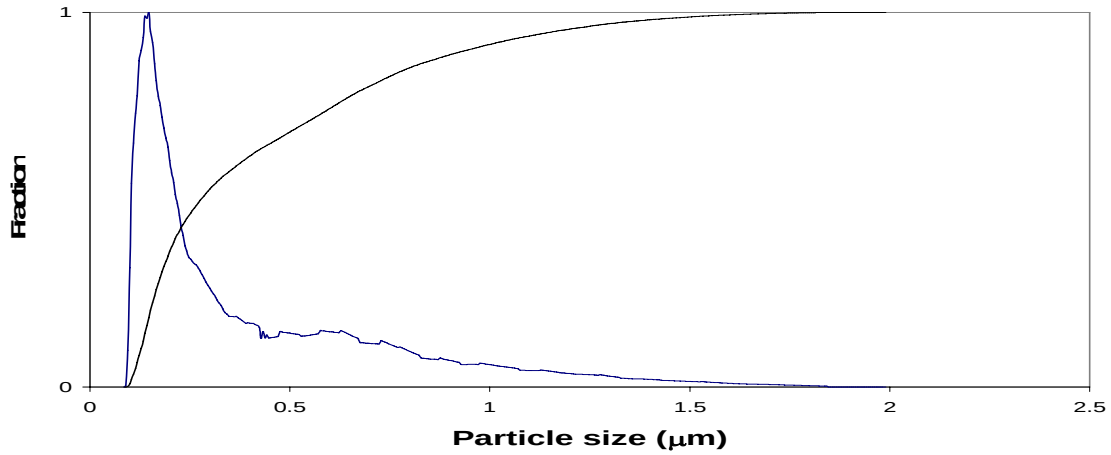

Figure 51: Averge size: 0.429μm (2nd Exp. 2)

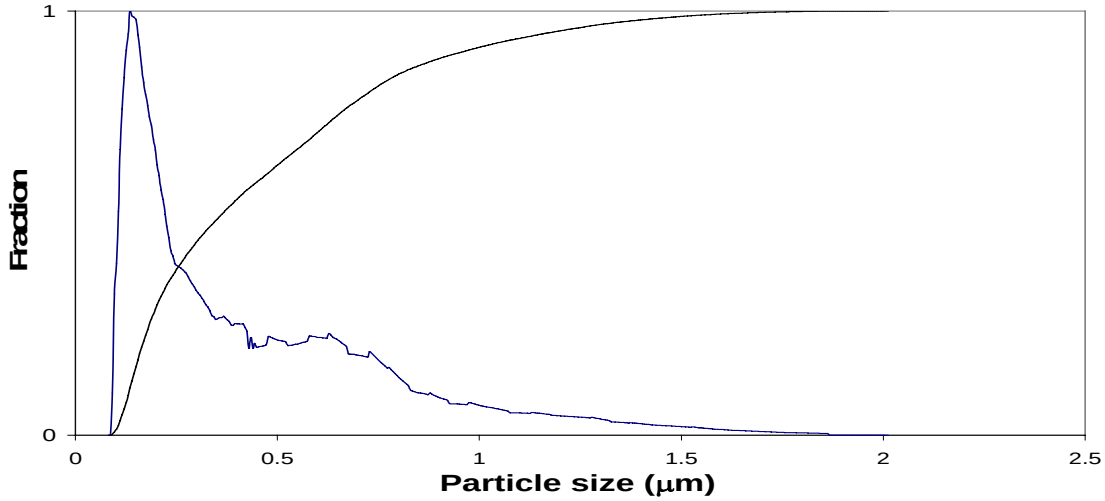

Figure 52: Averge size: 0.440μm (3rd Exp. 2)

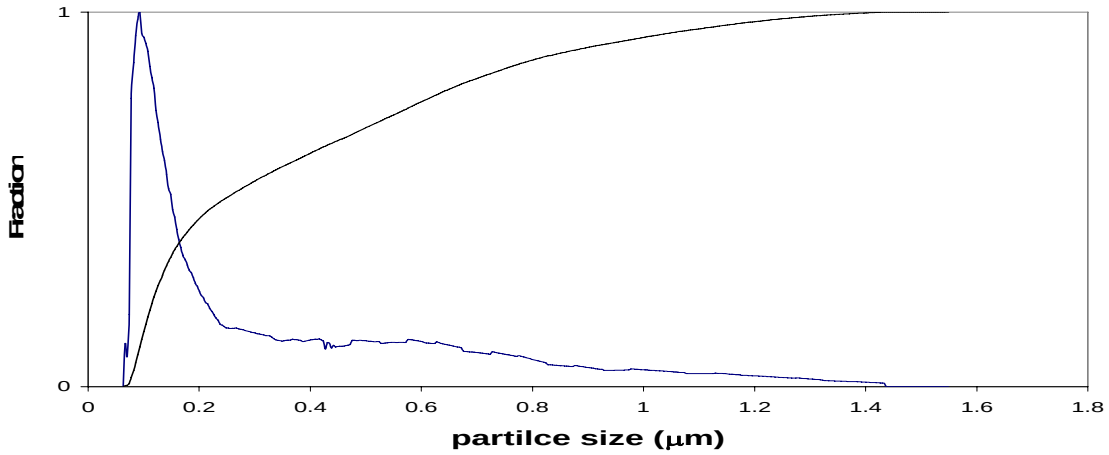

Figure 53: Averge size: 0.388μm (1st Exp. 3)

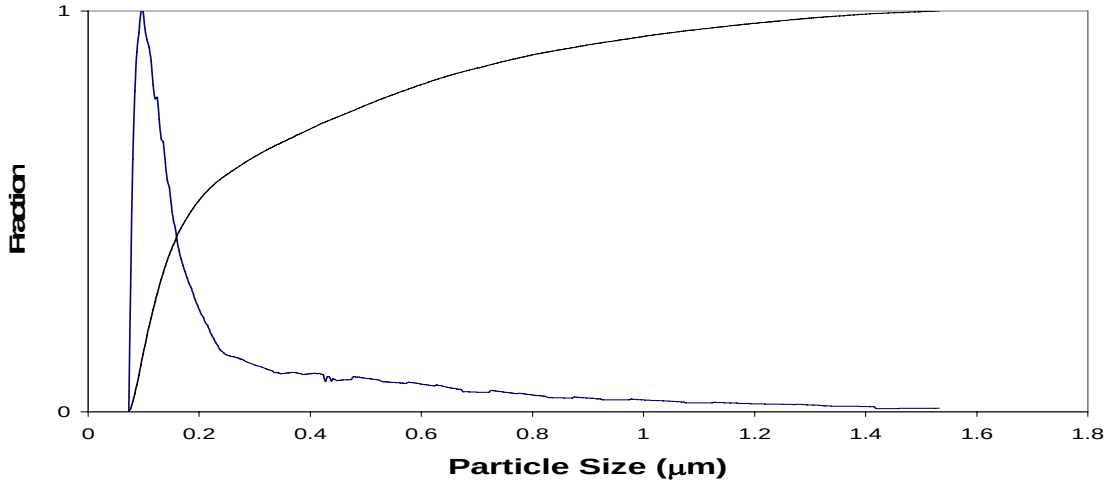

Figure 54: Averge size: 0.349μm (2nd Exp. 3)

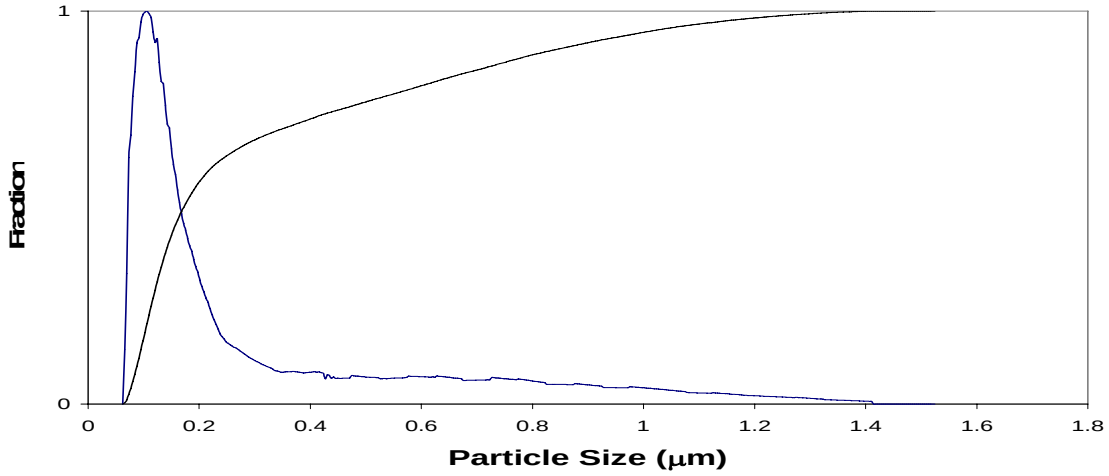

Figure 55: Averge size: 0.328μm (3rd Exp. 3)

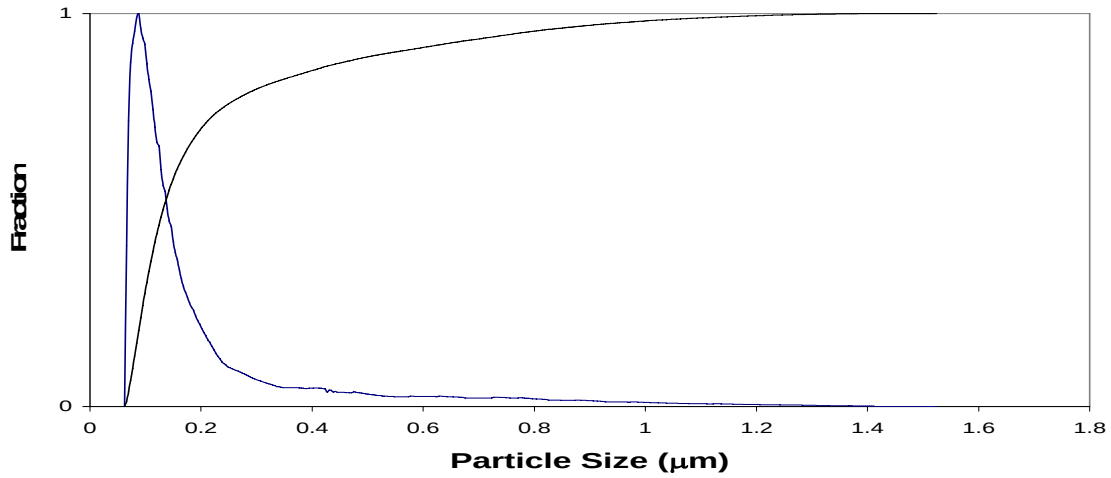

Figure 56: Averge size: 0.225µm (1st Exp. 4)

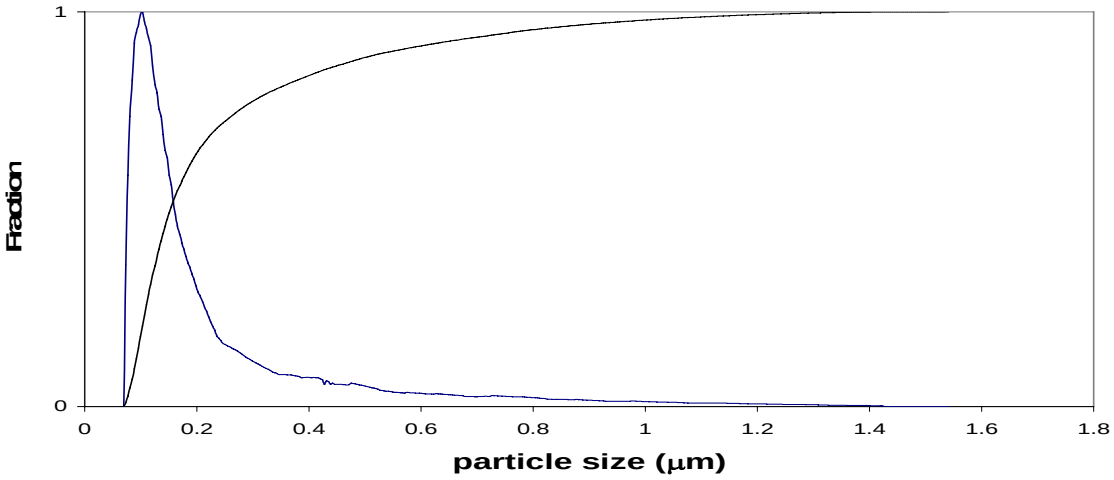

Figure 57: Averge size: 0.248µm (2nd Exp. 4)

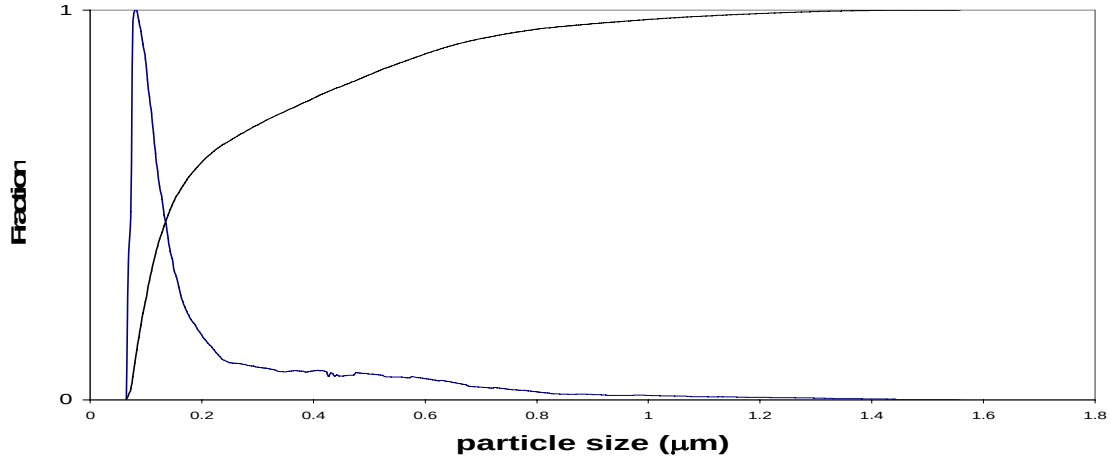

Figure 58: Averge size: 0.269µm (3rd Exp. 4)

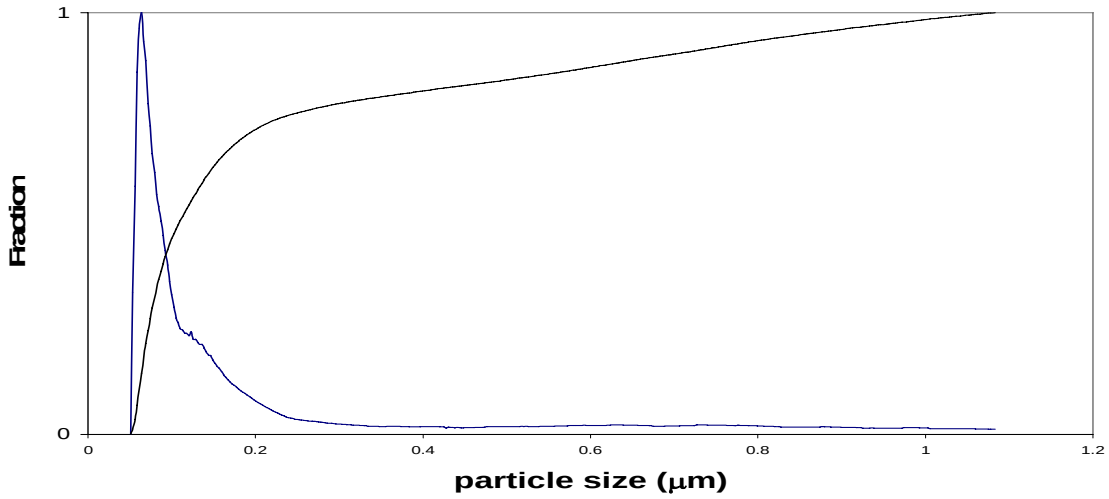

Figure 59: Averge size: 0.239μm (1st Exp. 5)

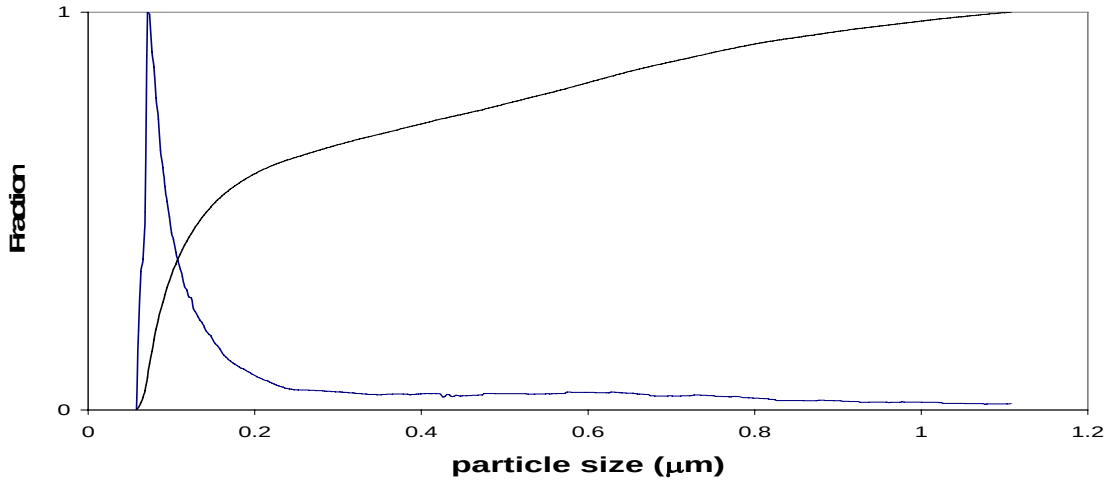

Figure 60: Averge size: 0.253μm (2nd Exp. 5)

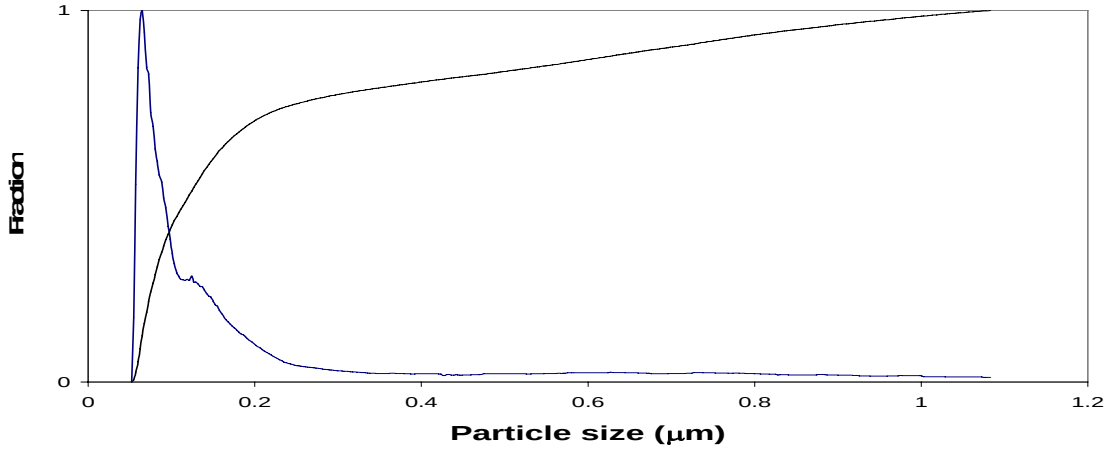

Figure 61: Averge size: 0.247μm (3rd Exp. 5)

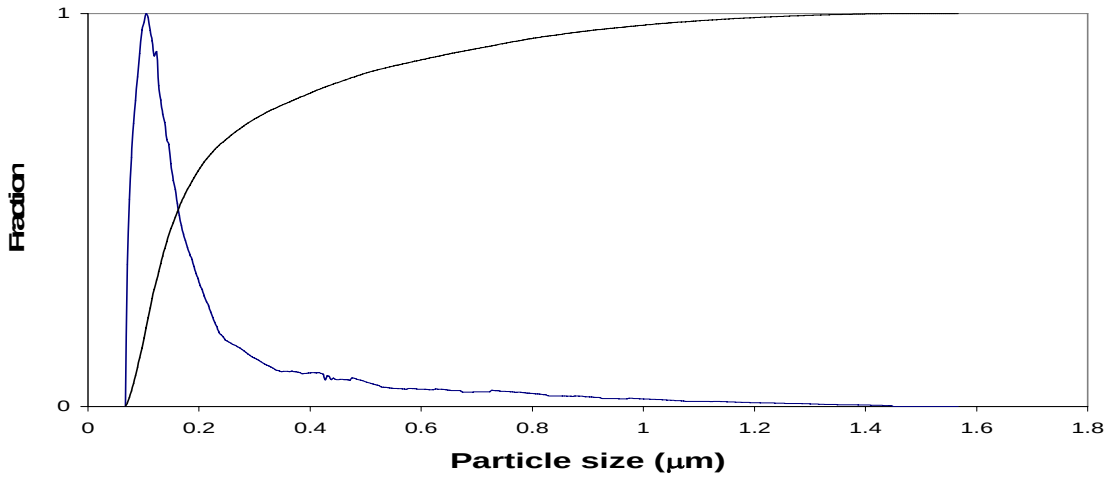

Figure 62: Averge size: 0.275μm (1st Exp. 6)

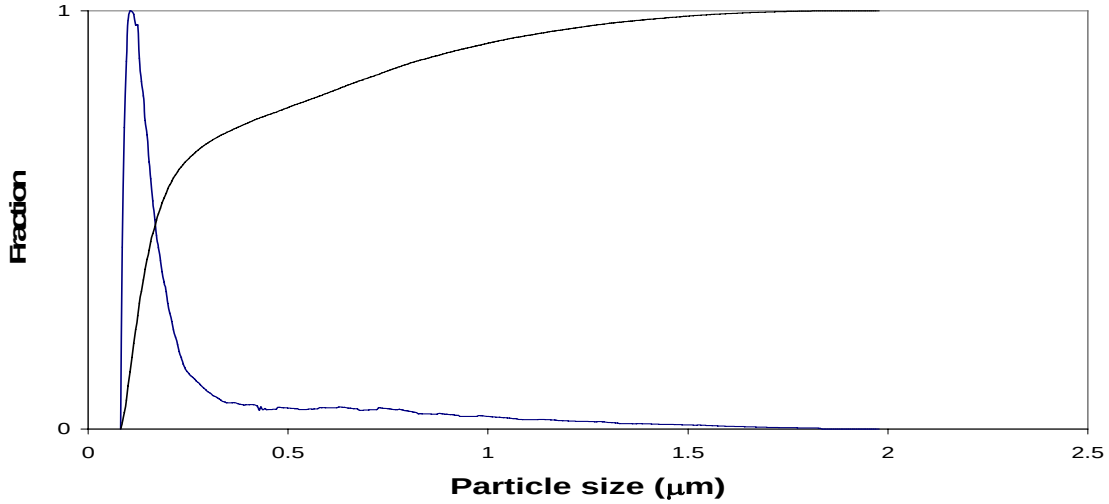

Figure 63: Averge size: 0.349μm (2nd Exp. 6)

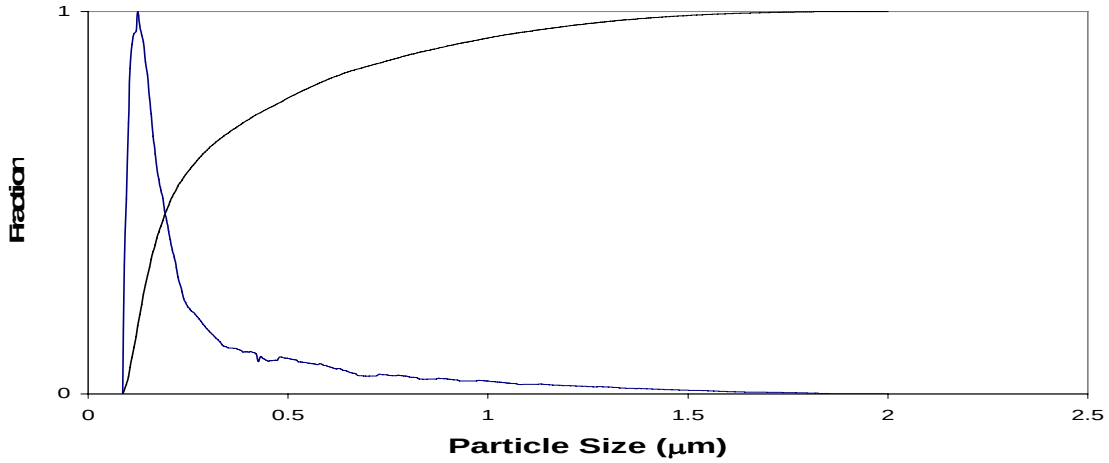

Figure 64: Averge size: 0.357μm (3rd Exp. 6)

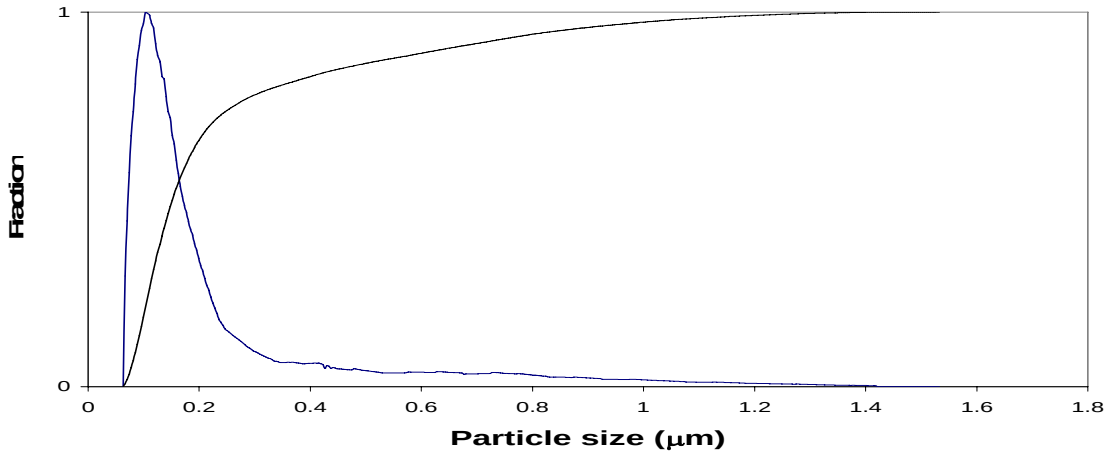

Figure 65: Averge size: 0.256μm (1st Exp. 7)

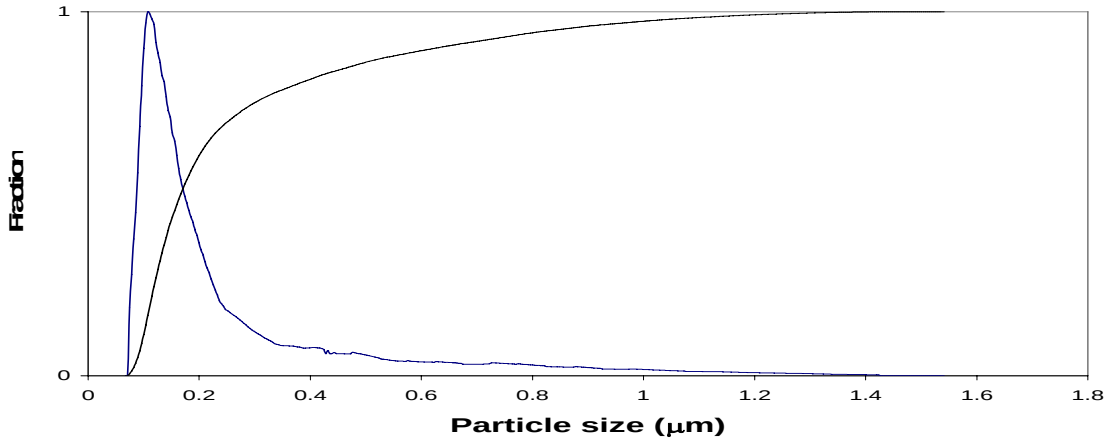

Figure 66: Averge size: 0.270μm (2nd Exp. 7)

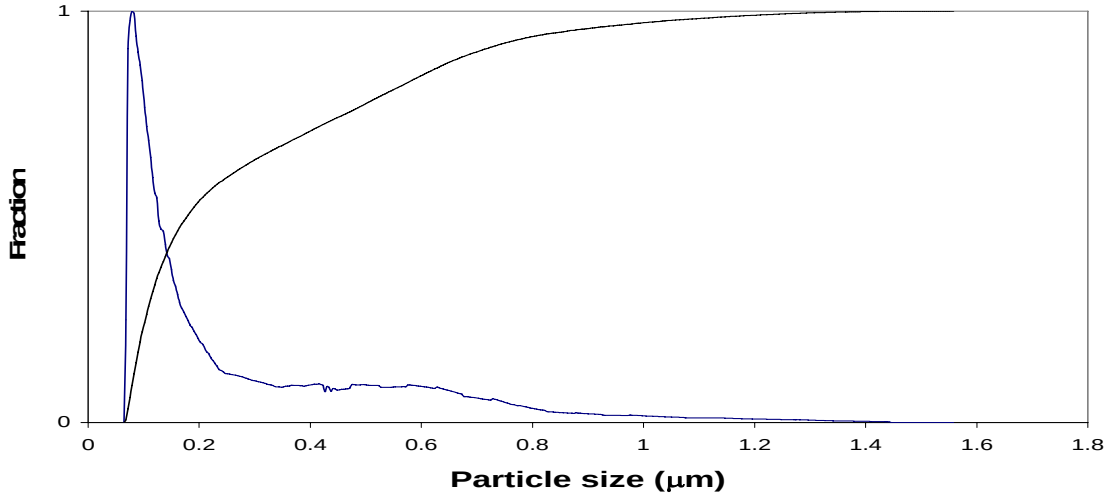

Figure 67: Averge size: 0.309μm (3rd Exp. 7)

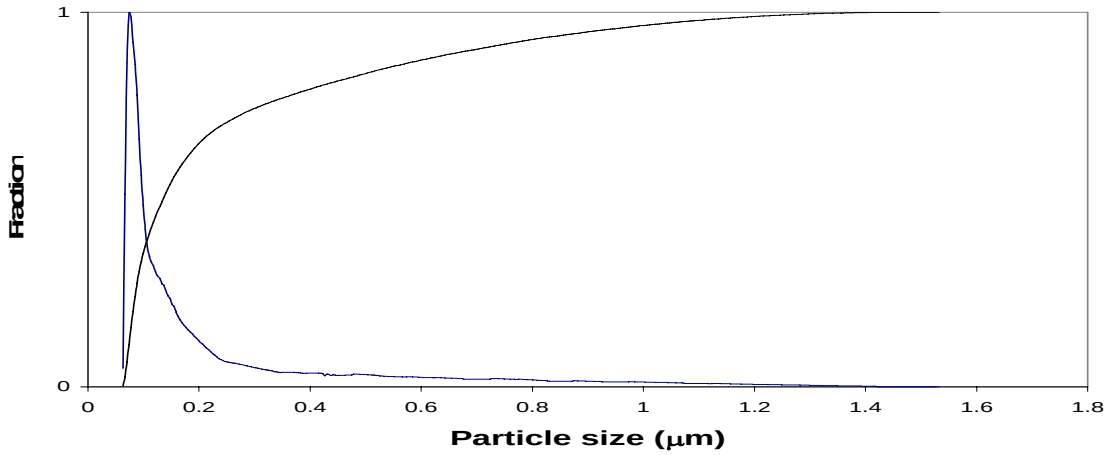

Figure 68: Averge size: 0.258μm (1st Exp. 8)

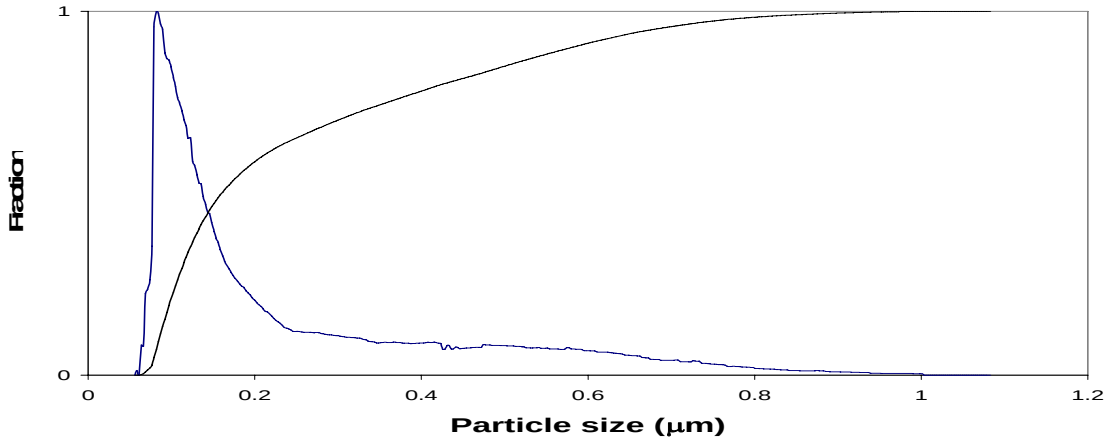

Figure 69: Averge size: 0.259μm (2nd Exp.8)

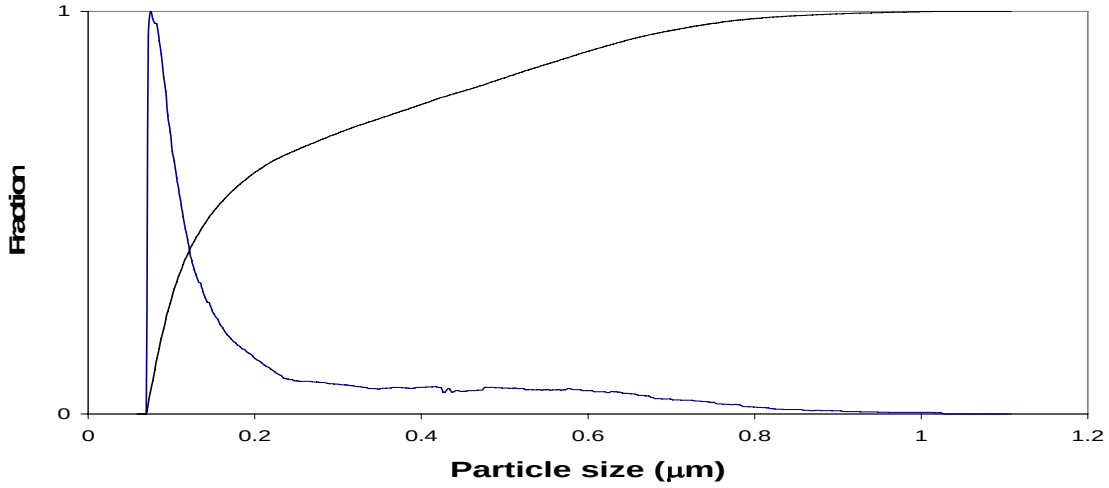

Figure 70: Averge size: 0.264μm (3rd Exp. 8)

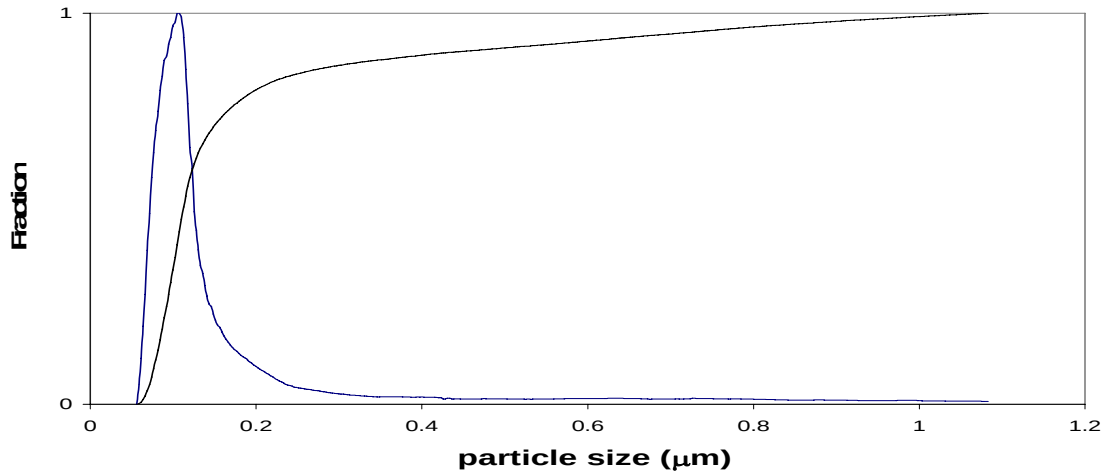

Figure 71: Averge size: 0.194μm (1st Exp. 9)

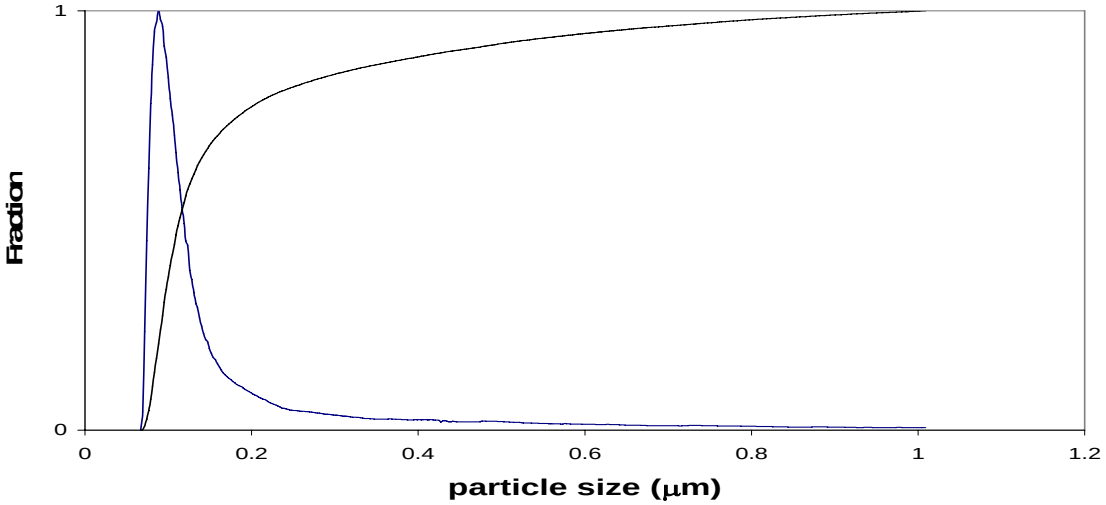

Figure 72: Averge size: 0.192μm (2nd Exp. 9)

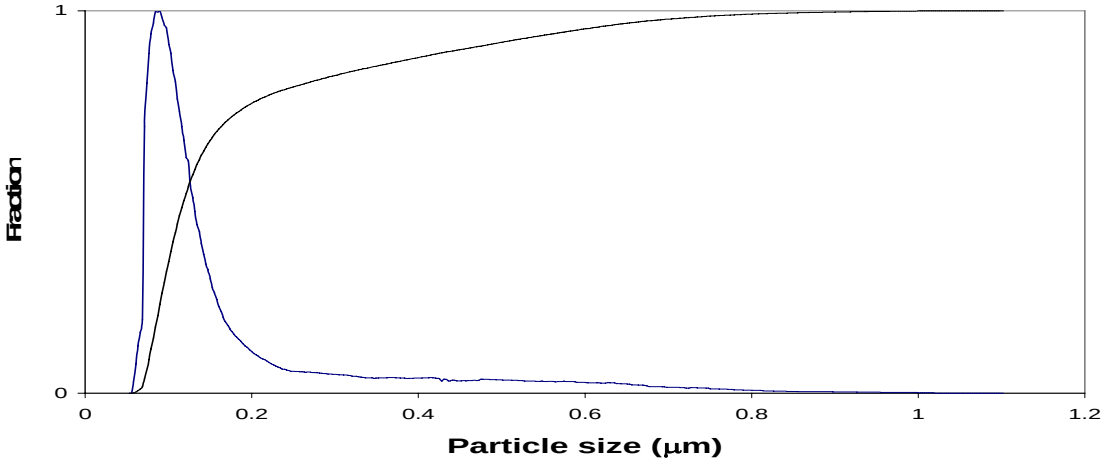

Figure 73: Averge size: 0.192μm (3rd Exp. 9)

Chapter 4 Preparation and Characterization of Polymer TiO_2 Nanocomposites

4.1 Introduction

Styrene based polymer materials represent an intensively investigated and rapidly developing field, extending from the simplest homo-polystyrene through a large group of thermoplastics based on the random copolymers of styrene with various monomers, block copolymers of styrene, to polymer blends with various other polymers or fillers and thermosetting resins. An enormous amount of theoretical and technological knowledge has been accumulated over the last several decades. But the work is still rare on PS-filled nanocomposites where the inorganic phase is dispersed at the nanoscale level in the polymer matrix. This project aimed at proving the new concept of in-situ free radical copolymerization to synthesize polystyrene TiO_2 nanocomposites. To overcome the aggregation of nanoparticles is the biggest challenge for the approach described here.

In the first step, TiO_2 surface modification significantly reduced the size of the modified TiO_2 to the range around 200 nm from the average aggregated (from the as-received TiO_2 nanopowder) with micrometer size. However, at 200nm the particles are still too large to affect composites properties and benefit from the primary nanoparticles 21nm.

In the second step, in-situ polymerization will be used to provide further particle size reduction. the grafted vinyl groups on the TiO_2 nanoparticles surfaces can act not only as surfactant to decrease agglomeration but also a comonomer which can react with styrene monomer. Hereby the growing polymer chains can separate the 200 nm aggregated particles resulting in a much finer dispersion of nanoparticles in the polystyrene matrix.

This chapter deals with synthesis and characterization of polystyrene TiO_2 nanocomposites. Section 4.2 describes experimental setup and analytical methods

including differential scanning calorimetry (DSC) and thermogravimetrical analysis (TGA). Results are discussed in Section 4.3, followed by the summary in Section 4.4.

4.2 Experimental

4.2.1 Materials

The modified TiO_2 being used here was based on the above Experiment 4 in Section 3. The free radical polymerization initiator 2.2'-azobis isobutyronitrile (AIBN) was donated by Polyscience Inc. The styrene monomer purchased from VWR was purified by molecule sieve to remove the inhibitor tertbutylcatechol (TBC). Nitrogen gas with 5.0 purity was used as purchased from Praxair Inc.

4.2.2 Nanocomposite Synthesis

Bulk polymerization of styrene was completed in a borosilicate glass vial. The process (see Figure 74) began with dispersing the modified TiO_2 with the monomer under 30 min ultrasonication in a sealed vial, after which the vial was open to allow addition of the accurately weighed initiator. Then the vial was vacuumed for three cycles and purged with N_2 for 10min right before polymerization in order to expel O_2. If the reaction could not be started once the vials were prepared, they were stored in liquid nitrogen. Before beginning the reaction, the vial was thawed to room temperature and placed in a temperature-controlled shaker (PL-SP 260, Polymer Laboratories, UK). The shaker was used for polymerization reaction apparatus with two purposes, one of which was to control the desired temperature and the other to have the same function as a mixer.

After the desired polymerization time, vials were taken out of the shaker and then immediately frozen in ice to stop the reaction. Once the vials were completely frozen and there was no doubt that the reaction had stopped, they were once again thawed, cut open and their contents were washed into the flasks with tetrahydrofuran (THF). After all their contents were removed, ethanol was used to precipitate the polymer inside the flasks and

then filtered out with filter paper. Before placing the polymer into the filter papers, they were weighed for gravimetric calculation purposes.

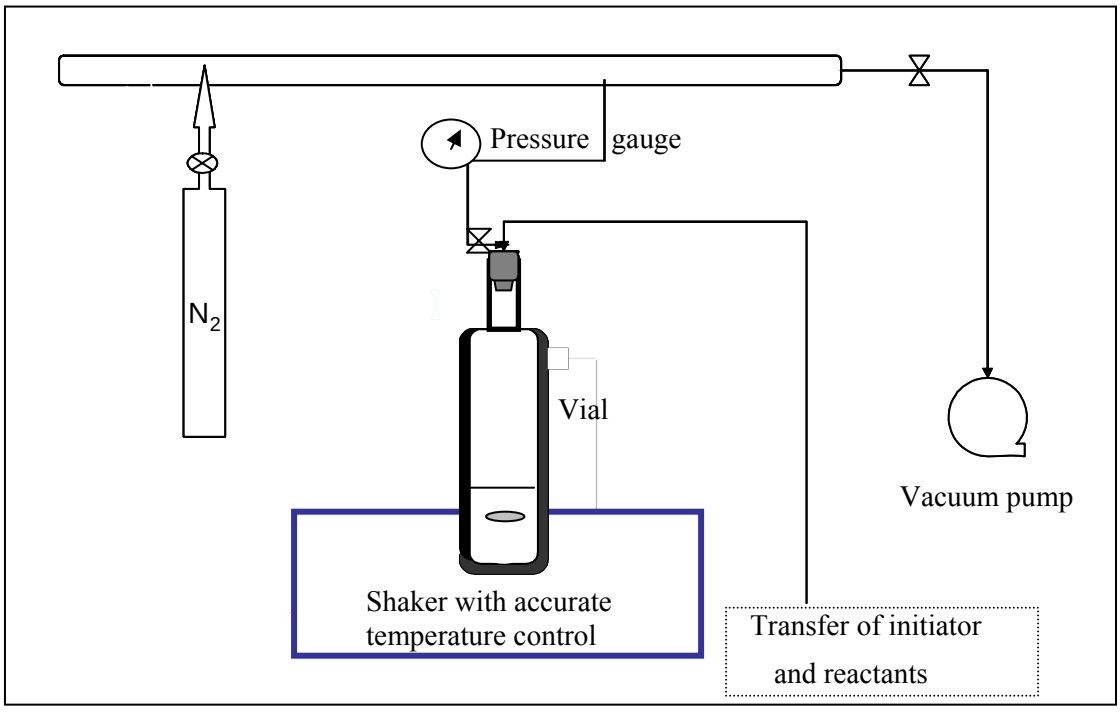

Figure 74: Experimental Setup of polymerization process

A list of the experiments is provided in Table 7, which was labeled by concentration of modified TiO_2 (referred as MT) in the monomer styrene (PS-0=0 g/l, PSTN1=50 g/l, PSTN2= 10 g/l, PSTN3=2 g/l). The other factors such as the temperature (T = 60^{o}C), the initiator concentration (C = 0.005 M) were constantly set.

Table 7: Experimental conditions polymerization runs

Experiment label	Temperature (^oC)	Concentration of initiator (mol/l)	Concentration of MT (g/l)
PS-0	60	$5*10^{-3}$	0
PSTN1	60	$5*10^{-3}$	50
PSTN2	60	$5*10^{-3}$	10
PSTN3	60	$5*10^{-3}$	2

4.2.3 Nanocomposite Characterization

4.2.3.1 Fractionation

In the characterization of polymer nanocomposites samples, a fractionation method was required to separate the nanocomposite fraction from the homopolymer fraction. Two types of the following fractionation methods were performed.

Fractionation A:

A Soxhlet extraction was first employed to divide two fractions with hot solvent (toluene or xylene). Figure 75 gives a picture of the Soxhlet extraction apparatus. A solvent reservoir is heated such that a suitable amount of vapor can be condensed overhead of the 150-mesh stainless steel (or thimble) for toluene or for xylene. The warm solvent then flows over the polymer in the mesh steel dissolving and extracting the soluble fraction of the sample. When enough vapor has been condensed, the solvent will drain through the siphon tube into the solvent reservoir. Prior to the extraction procedure, the mesh steel was put inside the Soxhlet apparatus, refluxed with solvent for one hour, dried and then weighed in order to reduce any error caused by the weight loss of the thimble or steel. In the extraction process, solvent was refluxed over the sample for 24 h. The extracted fraction in hot solvent was poured into ethanol for precipitation, filtered out and washed ethanol repeated times over filter papers. Both extracted and non-extracted fractions were dried in the oven (approximately 60^oC) until constant weight.

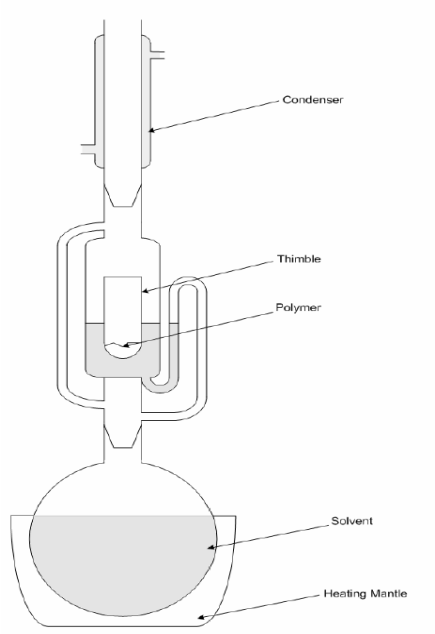

Figure 75: The Soxhlet extraction apparatus

Fractionation B:

The following procedure (conveniently called as centrifugation separation) was adopted and modified from Angot and coworkers [Angot, 1998]. Approximately 10 ml of boiling toluene was slowly added to dissolve 0.5 g of the sample in a 20 ml vial while stirring and heating and then capped and put into a heated ultrasonic bath for one hour until it became uniform solution and no polymer particles appeared. After that the vial was left to cool to room temperature and the solution was then poured into a centrifuge tube.

The solution was separated into two phases by centrifugation for about 3 h, at 4000 rpm, until the upper supernatant phase become totally clear. The lower sediment phase was isolated and repeated three more times with the above redispersion and centrifuging-sedimentation procedures. The supernatant phase was poured into a round bottom flask to evaporate. Both the sediment and supernatant phases were dried at 60^{o}C until constat weight.

4.2.3.2 Melt Pressing

Films of these nanocomposite samples were prepared by melt pressing for further investigations. A few grams of the nanocomposites were sandwiched between two smooth transparent PET films and placed between two steel plates. The plates of the hydraulic press were heated to about 170°C. The steel plates with samples in between were put in the hot hydraulic press. After melting the polymer (approximately 5 min), the samples were pressed (1000 psi). After 10 min, the press was released to let the air bubbles in the polymer melt to move out. After 30 seconds, the sample was pressed again for another 1 minute. Then the sample were taken out and cooled down by air to obtain the film specimens.

4.2.3.3 SEM

The morphology of the nanocomposites was also observed with a LEO scanning electron microscope. The polymer nanocomposite films were frozen by immersion in liquid nitrogen to allow fracturing and then mounted on aluminum stubs by using conductive adhesive tabs with fracture surface facing up. Prior to SEM examination, the samples were sputter-coated with 15–20 nm thick gold for electron conduction. The pressure in the vacuum chamber for SEM analysis was approximately $2.5x10^{-6}$ mbar, and the electron gun current was 10 kV. SEM pictures were recorded electronically in a personal computer.

4.2.3.4 FT-IR

The nanocomposite samples were analyzed by a FTIR spectroscopy in transmission mode using a KBr technique which was described in Section 3. The spectra were recorded in the wavelength range from 400 to 4000 cm^{-1}, after 32 scans, with resolution of 4 cm^{-1}. Calibration of the wavenumber was automatically done by the instrument with using an internal polystyrene film. Spectra reported here were subtracted from a background spectrum obtained with pure KBr.

4.2.3.5 Differential Scanning Calorimetry (DSC)

Differential scanning calorimetry was measured with a model Q10 Differential Scanning Calorimeter (TA instruments) under nitrogen atmosphere. Polymer nanocomposite samples were sealed in aluminum pans and then scanned from 35 to 250^{o}C by a heat/cool/heat step at a heating rate of 10 ^{o}C ·min^{-1}. Data obtained from the second heating-run were used for analysis to account for knowledge of thermal history of the sample. Prior to experiments, all the samples were dried in vacuum at 75^{o}C for 24 h. DSC was also run for an empty aluminum DSC sample cell, and the obtained DSC curve was used as the real baseline for DSC measurement.

4.2.3.6 Thermogravimetric Analysis (TGA)

The thermogravimetric analysis was carried out with a model Q50 Themogravimetric Analyzer in the temperature range from 20^{o}C to 800^{o}C at a heating rate of 20^{o}C ·min^{-1}, which was conducted in a nitrogen atmosphere. Prior to each run, the empty sample pan was completely tared to get accurate balance. Samples for the TGA studies were dried in oven at 60^{o}C for at least 10 hrs.

4.2.3.7 UV-Vis

The ultraviolet and visible spectroscopic study was carried out with a spectrophotometer in a wavelength range of 200 to 800 nm. The nanocomposites samples before fractionation were dissolved in boiled toluene for the test. Although the solubility of the polymer nanocomposites in toluene was unknown, enough could be dissolved for the purposes of the analysis. An appropriate amount of viscous sample solutions were transferred onto the clear sidewall of a quartz glass respectively to form a uniformly flat and thin polymer film with relatively similar thickness. An IR lamp was used for accelerating the drying of the samples before each testing. Spectra of the nanocomposites obtained here were subtracted from a blank quartz glass without or with homopolystyrene.

4.3 Results and Discussions

4.3.1 Polymerization Mechanism

The mechanism of free radical polymerization is well studied for the polymerization of styrene by monofunctional initiator AIBN. The general structure and decomposition pathway of AIBN are represented in Figure 76. It decomposes to form two carbonyloxyl radicals and an N_2 molecule.

Figure 76: Decomposition of AIBN

This radical is extraordinarily reactive and readily react with certain monomers or molecules containing double bonds that are succetible for free radical attack. For a styrene radical homopolymerization, each radical initiates, propagates and terminates to generate a polystyrene chain made entirely of the monomer styrene [Odian, 1991]. In the following equations 4-1 to 4-5, I is an AIBN initiator molecule, $R_{in}^{\bullet}$ an initiator radical, M a styrene monomer unit, $R_1^{\bullet}$ a primary radical; $R_n^{\bullet}$, $R_{n+1}^{\bullet}$, $R_m^{\bullet}$ represents radical chains with n, n+1, or m units respectively; P_n, P_m, P_{n+m} are dead polymer molecules of chain length n, m, n+m. k_d, k_{p1}, k_p, k_{tc}, k_{td} are initiation, primary propagation, propagation combination termination, and disproportionation termination rate constants respectively.

Initiation:

$$I \xrightarrow{k_d} 2\ R_{in}^{\bullet} + N_2 \quad \cdots\cdots\cdots (4-1)$$

$$R_{in}^{\bullet} + M \xrightarrow{k_{p1}} R_1^{\bullet} \quad \cdots\cdots\cdots (4-2)$$

Propagation:

$$R_n^{\bullet} + M \xrightarrow{k_p} R_{n+1}^{\bullet} \quad \cdots\cdots\cdots (4-3)$$

Termination:

$$R_n^{\bullet} + R_m^{\bullet} \xrightarrow{k_{tc}} P_{n+m} \quad \cdots\cdots\cdots (4-4)$$

$$R_n^{\bullet} + R_m^{\bullet} \xrightarrow{k_{td}} P_n + P_m \quad \cdots\cdots\cdots (4-5)$$

Figure 77: Mechamism for free radical polymerization of styrene by AIBN

However, when dealing with a copolymerization, there are four such reactions to think about: two homopropagation and two cross-propagation reactions [Odian, 1991]. In equations 4-6 to 4-9, $R^{\bullet}_{n,1}$ is a radical of length n ending in a unit of the styrene monomer and M_1 the styrene monomer. $R^{\bullet}_{n,2}$ is a radical of length n ending in a unit of the vinyl group on modified TiO_2 and M_2 the vinyl group on MT. k_{11}, k_{12}, k_{21}, k_{22} are the rate constants of the monomer 2nd subscript reacted with a growing chain (of any length) with a terminal unit of monomer 1st subscript.

$$R^{\bullet}_{n,1} + M_1 \xrightarrow{k_{11}} R^{\bullet}_{n+1,1} \quad \cdots\cdots\cdots (4-6)$$

$$R^{\bullet}_{n,1} + M_2 \xrightarrow{k_{12}} R^{\bullet}_{n+1,2} \quad \cdots\cdots\cdots (4-7)$$

$$R^{\bullet}_{n,2} + M_1 \xrightarrow{k_{21}} R^{\bullet}_{n+1,1} \quad \cdots\cdots\cdots (4-8)$$

$$R^{\bullet}_{n,2} + M_2 \xrightarrow{k_{22}} R^{\bullet}_{n+1,2} \quad \cdots\cdots\cdots (4-9)$$

Figure 78: Proposed copolymerization mechanism of styrene and MT by AIBN

A proposed model suggested by Zhang and Simon [Zhang, 2005] in hybrid PE-Al_2O_3 nanocomposites system is also introduced here to explain different structures in nanocomposites synthesized by *in situ* polymerization shown in Figure 79. Five categories of structures are proposed in PS-TiO_2 nanocomposites: a) homopolystyrene chain; b) TiO_2 nanopowder connected to the end of the polymer chains; c) TiO_2 nanopowder connected in the middle of the polymer chains; d) Several TiO_2 nanoparticles first self-propagated and then connected to the polymer chains creating a network; e) TiO_2 nanopowders connected by a long polyethylene chain (larger distance between the powders compared with particle diameter).

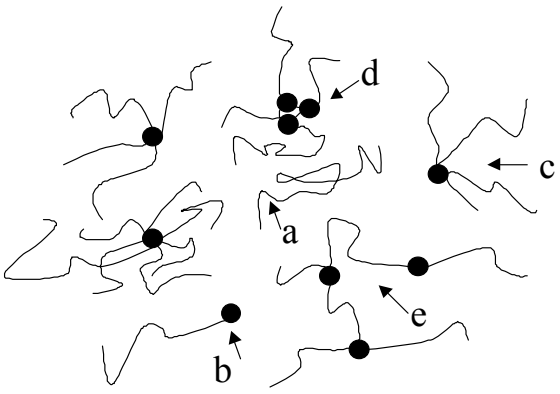

Figure 79: Proposed model for distribution of structures on hybrid PS-TiO_2 nanocomposites [Zhang, 2005]

From research done on radical polymerization by a monofunctional initiator, the mechanism shows that the relationship between the polymerization rate and degree of polymerization is inversely proportional based on the following equation 4-10. Attempts to increase the rate of polymerization will cause a decrease in the polymer chain length. In addition, the rate of polymerization depends on many variables according to the equation 4-11, including the rate of constants which are temperature dependent [Rudin, 1999].

$$\nu = k_p^2 [M]^2 / (2 k_t R_p) \quad \cdots\cdots\cdots (4-10)$$

$$R_p = k_p [M] \left(f k_d [I] / k_t \right)^{1/2} \quad \cdots\cdots\cdots (4-11)$$

where ν represents the kinetic chain length defined as the average number of monomer molecules consumed by each radical; k_t, k_p, k_d are termination, propagation, and initiation rate constants respectively which are assumed to be an Arrhenius function and consequently increase with temperature; $[M]$ is the monomer concentration; R_p is the rate of polymerization; f is the initiation efficiency factor; $[I]$ is the initiator concentration.

In the polymerization method used here, homopolystyrene was firstly and repeatedly synthesized to find a suitable polymerization temperature, time and initiator concentration. Under the same conditions, monomer styrene were *in-situ* polymerized with TiO_2 as received (no MPS treatment) to test the activity of the initiator AIBN in the presence of hydroxyl groups on TiO_2 surface. It was shown that TiO_2 did not influence the functionality of the initiator for carrying out polymerization of styrene. Hence we could possibly regulate polymerization time to control the final weight percentage (wt%) of TiO_2 nanopowder in the polymer matrix. For example, if we want to increase the TiO_2 fraction, one effective way we could use is to decrease polymerization time for the similar initial reaction conditions. The results of all designed polymerization runs are demonstrated in

Table **8**.

Table 8: Polymerization results with different loadings of modified TiO_2

Exper.	**Styrene**	**MT**	**Initiator**	**Temp.**	**Time**	**Yield**[#]	**Conversion**	**TiO_2 loading**
	(ml)	(g/l)	(mol/l)	(^oC)	(hr)	(g)	(%)	(wt%)
PS-0	10	0	$5*10^{-3}$	60	24	2.00	22.03	0
PSTN1	10	50	$5*10^{-3}$	60	24	2.50	22.02	19.98
PSTN2	10	10	$5*10^{-3}$	60	24	2.11	22.09	4.74
PSTN3	10	2	$5*10^{-3}$	60	24	2.01	21.93	0.994

data obtained from an average of three repeated experiments

4.3.2 Chemical Composition

To identify if the TiO_2 nanopowder was embedded in the polystyrene matrix and chemically bonded to polymer chains, FT-IR spectroscopy was employed. This technique has been reported in the literature for the investigation of polymer alumina nanocomposites [Rong, 2002]. In Chapter 3, the characteristics of unmodified and modified TiO_2 surface have been clearly investigated to get evidence of Ti-O and -OH bonds, as shown in Figure 17: FTIR spectra of (a) pure MPS; (b) MPS-modified TiO2. As we

know, the fundamental vibrations of solids are localized in the low frequency region (<1200 cm^{-1}) of the midrange (400 to 4000 cm^{-1}) IR spectrum. However, the vibrational spectrum of such surface hydroxyl groups is quite complex and the intensity of peak changes significantly upon the adsorption of moisture [Morterra, 1996]. For simple identification of TiO_2, the Ti-O bond is sufficient. It is clearly located in the range from 400 to 900 cm^{-1} and it does not overlap with other typical polystyrene bands.

Homopolystyrene, polystyrene TiO_2 nanocomposites, and TiO_2 as received were investigated and their typical FT-IR spectra are presented in Figure 80. The spectrum of polystyrene TiO_2 nanocomposites is almost a combination of the spectra of homopolystyrene and TiO_2 nanopowder, showing typical absorptions for homopolystyrene with characteristic phenyl ring stretching bands at 1602.7, 1492.7 and 1452.2 cm^{-1}, and the ring out of plane band at 698.1 cm^{-1}. In addition, the spectrum of PS-nanocomposites shows the significant absorption below 900 cm^{-1} representing Ti-O band of TiO_2, which indicates the TiO_2 nanopowders are located in the polystyrene matrix of the nanocomposite. These observations are in agreement with analogous procedures reported in the literature [Rong, 2005; Chen, 2000].

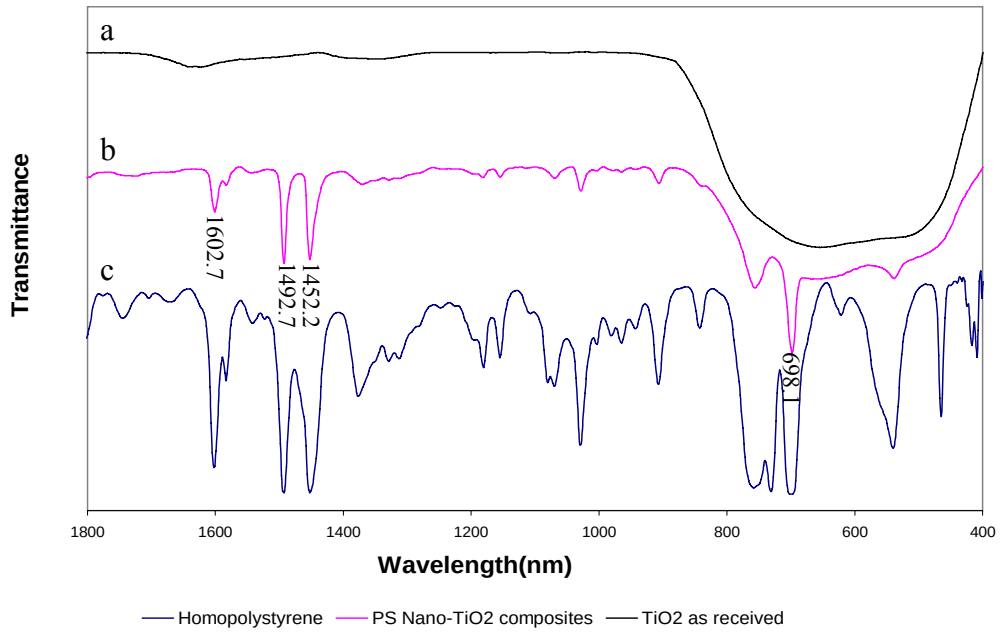

Figure 80: FTIR spectra (1800-400 cm^{-1} wavelengths) of (a) TiO_2 as received; (b) polystyrene TiO_2 nanocomposites; and (c) homopolystyrene

The spectra in Figure 80 represent that TiO_2 nanopowders are present in the polystyrene matrix. However, it does not differentiate between a physical mixture and a hybrid composite with chemical bonding linking polystyrene and TiO_2. In order to further confirm that the chemical bond between organic (PS) and inorganic (TiO_2) phases really exists, fractionation of the nanocomposites was carried out with the Soxhlet extraction or centrifugation separation method.

Initially the sample was extracted with boiling toluene throughout a Soxhlet extractor. According to the proposed model (Figure 79), it is expected that the nanocomposite samples should have a fraction of PS not bonded to the TiO_2 nanopowders and a fraction bonded to the TiO_2 nanopowders. It was clear that the homopolystyrene fraction dissolves in toluene and could be extracted by the hot solvent. However it was unknown if the fraction of polystyrene chemically bonded to TiO_2 nanopowders would also

dissolve to some extent to be extracted or not. From the results after Soxhlet extraction, almost no sample was left in the mesh steel.

Subsequently, the extracted solution was taken to separation by centrifugation. After this second fractionation method there were two separated sediment and supernatant phases clearly observed in the system. For comparison, homopolystyrene was dissolved in hot toluene and the centrifugation separation was also employed. It was found that there was only one clear phase in the PS-toluene solution after its centrifugation. All these evidences suggest that the fraction of polystyrene chemically bonded to TiO_2 nanopowders is dissolvable in hot toluene to a certain extent. Hence, centrifugation separation is the more effective method to carry out the fractionation of these nanocomposites.

After complete fractionation by centrifugation, the chemical composition of the supernatant and sediment fractions was analyzed by FT-IR spectroscopy. Typical results are represented in

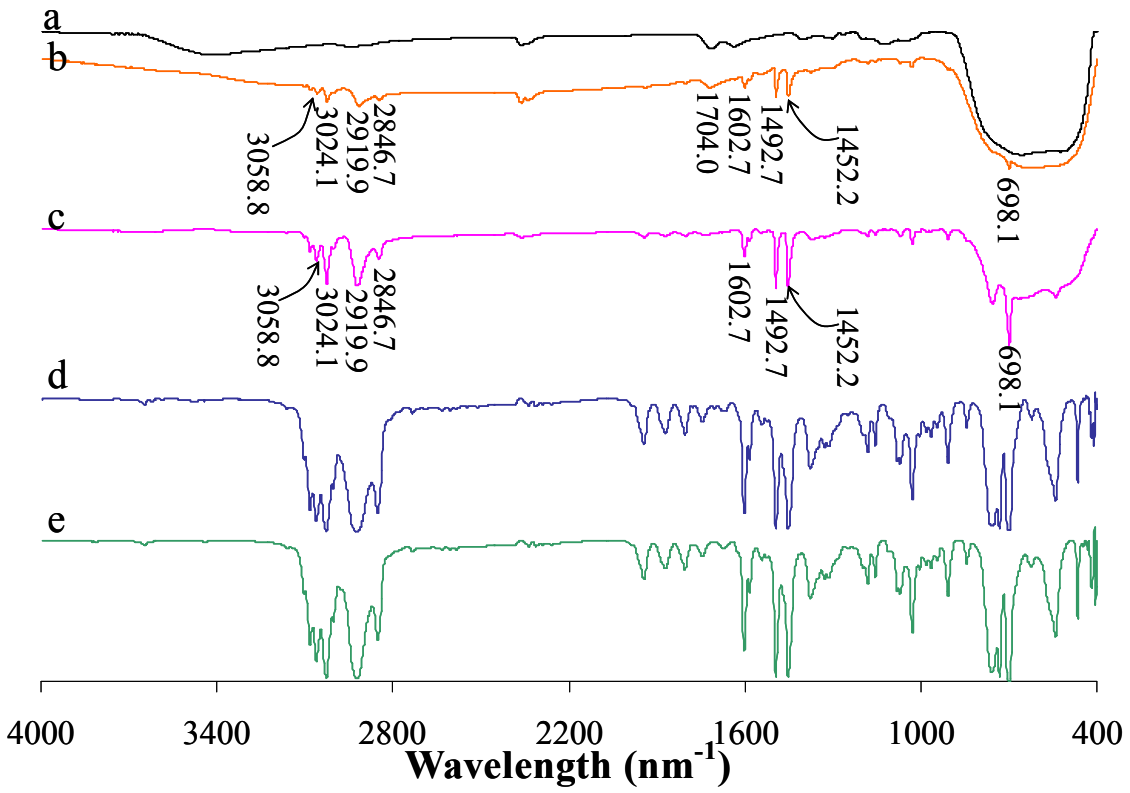

Figure 81. Comparing with those of FT-IR spectra of TiO_2 modified by MPS, homopolystyrene, PS-TiO_2 nanocomposites before and after centrifugation, it is found that the FT-IR spectrum for the supernatant fraction only showed typical polystyrene bands, no Ti-O absorbance bands of TiO_2. The sediment fraction is identified by bands such as the C-H benzenic stretching vibration at 3058.8 and 3024.1 cm^{-1}, the C-H stretching vibration at 2919.9 and 2846.7 cm^{-1}, the benzenic ring stretching vibration at 1602.7, 1492.7 and 1452.2 cm^{-1}, and the ring out of plane bend at 698.1 cm^{-1} [Rong, 2005; Chen, 2000], where the characteristic bands for polystyrene are clearly seen; additional strong absorbance below 900 cm^{-1} indicating Ti-O band of TiO_2. In the meantime, the C=O vibration band at 1704.0 cm^{-1} is also shown in the spectrum of sediment fraction. All these evidences indicate that polystyrene is chemically bonded to the TiO_2 nanopowder since the homopolystyrene has been fractionated from the powder surface by centrifugation separation.

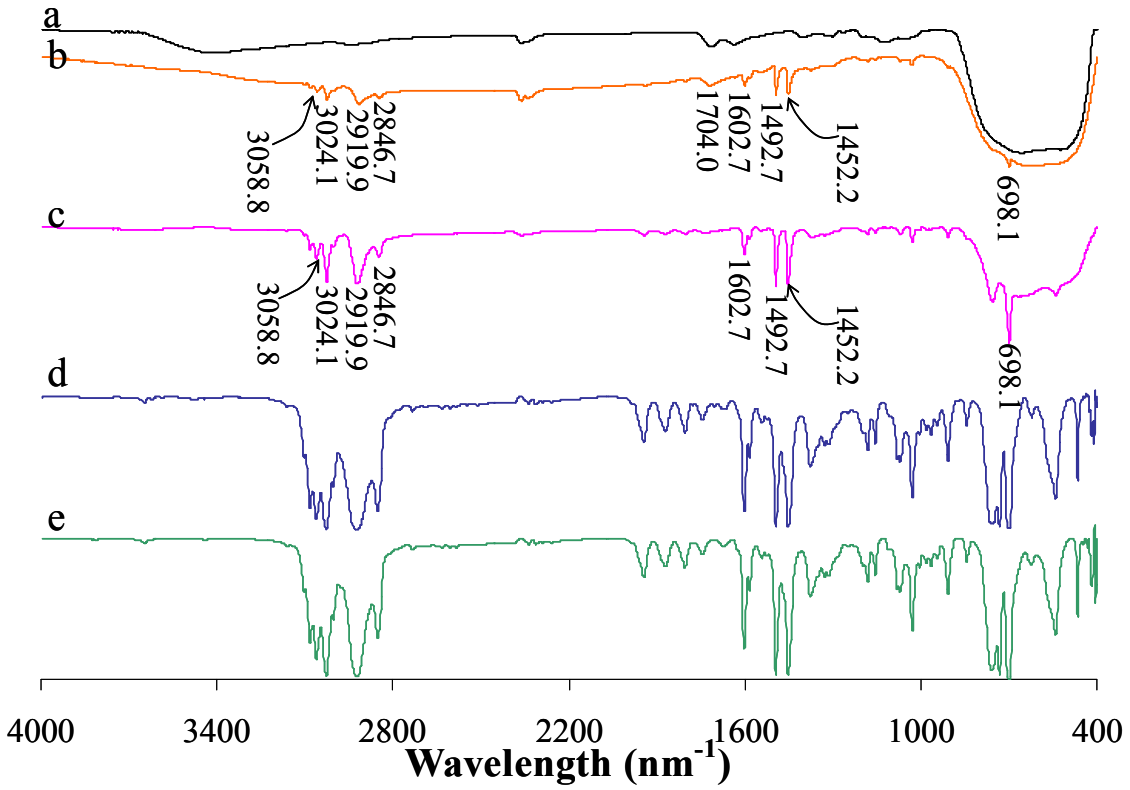

Figure 81: FTIR spectra (4000-400 cm^{-1}) of (a) modified TiO_2; (b) sediment of PSTN; (c) PSTN before fractionation; (d) homoPS; (e) supernatant of PSTN

Therefore, through these FT-IR investigations on fractionated samples, the following two points have been found out: a) there are at least two types of polymer chains in these nanocomposites – homopolystyrene and polystyrene covalently bonded to the surface of TiO_2 nanoparticles (hybrid organic-inorganic phase); b) during the copolymerization of styrene and vinyl groups on modified TiO_2, the hybrid phase is not completely crosslinked and may be somehow soluble in organic solvents such as toluene. As a conclusion, it was possible to graft polystyrene chains to the surface TiO_2 nanopowder creating a hybrid organic-inorganic nanocomposite.

However, it is difficult to attribute the faster polymerization rates observed in the first stages to either the homopolymerization of styrene or copolymerization of styrene and vinyl groups of modified TiO_2. One hypothesis is that the copolymerization of styrene and vinyl groups of modified TiO_2 happened from the very beginning of the polymerization and finished after the consumption of all vinyl groups on the TiO_2 surface. After that, the homopolymerization of styrene would be the only possible mechanism. Because polystyrene chains were still being produced, it was possible to control the final weight of TiO_2 nanopowder in the nanocomposites by simply controlling polymerization time. However, this hypothesis has not been confirmed and it is still unknown when the homopolymerization started and how it would influence the resulting materials. Further experiments should be designed to study the mechanism and kinetics of this system, especially the relationship between polymerization conversion and structure.

4.3.3 Quantification of PS Grafted on TiO_2

The quantification of polystyrene grafted on the TiO_2 nanopowder was obtained and calculated from the thermal gravimetric analyses (TGA). Three nanocomposites samples, before fractionation (below referred to as b.f.) and after fractionation (reffered to as a.f.),with modified TiO_2 (concentrations 50, 10 and 2 g/l) and polymerized under similar conditions were analyzed with TGA. Samples of TiO_2 nanopowder as received, modified

TiO_2 used in polymerizations, homopolystyrene produced with similar polymerization conditions were also analyzed. Thermograms are shown in Figure 82.

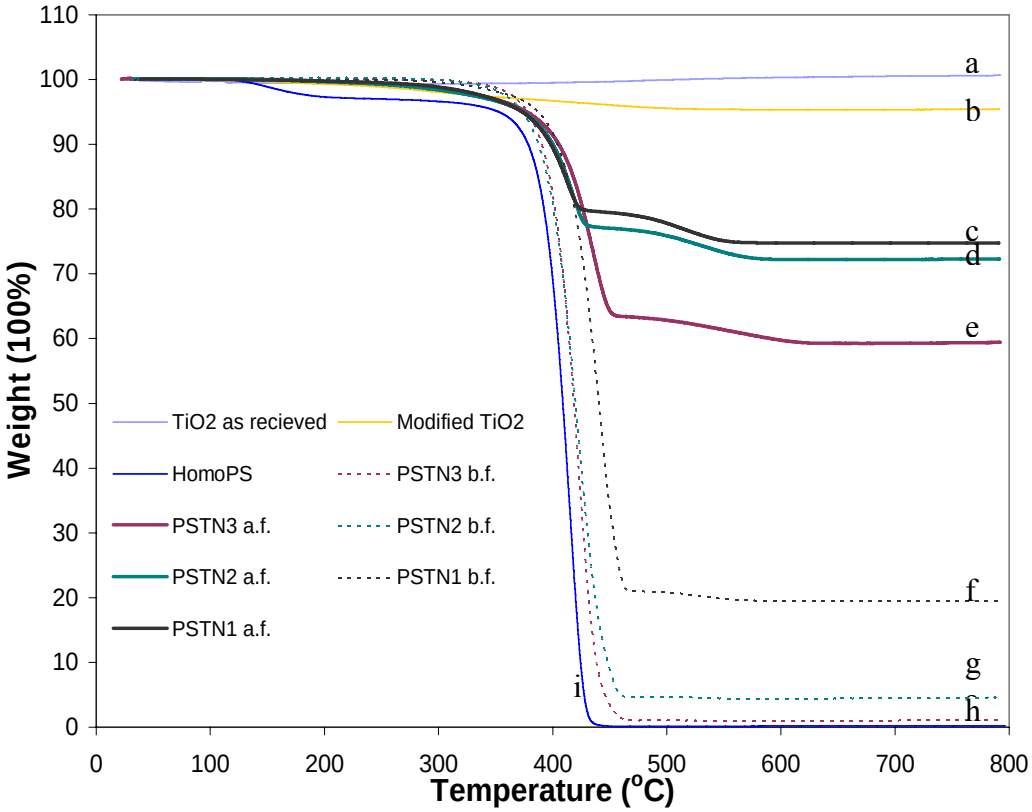

Figure 82: TGA curves of the samples (a) TiO2 as received; (b) modified TiO_2; (c) PSTN1 a.f.; (d) PSTN2 a.f.; (e) PSTN3 a.f.; (f) PSTN1 b.f.; (g) PSTN2 b.f.; (h)PSTN3 b.f.; (i) homoPS

From the TGA curves, the initial weight percent, residual weight percent, weight loss of all the samples can be calculated. The weight percent of grafted modifier and polystyrene are calculated according to equations 4-12 and 4-13 respectivel; results are presented in Table 9. The relationship between the weight percent of grafted PS on TiO_2 and the initial concentration of TiO_2 is also shown in Figure 83.

$$\text{Grafted MPS on } TiO_2\,(\text{wt\%}) = \frac{\text{Initial (wt\%)} - \text{Residual (wt\%) of modified } TiO_2}{\text{Residual of modified } TiO_2} \quad \textbf{(4-12)}$$

$$\text{Grafted PS on } TiO_2\,(\text{wt\%}) = \frac{\text{Resiual (wt\%) of modified } TiO_2 - \text{Residual (wt\%) of the PSTN after fractionation}}{\text{Residual (wt\%) of the PSTN after fractionation}} \quad \textbf{(4-13)}$$

Table 9: Weight changes of the samples from TGA

Samples	Initial wt. (%)	Residual wt. (%)	Weight loss (%)	Grafted MPS (%)	Grafted PS (%)
TiO_2 as received	100	100.65	-0.65	-	-
Homo-PS	100	0.13	99.87	-	-
PSTN3 b.f.	100	1.07	98.93	-	-
PSTN2 b.f.	100	4.57	95.43	-	-
PSTN1 b.f.	100	19.53	80.47	-	-
Mod. TiO_2	100	95.4	4.6	4.82	-
PSTN3 a.f.	100	59.41	40.59	4.82	60.6
PSTN2 a.f.	100	72.30	27.70	4.82	32.0
PSTN1 a.f	100	74.77	25.23	4.82	27.6

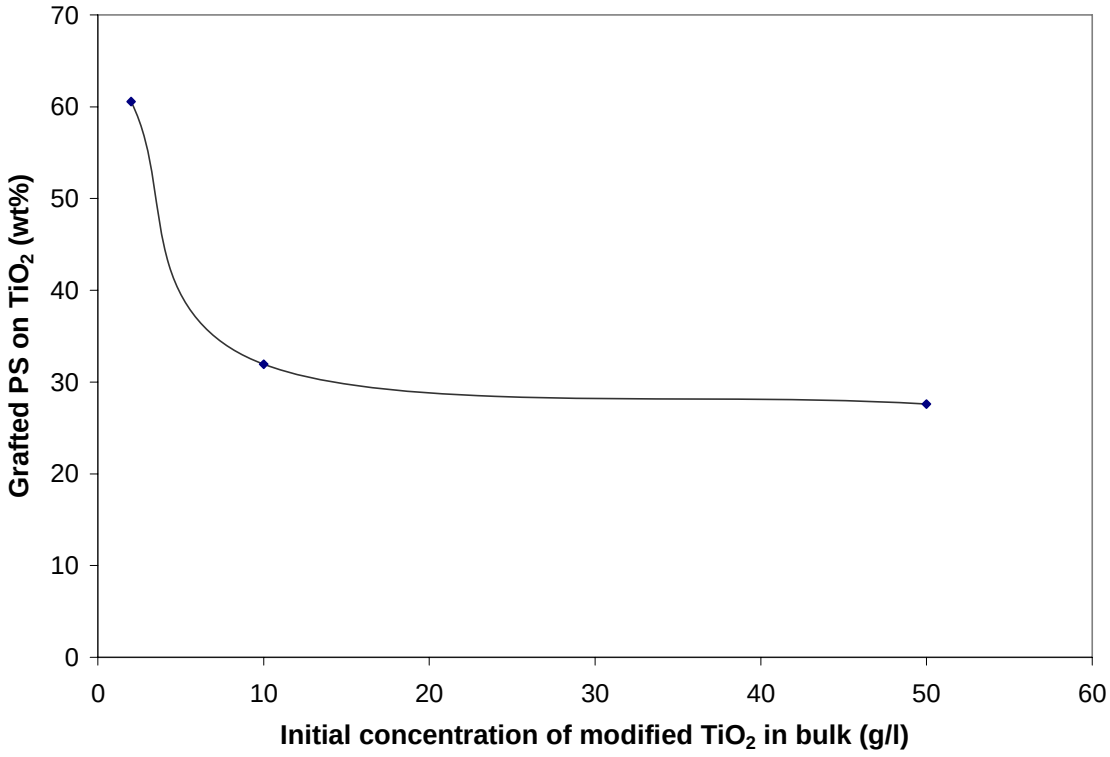

Figure 83: Grafted PS on TiO_2 vs MT initial concentration

As shown in Table 9, the grafted MPS on TiO_2 is calculated as 4.48 wt%, which is less than the 5.32wt% [=initial fraction of MPS to TiO_2 (40 wt%) * SGC (13.3%)] estimated by ^{1}H-NMR in the previous section. The reasonably small gap is attributed to: 1) different instrumentations have different accuracy and sensitivity; 2) in TGA quantification, Si in MPS does not pyrolyzes completely in the temperature range tested.

It is also clearly found from Table 9 and Figure 83 that the amount of grafted PS on TiO_2 nanoparticles is inversely proportional to the initial feed concentration of modified TiO_2. Low concentration of modified TiO_2 provides a high amount of grafted polystyrene on TiO_2 nanopowder. When the initial concentration of modified TiO_2 decreased from 50 g/l to 2 g/l in bulk, the weight percent of grafted polystyrene increased from 27.6% to 60.6%.

The inverse in grafting density with concentration of modified TiO_2 nanoparticles is in agreement with the characteristic feature of the grafting process, which may be explained by the following two factors. First, from a survey of the literature on grafting free radical polymerization from solid surfaces [Minko, 1999], the rate of grafting is proportional to the surface concentration of initiator and the rate of the reaction process depends on the availability of reactive group. With the same initiator concentration, when the concentration of modified TiO_2 decreases, the TiO_2 unit surface concentration of initiator increases. In addition, as discussed above, in this system methacrylate groups on TiO_2 surface could possibly reacted with themselves or copolymerize with the monomer styrene. With the same monomer concentration, when fewer modified particles were supplied, the fewer methacrylate groups were available and the opportunity for the methacrylates to polymerize with themselves was lower. Therefore, more reaction between vynil methaclrylate and styere was possible increasing the grafting reaction. Second, modified TiO_2 powders are less likely to agglomerate and have their dispersibility improved, in the bulk monomer or polymer media, with decreasing initial concentration of TiO_2 in the feed. The increased dispersibility at low initial concentration

of modified TiO_2 could also decrease the diffusion limitations of polymer growing chains.

4.3.4 Thermal Properties

Thermal stability and degradation.

The thermal stability and degradation characteristics of the nanocomposites samples can be also revealed from TGA thermograms. The 1st derivative thermogravimetric (DTG) curves shown in Figure 84.

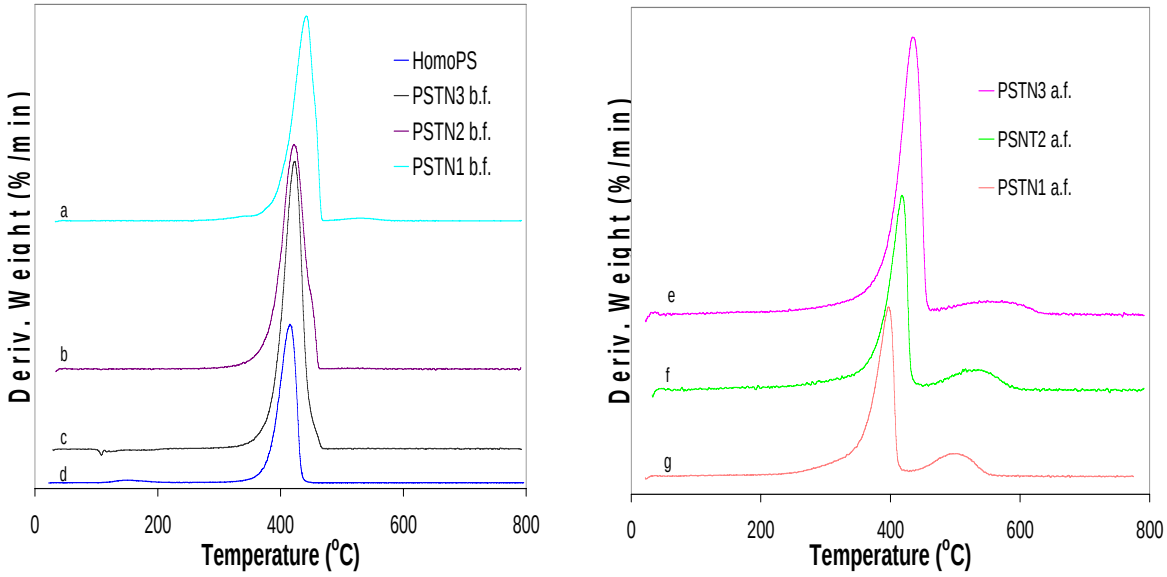

Figure 84: DTG curves of the samples (a) PSTN1 b.f.; (b) PSTN2 b.f.; (c) PSTN3 b.f.; (d) HomoPS; (e)PSTN3 a.f.; (f)PSTN2 a.f.; (g) PSTN1 a.f.

The TGA thermograms (Figure 74) and DTG (Figure 76) curves give a direct view of thermal degradation of the nanocomposite samples before and after fractionation. Temperature of decomposition at 5% weight loss (T_d 5%) and T_d 10% weight loss, temperature of maximum decomposition peak (T_d) of 1st derivative and residual weights were obtained from those curves and are listed in Table 10.

Table 10: Degradation temperatures of the samples from TGA and DTG

Samples	T_d 5 % wt. loss (^oC)	T_d 10 % wt. loss (^oC)	T_d peaks of 1st derive (^oC)	Residual Weight (%)
Homo-PS	352.6	378.5	417.6	~0
PSTN3 b.f.	372.9	386.7	424.4	1.07
PSTN2 b.f.	373.1	387.3	425.2	4.57
PSTN1 b.f.	387.4	404.0	442.0	19.53

Degradation temperatures reveal that the addition of TiO_2 can improve the thermal stability of the PS-TiO_2 nanocomposites. The 5% weight loss temperatures T_{d5}s, for instance, are increased from 342.3 ^oC, then 372.9^oC, 373.1 ^oC, to 387.4^oC when TiO_2 content (wt%) on the nanocomposites increased from 0% to 1.07%, then to 4.57% and finally to 19.53%, respecively.

For the maximum degradation temperatures of 1st DTG, a small improvement was found with increasing TiO_2 addition even though there is not a regular linear relationship. This phenomenon seems to be contrary to that reported in the literature review. According to the literature, the photoactivity of TiO_2 could make the polymer to degrade more easily and therefore decrease the degradation temperature of the polymer. In our system we propose that the modifier, in form of silane coupling agent on the surface of TiO_2, may have contributed to the improvement in thermal stability. In order to make clear evidence that how MPS and TiO_2 have influence on the T_d of the polystyrene individually, the fractionated sediment of each nanocomposites samples were also tested as shown in TGA and DTG curves. Their peak values are presented
Table 11.

Table 11: Peak values (T_d) of the nanocomposites samples from DTG

Samples	Grafted PS (wt%)	TiO_2 (wt%)	1st Peak (^oC)	2nd Peak (^oC)
Homo-PS			417.6	
PSTN3 a.f.	60.6	39.4	433.9	549.8
PSTN2 a.f.	32.0	68.0	417.8	515.7
PSTN1 a.f.	27.6	72.4	412.9	512.7

In an inert atmosphere, the classic homopolystyrene pyrolysis is a complete polymer chain breakage occurring at temperatures below 450^{o}C. However, the pyrolysis mechanism of polystyrene TiO_2 nanocomposites is not quite clear. Apparently, two peaks are observed in the DTG diagrams of the PSTNs after fractionation, which can also be interpreted with the pyrolysis mechanism being proposed here that they occur mainly in two steps. The first step is the decomposition beginning with a rapid breakage of the main grafted polystyrene chains in the temperature ranges between 350^{o}C and 450^{o}C, which represents their first DTG peak; then followed by the second step with a relatively slow elimination of MPS elements above 450^{o}C up to 620^{o}C to make the second peak appear.

An initial look at the temperature of maximum decomposition peak (T_d) shows an behavior. The values of T_d 1st peak in the DTG curves for the fractionated PSTNs, at low initial TiO_2 loading of 1.07 wt% (before fractionation) increased from 417.6^{o}C to 433.9^{o}C. Whereas, at initial TiO_2 loading of 4.57 wt% (before fractionation) T_d was about the same as homopolystyrene and at high initial TiO_2 loading of 19.53 wt% (before fractionation) the value of T_d was smaller than that for homopolystyrene. Recall that after the fractionation, the amount of grafted PS was 60.6 wt%, 32.0wt% and 27.6 wt% on those PSNTs with initial TiO_2 content (before extraction) of 1.07 wt%, 4.57 wt% and 19.53 wt% respectively (Table 9). Therefore the TiO_2 content after the fractionation were 39.4 wt%, 68.0 wt% and 72.4 wt% on those PSNTs with TiO_2 which had the initial TiO_2

contend (before extraction) of 1.07 wt%, 4.57 wt% and 19.53 wt% respectively (see Table 11). This thermal decomposition temperature behavior is rationalized in terms of the final compositin after extraction. For the concentration range studied here, at low amounts of TiO_2 the thermal decomposition temperature increased and at high amounts of TiO_2 the thermal decomposition temperature decreased. Although this behavior is not completely understood at this moment, it is proposed here that this phenomenon can be explained by fact that the modifier MPS might be capable of improving the degradation temperature of the polymer and it plays a competitive role with TiO_2. A similar behavior has been previously identified for polybenzoxazine polymer. As reported by Agag and co-workers, the enhancement of the thermal stability of polybenzoxazine was explained by the attribution to the thermal insulation effect of metal oxide network which protected the polymer matrix [Agag, 2004].

Thermal transition temperature. Thermal transitions of the polymer nanocomposites were measured by differential scanning calorimeter (monitoring the heat flow vs temperature). Polystyrene is non-crystalline and therefore does not exhibit any crystallization or melting transitions. After two cycles at 10 ^oC/min, from room temperature up to 200^oC, the glass transition temperature (T_g) of polystyrene nanocomposites was obtained from the mid-point change for the transition region in the curve of the second heating scan. To correct the baselines of DSC curves, an empty aluminum cell was scanned in the same heating range. The corrected DSC curves are displayed in Figure 85. The glass transition temperatures of homopolymer and nanocomposites samples are presented in Table 12.

It was found that the T_g did not change significantly with the addition of TiO_2 nanopowder. The slight differences between the values for all the samples were within experimental error. This result may indicate that hybridization of TiO_2 in the nanocomposites do not influence the glass transition behavior of polystyrene matrix. To date, the exact reasons of this result are unknown because of the very limited number of experiments which we have done.

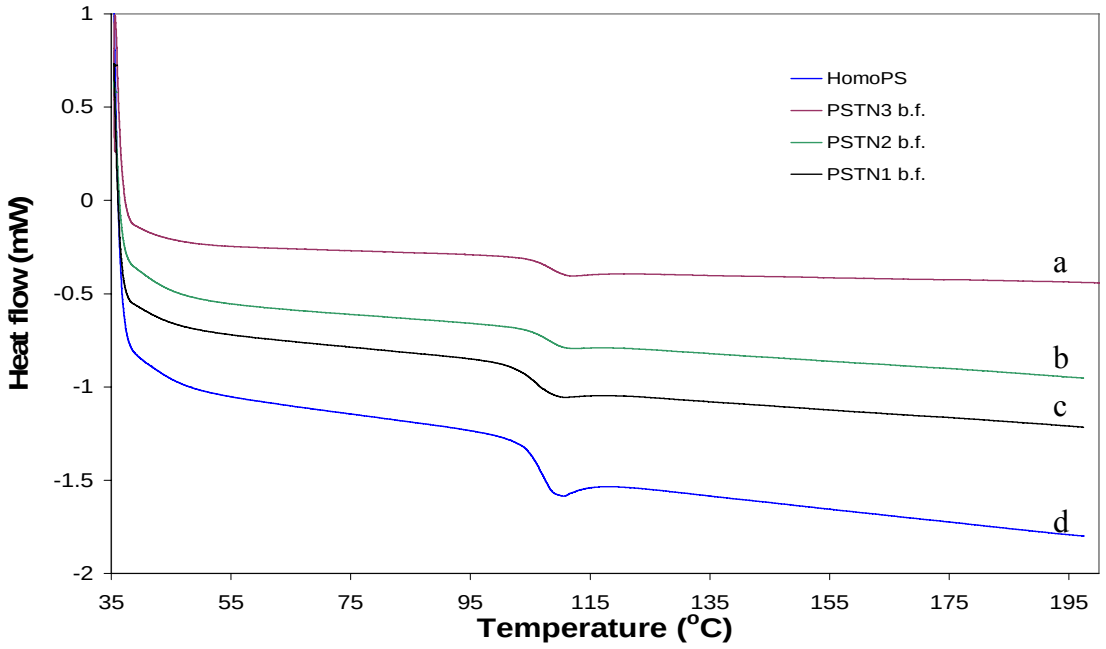

Figure 85: DSC thermal curves of the samples (a) PSTN3 b.f.; (b) PSTN2 b.f.; (c) PSTN1 b.f.; (d) HomoPS

Table 12: T_g temperatures from DSC thermograms

Samples	T_g (°C)
Homo-PS	106.8
PSTN 3 b.f.	108.6
PSTN 2 b.f.	108.2
PSTN 1 b.f.	106.5

4.3.5 Morphology Analysis

The morphology of polystyrene-TiO_2 nanocomposites was observed with scanning electron microscopy (SEM) by examining the cross section of nanocomposite film after cold fracture of films prepared by melt pressing. Results are shown in Figure 86, and Figure 87. After comparing with the morphology of modified TiO_2 in toluene suspension (Figure 29-b), it is apparent that there is a significant change on the TiO_2 particle size

within the polymer matrix after in-situ polymerization. These micrographs are in agreement with the proposed polymerization model presented in previous sections. When polymerization starts with aggregates of modified TiO_2, it is most likely that the TiO_2 nanoparticles are being coated by polystyrene during in situ copolymerization between styrene and double bonds of silane coupling agent on TiO_2 surface and the growing polymer chains force the TiO_2 aggregates to fragment.

It was discussed previously that in these nanocompoistes there are two types of polymer chains, polystyrene chains chemically bonded to TiO_2 and homopolystyrene. Even when relatively low amounts polystyrene chains are bonded to the TiO_2, the homopolymer chains could also form entanglements and provide a source for fragmentation.

Figure 86, and Figure 87 clearly confirm that there are polymer chains surrounding TiO_2 nanoparticles and nanoparticles (diameter in the range of 20-50 nm) are relatively uniform dispersion throughout the whole polymer matrix. They also indicate that there is a good adhesion between organic and inorganic phases and the distance between TiO_2 nanoparticles is much larger than the diameter of the nanoparticles.

From the energy dispersive X-ray (EDX) analysis (see Figure 88), done during the SEM, it is also evident that there are Ti and Si elements coming from TiO_2 nanopowders and the MPS silane coupling modifier in the sample. This is a further evidence about the chemical compostion of the nanocomposite and that the modified TiO_2 nanoparticles are embedded within the polystyrene matrix.

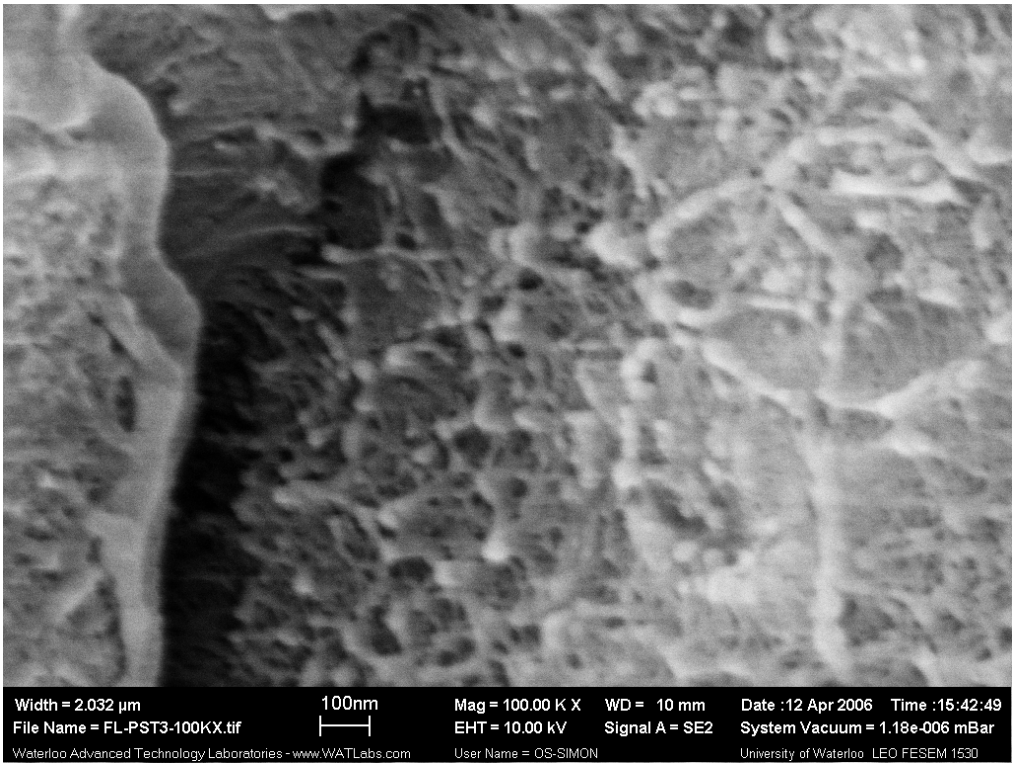

Figure 86: SEM pictures of PS TiO_2 nanocomposites after cold fracture; Mag =100kX

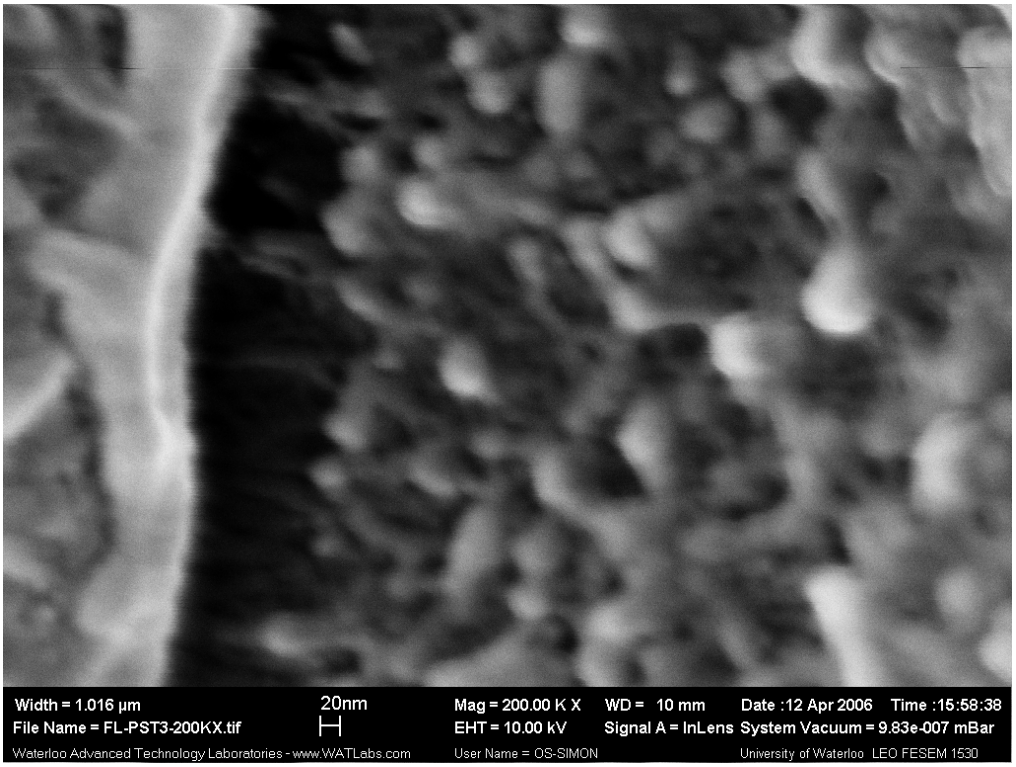

Figure 87: SEM high magnification pictures of PS TiO_2 nanocomposites after cold fracture; Mag =200kX

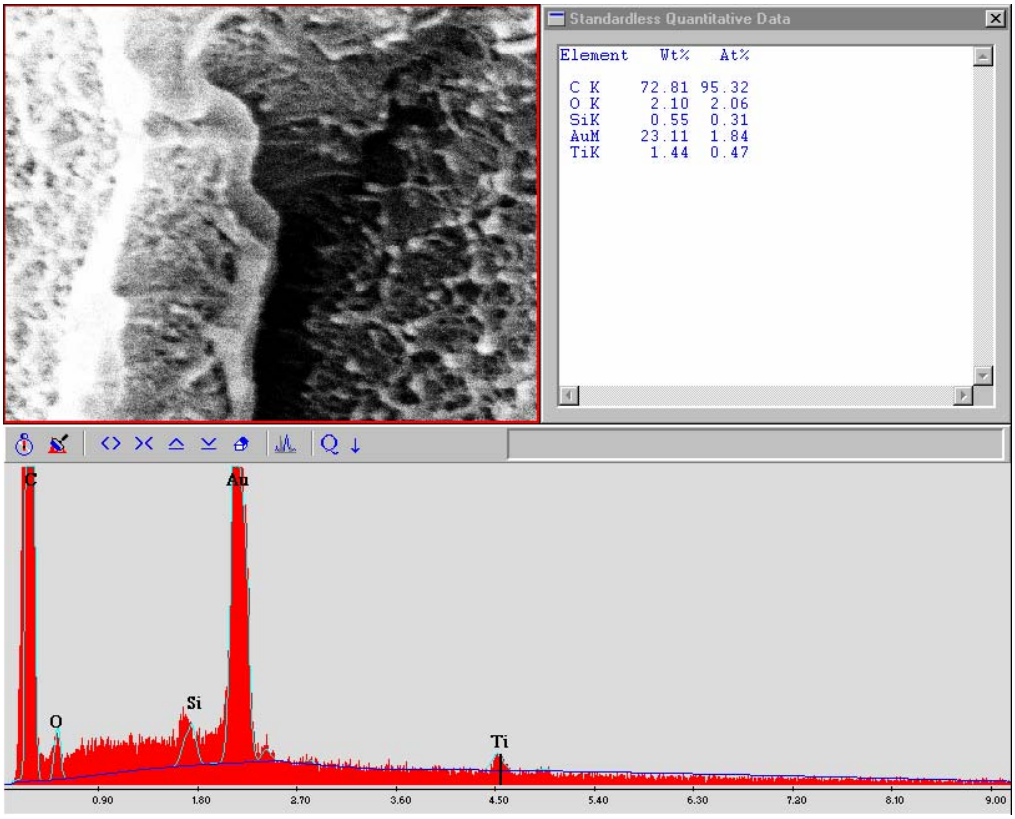

Figure 88: Element analysis for PS TiO_2 nanocomposites SEM observation

4.3.6 Optical Properties

It is proposed that the small TiO_2 nanoparticles size and the homogeneous dispersion in the polymer matrix could lead to improved optical properties of the nanocomposites. This is based on the theory that the scattering of visible light is markedly dependent on the size of particles. To confirm this hypostesis, measurement of the optical properties of the nanocomposite samples was carried out with a UV-Vis spectrophotometer.

The testing samples were prepared by addition of same amount of the obtained nanocomposites with different fractions of TiO_2 before fractionation into boiled toluene solutions. Films with relatively uniform thickness were obtained on the sidewall of a quartz glass after solvent evaporation. For the material with the higher TiO_2 content, in this case PSTN1 containing 19.53% TiO_2, a powder was obtained instead of a uniform film after solvent evaporation. Data from this sample will not be discussed. The UV-Vis

spectra of PSTN3 and PSTN2 nanocomposites containing 1.07% and 4.57% of TiO_2 respectively, along with homopolystyrene, are shown in Figure 89. Their absorbances at wavelengths 400nm (A_{400}) and 300nm (A_{300}) were recorded and are summarized in Table 13.

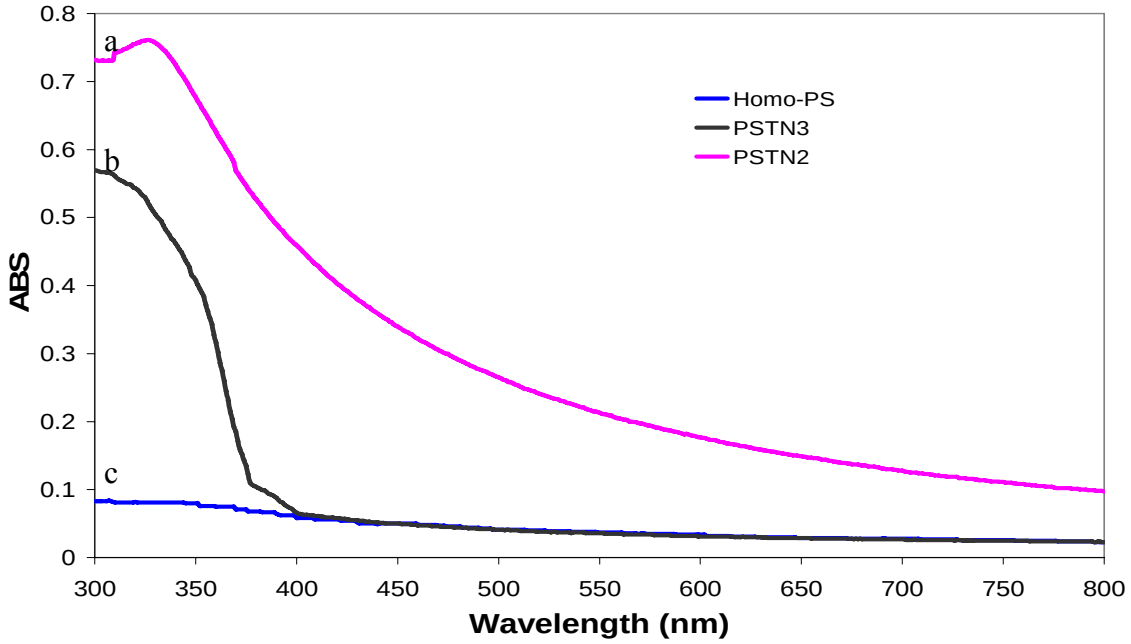

Figure 89: UV-Vis spectra of (a) PSTN2 containing 4.57% TiO_2; (b) PSTN3 containing 1.07% TiO_2; and (c) homopolystyrene

Table 13: Optical properties of the samples with different fractions of TiO_2 (f_{TiO_2}): absorbances at wavelengths 400 nm and 300 nm

Sample	f_{TiO_2} (wt%)	A_{400}	A_{300}
Homo-PS	0	0.058	0.083
PSTN3 b.f.	1.07	0.060	0.570
PSTN2 b.f.	4.57	0.459	0.732

Small values of absorbances at the visible and UV region were observed for homopolystyrene film, which is reasonable transparency but has no function of filtering out UV light. However, relatively strong absorbance in the UV region and small absorbance at the visible region, which also means a typical optical property of the combination of visual transparency and UV filters close to the visual wavelengths, were observed for the PSNT3 nanocomposites containing 1.07% TiO_2. With the further addition of TiO_2, sample PST2 with 4.57% TiO_2, the material appeared opaque to eye observation and had significant absorbance in the visible region as well as in the UV region. At this level (4.57%), the performance of the material as a visually transparent UV filter was reduced.

The spectrum of homopolystyrenre was used as background for subtraction, from the UV-Vis spectra of the nanocomposites PSNT3 and PSNT2 (see Figure 90). After subtraction both exhibited an adsorption maximum of the TiO_2 nanoparticles at 225 nm, in accordance with the results found by Nussbaumer and co-worker. A similar behavior was demonstrated for the UV characteristics of TiO_2 nanocomposites with polyvinyl alcohol (PVAL), polyvinyl acetate (PVAC), polyvinylpyrrolidone (PVPO), and polyvinyl pyridine (PVPY) matrices [Nussbaumer, 2003].

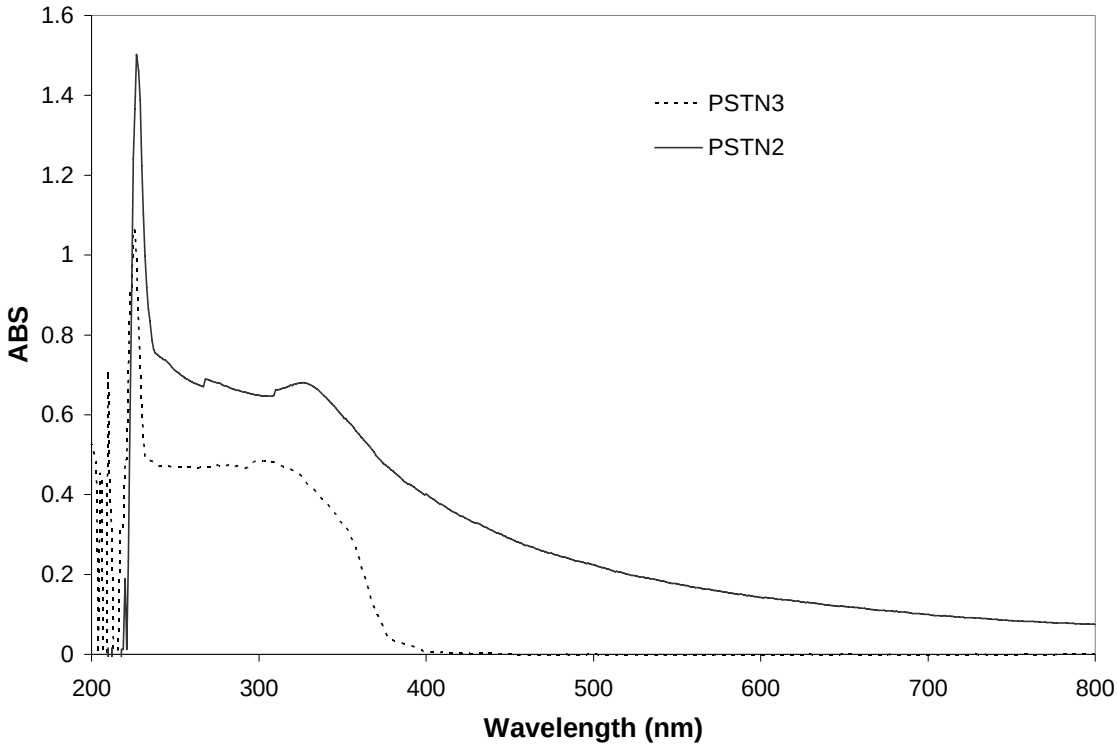

Figure 90: UV-Vis spectra of PS-TiO_2 nanocomposites with two different TiO_2 contents (dashed line) PSTN containing 1.07% TiO_2; (solid line) PSTN containing 4.57% TiO_2 The absorbance has been subtracted from the homopolystyrene background.

4.4 Summary

A bulk polymerization method was employed to synthesize polystyrene TiO_2 nanocomposites. The free radical copolymerization of styrene monomer and double bonds on the surface of modified TiO_2 was initiated by AIBN, in concurrence with homopolymerization of styrene in this system. These nanocomposite materials, which contain some fraction of polystyrene covalently grafted to TiO_2 surface, did not form completely crosslinked gel and were soluble in hot organic solvents. The amount of polystyrene grafted on TiO_2 was a function of the concentration of chemical in the polymerization.

The in situ polymerization approach used here is able to disrperse the nanopowder with the polymer matrix and to stabilize the dispersion after polymerization. The first is

attributed to the mechanism of fragmentation during polymer chain growth and the later is attributed to the covalt bonding between the polymer chains and the nanoparticles.

The hybrid nanocomposites were shown to have improved optical properties as compared to those of pristine polystyrene due to the hybridization of nano-sized TiO_2. The combination of visual transparency and strong UV absorption close to the visual wavelengths, a typical optical property of TiO_2, was conserved in PS nanocomposites with 1.07 wt% TiO_2. It was also demonstrated that TiO_2 did not have a significant detrimental effect on the thermal properties, as it would be expected due to the oxidatively degradable ability of TiO_2. The glass transition temperature maintained the same temperature in comparison with neat polystyrene.

4.5 References

Agag, T.; Tsuchiya, H.; Takeichi, T.; *Polymer*, 2004, 45, 7903

Angot, S. K. S.; Taton, D.; Gnanou, Y.; *Macromolecules*, 1998, 31, 7218

Chen, G.; Liu, S; Zhang, S.; Qi, Z.; *Macromol. Rapid Commun*., 2000, 21, 746

Minko, S.; Gafijchuk, G.; Sidorcnko, A.; Voronov, S.; *Macromolecules*, 1999, 32, 4525

Morterra, C.; Magnacca, G.; *Catal. Today*, 1996, 27, 497

Nussbaumer, R. J.; Caseri, W. R.; Smith, P.; Tervoort, T.; *Macromol. Mater. Eng*., 2003, 288, 44

Odian, G.; *Principles of Polymerization*, John Wiley and Sons, Inc., New York, 1991

Rong, Y.; Chen, H. Z.; Wu, G.; Wang, M.; *Mater. Chem. Phys*., 2005, 91, 370

Rudin, A.; *the Elements of Polymer Science and Engineering*, Academic Press, San Diego, 1999

Chapter 5 General Conclusions and Recommendations

The elaborated strategy has been developed to synthesize polystyrene TiO_2 hybrid nanocomposites which have the polymer chains covalently grafted onto the ceramic nanopowder with the aid of a silane coupling agent. Several characterization techniques, such as fractionation, FTIR, BI-DCP sizer, SEM and UV-Vis, were employed to provide the proof for the success of chemical bonding, their particle size and morphology structure and properties. It was shown that these nanomaterials could act as visually transparent UV filters without loss of thermal properties of the polymer.

The synthesis of nanocomposites was effectuated by surface modification and grafting polymerization steps. The objective of the first step was to turn the character of the surface into hydrophobic, to improve dispersibility of nanoparticles in orgainic media decreasing average particle size, and to introduce vinyl groups which are capable of copolymeizing to the surface of TiO_2 nanopowder. The surface modification with a silane coupling agent was acomplishied by hydrolysis and condensation reactions. ^{1}H-NMR analysis quantified that initial TiO_2 concentration at 50 g/l and MPS contentraction at 0.08 M in ethanol were close to the most adequate reaction concentration for the highest surface grafing density. BI-DCP particle sizer investigated that the average size of modified TiO_2 in ethanol decreased from >1200 nm for unmodified TiO_2 (as received) to the range of 200-400 nm depending on surface density of the silane grafting. In the second, polymerization of styrene with the vinyl groups on the modified TiO_2 was carried out by free radical AIBN initiator in bulk medium.

FTIR spectroscopy and fractionation were used to get evidence of how TiO_2 nanopowders existed in the polystyrene matrix. Fractionation with centrifugation showed that these nanocomposite materials, which contain some fraction of polystyrene covalently grafted to TiO_2 surface and one fraction of homopolystyrene, did not form

completely crosslinked gel and were soluble in hot organic solvents. FTIR proved that the covalent chemical bonding between the polymer chains and inorganic phase via grafted MPS was present in these hybrid nanocomposites. TGA quantitative analysis has shown that the amount of polystyrene grafted on TiO_2 was between 30 and 60 g per 100 g TiO_2.

It was observed by SEM that the dispersion of TiO_2 nanoparticles inside the polymer matrix was relatively uniform. Also the particles had a very good adhesion with polymer domain. The nanoparticles aggregation could be avoided by the in-situ polymerization step together with first surface modification process. The growing bonded polymer chains, as well as entangled homopolymer chains, have fragmented the aggregated nanoparticles leading to an ultrafine dispersion of nanoparticles in the matrix.

Investigation with UV-Vis spectroscopy has found that the dispersion of TiO_2 particles at nanoscale level could improve optical properties of the polymer nanocomposites. Good transparency was observed (to the eye) for the PS nanocomposites films for TiO_2 addtions of 1.07%. The fact that the nanocomposites are transparent indiciates that the nanoparticles are not agglomerated as observed by SEM. In addition, strong UV absorption of the nanocomposites was observed because of the incorporated TiO_2 particles, which exhibited an absorption maximum at 225 nm. Thus this sample could act as an efficient optically transparent UV filter.

Because of the good miscibility of polystyrene with various kinds of hydrophobic polymers, it is suggested that these PS TiO_2 nanocomposites are ideal starting materials to fabricate wide range of new nanocomposites, e.g. based on poly(styrene-co-acrylonitrile), poly(acrylonitrile-co-butadiene-co-styrene), to insert optically UV filtering properties of TiO_2 nanopowder potentially. In addition, grafting different polymer chains to the surface of the nanoparticles can increase the compatibility of other polymer blends, like polyethylene, polypropylene, ethylene/propylene rubber, polyvinyl acetate, natural rubber, etc.

We also make recommendation that further research remain to be carried out to explore different synthesis techniques yielding the different structures and to fully understand the structure/properties relationship. Comparison experiment by only simple mixing of polystyrene and TiO_2 as received (without surface modification) can be carried out to see how the particle size possibly from micro- to nano-meter affects the properties of composites. Characterization of microtomed sections of final nanocomposites using TEM or AFM may give a better description of the degree of dispersion. Testing of mechanical properties including tensile and impact should be studied to verify the improvents due to the inclusion of TiO_2 nanoparticles. Other vinyl monomers such as ethylene or propylene and other ceramic nanopowders such as SiO_2, Al_2O_3, ZnO which have not been investigated yet will be a vast range of possibilities to be explored by using surface modification with silane coupling agents and in-situ polymerization strategy we proposed here.